COMBINATORIAL NANODOT STRIPE ASSAY TO STUDY CELL HAPTOTAXIS

Mcolisi Dlamini
Department of Biological and Biomedical Engineering
McGill University, Montréal

December 2018

A thesis submitted to McGill University in partial fulfillment of the requirements of the Master of Engineering.

ABSTRACT

Haptotaxis, a cellular migration response to surface-bound biochemical cues, is essential for life processes such as angiogenesis, tissue repair, and embryonic development. *In vitro,* haptotaxis signaling processes are typically studied using protein gradient patterns. However, while these gradients provide global cell distributions for haptotaxis results, they do not easily and clearly provide precise information about the choices that cells make locally on different protein surface densities that exist within the gradient. Herein, we introduce the nanodot stripe assay (NSA) in order to (i) easily examine cell migration choices to different protein surface densities and (ii) to investigate the effect of protein nanodot cluster sizes on cell migration behavior. Each NSA design consists of a pair of alternating nanodot arrays of discrete and non-continuous surface density of either 0, 1, 3, 10, 30, 44 or 100% coverage. The NSA configuration challenges cells with a binary choice of low versus high surface densities of all possible combinations at once. The cell-surface affinity of the reference surface (RS), the area between patterned cues was adjusted towards maximizing cell response to the nanopatterned guidance cue. The RS was backfilled with a mixture of polyethylene glycol (PEG) and poly-D-lysine (PDL) with a low and high cell-surface affinity, respectively, and three RS combinations of 100:0, 90:10 and 75:25 %PEG:%PDL were tested with the NSA. The 90:10 %PEG:%PDL RS resulted in optimal C2C12 myoblasts haptotaxis responses to patterned netrin-1 nanodots. To study the effect of nanodot size, netrin was patterned as 200 × 200 nm^2, 400 × 400 nm^2 and 800 × 800 nm^2 dots. The migration response was found to be indifferent to the nanodot size. The NSA revealed that the myoblasts preferentially migrated onto higher netrin-1 density stripes when challenged with nanodot stripes with a threefold and greater density difference. Finally, by comparing the cell migration on NSA and stepped gradients, a response consistent with directional persistence could be identified on the stepped gradients. The NSA provides a powerful haptotaxis platform to advance the understanding of contact-mediated migration and signaling of motile cells to surface-bound protein cues.

Résumé

L’haptotaxie, une réponse de migration cellulaire a la biochimie des surfaces, est essentielle pour des processus vitaux tels que l'angiogenèse, la réparation tissulaire et le développement embryonnaire. In vitro, les processus de signalisation de l’haptotaxie sont généralement étudiés en utilisant des motifs de gradients de protéines sur des surfaces. Cependant, alors que ces gradients fournissent des distributions de cellules pour des résultats d'haptotaxie, ils ne fournissent pas facilement et clairement des informations précises sur les choix que font les cellules sujettes à des différences locales de densités de protéines sur la surface. Ici, nous introduisons le test de la bande de nanopoint (BNP) afin de (i) examiner facilement les choix de migration cellulaire à différentes densités de surface protéiques, et (ii) étudier l'effet de la taille des nanopoint de protéines sur la migration cellulaire. Chaque BNP consiste en une paire de matrice de nanopoint discret et alternant de façon discontinue entre des densités de soit 0, 1, 3, 10, 30, 44 ou 100%. La configuration du BNP présente ainsi les cellules avec un choix binaire de densités de surface faibles ou élevées couvrant toutes les combinaisons possibles. Pour étudier l'effet de la dimension des nanopoint de protéines, des nanopoint de 200 × 200 nm^2, 400 × 400 nm^2 et 800 × 800 nm^2 ont été testés. De plus, pour révéler la migration cellulaire, l'affinité de la surface cellulaire a la SR a été ajustée pour maximiser la réponse cellulaire au guidage du motif de nanopoint. Le SR a été remblayé avec un mélange de polyéthylène glycol (PEG) et de poly-D-lysine (PDL) avec une affinité faible et élevée à la surface des cellules, respectivement. Trois combinaisons de SR ont été testées; 100:0, 90:10 et 75:25 %PEG:%PDL. Le PEG 90%:10% PDL SR a résulté à des réponses optimales de l’haptotaxie des myoblastes C2C12 spécifiques aux nanopoints de netrin-1, et ont été conservés avec toutes les tailles de nanopoints. Les myoblastes ont migré préférentiellement vers les bandes de haute densité de nétrine-1 lorsque présentés avec des bandes de nanopoint avec une différence de densité de triple et plus. Par rapport aux résultats du test par gradient, les choix des cellules présentées au bande du BNP étaient exempts d’effet persistant de la migration cellulaire. Le BNP fournit une plate-forme d’haptotaxie puissante pour améliorer la compréhension de la migration et de la communication cellulaire face à des motifs de proteines sur les surfaces.

Acknowledgements

Thank you, Dr. David Juncker, for your support and guidance throughout this research project and its documentation. I acknowledge the Juncker lab members for providing a friendly and enabling environment, insightful discussions and support in general throughout my time in the lab. Special recognition is afforded to my lab mentor Mr. Grant Ongo, who provided life and scientific guidance when needed. I am thankful to Dr. Andy Ng for his help editing the attached manuscript, and to Mr. Philippe Decorwin-Martin for translating the thesis abstract to French. I am also indebted to Dr. Sebastien Ricoult and Mr. Donald MacNearney, Juncker lab alumni, for their valuable discussions with regard to my project, and their help troubleshooting at times. I would also like to extend my gratitude to the Kennedy lab at the Montreal Neurological Institute (MNI) at McGill University for the constant supply of the netrin-1 protein used in this project. I am further grateful to Dr. Timothy Kennedy who provided feedback and guided me through this research project as my informal supervisor.

I would also like to acknowledge the Biological and Biomedical Engineering (BBME) at McGill University for their financial support via international tuition fee waivers. Lastly, I want to thank the NSERC-CREATE Neuroengineering program that supported me financially and further provided interesting scientific lectures in this cross-disciplinary field.

TABLE OF CONTENTS

1. PROJECT DESCRIPTION

1.1. Motivation and synopsis

The motivation for this project is to advance the understanding of contact-mediated cell navigation responses as a result of cell interactions with surface-bound tactile guidance cues. This cell migration mode is defined as haptotaxis and is directed by the cell-surface affinity. Classically, haptotaxis has been studied using the stripe assay which tested the choice of cells seeded on stripes of proteins, allowing to evaluate the preference of cells based on their final positions on stripes.[1-4] Protein stripes are comparatively easy to generate, and traditionally have included a stripe with complete (100%) protein surface coverage and one without (0%) proteins. Hence, stripe assay results have been limited to 'on' and 'off' cues. However, instructive protein guidance cues *in vivo*, generally bound to the membrane, often produce surface density gradient distributions.[5] Therefore, physiologically relevant patterns in the form of continuous gradient arrays were designed, and provided a more natural response. However, because fluorescence imaging is not quantitative, and because protein immobilization is not proportional to solution concentration, the final concentration could be difficult to track, while only 'simple' gradients could be formed.

Our group previously introduced digital nanodot gradients (DNGs) that could be designed to represent arbitrary monotonic and non-monotonic functions using ordered and randomly positioned nanodots.[6] DNGs were made of 200 × 200 nm^2 nanodots and ranged from 0.02% to 44.44% surface coverages, which is precisely defined and quantified by tuning the density of nanodots. Whether classical or digital gradients, the overall cell migration on gradients report the global cell distributions. However, the final cell positions may not be indicative of whether cells respond to the changes of cues at different positions. Possibly, cells that responded at the lower end of the gradient and became polarized may simply continue to migrate along their established trajectory towards the higher end of the gradient due to migration directional persistence.[7] Here initial signaling events are sustained, conserving the cell's migration axis which in turn sustains actin polymerization at the current leading edge, leading to the cell migrating in a predetermined direction for some time, regardless of the cell's signal integrations from the local surface cues.[8]

Potentially, cells' directional persistence masks receptor saturation which has been shown to influence cell navigation behaviors in chemotaxis assays.[9]

Here, we introduce the nanodot stripe assay (NSA) which consists of seven stripes in total, with five nanodot stripes of 1%, 3%, 10%, 30% and 44% surface coverages, as well 0% and 100% density stripes. The NSA proposed here evaluates cell haptotaxis for each of the 21 binary stripe combinations in every experiment. This assay allows testing cell choices and haptotaxis sensitivity towards low and high overall nanodot densities, and for small and large differences in surface concentrations according to a logarithmic scale of a three-fold increase. The 44% nanodot stripe is an exception that was added as it represented the maximal nanodot density that could be fabricated. It had previously been shown that cells could not respond to protein nanodots smaller than 0.11 μm^2 (333 × 333 nm^2) in size.[10] To test this effect, we generated NSAs with 200 × 200 nm^2, 400 × 400 nm^2 and 800 × 800 nm^2 nanodots. Furthermore, haptotaxis assays are also sensitive to the area between patterned proteins, defined as the reference surface (RS), and which can dictate the ability of cells to respond to the patterned cues. Hence we tested different RS compositions with different cell-affinities made by mixing a non-affinity molecule (PEG) with a high-affinity molecule (PDL) at ratios from 75:25, 90:10 and 100:0 of %PEG:%PDL. In this research, netrin-1, a widely studied neuronal guidance cue, was used for examining and quantifying the haptotaxis response in the NSA, using C2C12 myoblast cells expressing the netrin-1 receptor, neogenin.

1.2. Project goals

The major goals for this research project are:

i. To design, fabricate and pattern nanodot stripes forming the NSA platform.
ii. To find the optimal cell-surface affinity for the reference surface (RS) most suitable for testing haptotaxis responses of C2C12 myoblast cells towards netrin-1 cues.
iii. To investigate the effect of different protein nanodot sizes on cellular haptotaxis responses and migration choices.
iv. To conduct NSA experiments and quantify cell choices.

1.3. Thesis format

This thesis is presented in a manuscript-based format. The introduction section provides the background for this work and aligns this research with existing relevant literature. The manuscript chapter is preceded by a discussion of research work that qualifies as part of this thesis but not the manuscript. Finally, the conclusion section offers a synthesis of the contributions of this research and includes ideas and suggestions for future work.

1.3.1. Contribution of authors

Mcolisi Dlamini designed the mask for the fabrication of the nanodots, performed all the experiments, extracted and analyzed the data and further prepared the attached figures. Dr. David Juncker conceived the design concept, and provided guidance during the designing process, experimentation and analysis, while supervising the entire research project. Dr. Tim Kennedy provided the netrin-1 proteins from his lab, and shared insights with regard to netrin guidance mechanisms. The thesis was prepared and written by Mcolisi Dlamini with help and supervision from Dr. David Juncker.

1.4. Declaration of novelty

This thesis introduces the Nanodot Stripe Assay (NSA), a novel platform that introduces combinatorial binary arrays of different protein coverages to easily study cell haptotaxis choices for a range of differences and average densities. This study also presents results of C2C12 myoblasts haptotaxis preferences to netrin-1 nanodot stripes.

2. INTRODUCTION

The introduction provides the background and literature review on haptotaxis. It is arranged in subsections focusing on (i) cell migration processes, (ii) haptotaxis in neuronal development, (ii) *in vitro* haptotaxis assays with regard to applied patterning techniques, results and limitations of these platforms, and finally (iv) a project rationale as a preamble to the manuscript chapter.

2.1. Cell migration theory and applications

2.1.1. Cell migration mechanism

Cellular migration in response to surface-bound biochemical cues is essential for life processes such as angiogenesis, homeostasis, and embryogenesis.[11] Endothelial cells, for example, have a vital function in embryonic vasculogenesis, angiogenesis and wound healing.[12] Among other factors, extracellular biochemical cues present in the cell's microenvironment dictate the direction pursued by motile cells. In cellular navigation, cells interact with and encode extracellular signals (convert to matching intracellular messages) from cues presented as gradients leading to a chemoattraction or chemorepulsion response. A higher signal on the leading edge of a cell can establish the cell's migration polarity, resulting in the cell having a front–rear axis.[13] Cell polarity triggers rapid actin polymerization, *i.e.* actin filament growth, causing the formation of a cell membrane protrusion at the leading edge (assuming the signal is a chemoattractant (Figure 1), otherwise repulsive signals trigger actin de-polymerization). The cell's transmembrane receptors on the protruded leading edge bind to cell adhesion molecules (CAMs) mainly integrins to link the cell to the underlying substratum. These receptor-ligand junctions establish contact points between the cell and the substrate, leading to the formation of macromolecular protein complexes called focal adhesions.[10,14,15] This receptor-ligand bond produces molecular clutches at the leading edge required to transmit the cell's internally generated forces to the substrate. Myosin motors collaborate with actin filaments to produce a contractile force that facilitates the shift of the bulk of the cell in the direction of motion. Translocation of the cell's bulk is modulated by actin retrograde flow where actin filaments move in the opposite direction to generate an opposite internal counter force (within the cell) to help propel the cell forward.[16,17] At the trailing edge, the cell detaches from the surface to allow for a forward motion of the cell. Detachment of adhesion

contacts is facilitated by actin depolymerization-promoting proteins like cofilin, and calpain, a proteolytic cleavage protein.

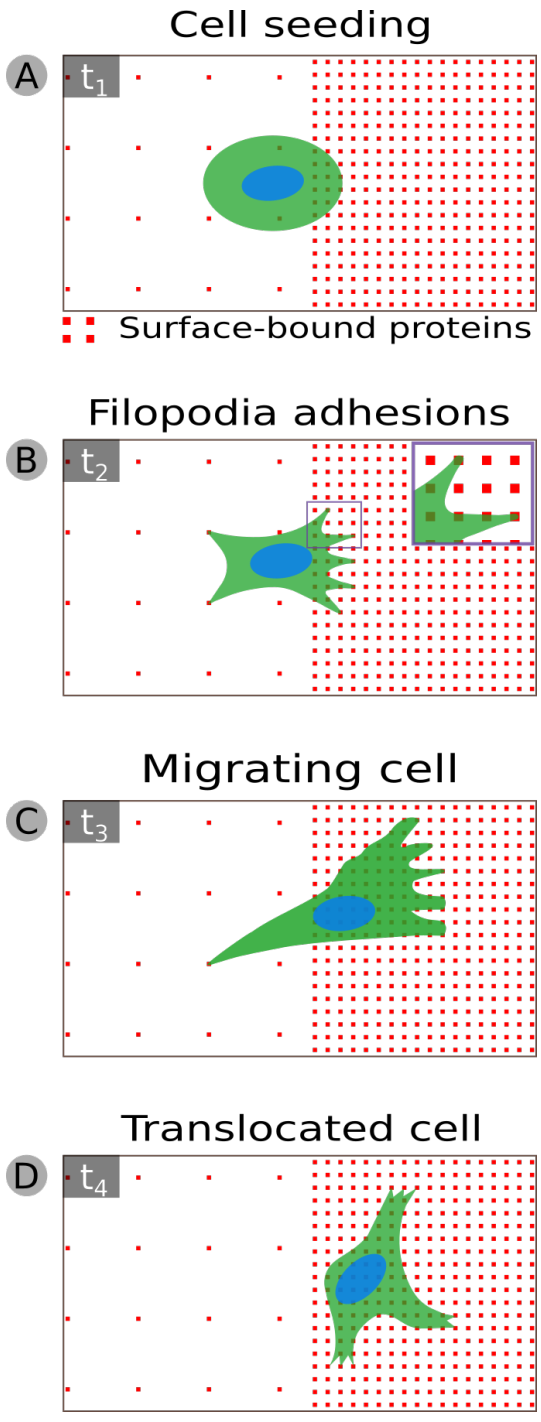

Figure 1: Cell migration on digital patterns of surface-bound proteins with two distinct densities. **A)** A cell being seeded onto a substrate with surface-attached proteins at different surface concentrations. **B)** Once on the surface, the cell scans its environment using membrane extensions called filopodia. Cell adhesion molecules on the filopodia bind to protein ligands leading to the formation of focal adhesions (see insert). More contact points are formed on the high density side (on the right) establishing the cells migration polarity, the right being the cell's front or leading edge. **C)** The membrane on the leading edge protrudes due to actin polymerization and adheres onto protein ligands farther on the right. Myosin-mediated contractile forces drive the movement of the bulk of the cell towards the right. Eventually, contact points at the trailing edge are disassembled. **D)** The cell migrated in the direction of a higher protein cue. Notice that the cell continuously scans its micro-environment for migratory signals.

(Not drawn to scale)

2.1.2. Haptotaxis – an overview

Soluble cues and chemotaxis: Biochemical gradients orchestrate directed cell migration either as: (i) soluble protein gradients or (ii) surface-bound protein gradients. Soluble gradients, also referred to as diffusible gradients, are generated *in vivo,* when proteins diffuse away from their source into the extracellular fluids. Following diffusion principles, the spatial protein concentration decreases farther from the protein excretion source. Polarized cell migration in response to such soluble gradients is defined as chemotaxis,[18] and facilitates metastatic tumor cell migration *in vivo*.[19] Chemotaxis is notably responsible for directing neutrophils to injury sites and sites of infection where they neutralize pathogens.[20]

Surface-bound cues and haptotaxis: Contrary to soluble gradients, surface-bound gradients result from proteins attaching to the substratum at varying surface concentrations (*i.e.* density). *In vivo* surface-attached protein gradients develop when protein molecules diffuse from their source and bind onto the membrane or onto any surface in the intercellular space. The eventual surface concentration will be higher closer to the protein source. Examples of surface-anchored cues include extracellular matrix (ECM) proteins like fibronectin, collagen, elastin and laminin; and neuronal guidance cues like ephrins, semaphorins, slits and netrins. Cell migration in response to these cues immobilized onto the substratum is defined as haptotaxis. Neuronal guidance cues orient growing neurites towards their desired synaptic targets during embryogenesis via haptotaxis.[21] Mesenchymal stem cells and dermal fibroblasts navigate on gradients of surface-bound ECM proteins at the interface of healthy and fibrotic tissues via haptotaxis en-route to wounded tissues.[22]

Haptotaxis and chemotaxis are differentiated by the type of gradient they respond to, and are facilitated by different molecular domains.[23] Haptotaxis was coined in 1965 by S. B. Carter, "conveying the idea that the movement of a cell is controlled by the relative strength of its peripheral adhesions".[24] Carter patterned the surface with palladium and observed that fibroblast cells preferentially migrated up the concentration gradient. Carter argued that haptotaxis was analogous to cell migration and mechanisms like chemotaxis were a subset of this supreme migration process.[25] He was corrected in 1979 by Keller *et al.* in an article entitled 'Chemotaxis is not a special case of haptotaxis'[26] where Keller showed that adhesion gradients alone do not induce

morphological changes on neutrophils, but soluble gradients do. Therefore, the two migration modes trigger unique cellular signaling pathways. Function blocking experiments further showed that inhibiting haptotaxis-responsible domains has no effect on chemotactic responses.[23] Haptotaxis and chemotaxis are now accepted as two different cell migration processes. However, it's imperative to note that many cells are capable of both chemotaxis and haptotaxis.

Predominately, the navigation directional compass for a cell is dependent on chemical and mechanical stimuli encoded from its microenvironment. Additionally, mechanical gradients at the cell-substrate interface are also capable of inducing durotaxis – directed cell migration in response to the surface's stiffness.[27-29] Environmental stimuli and their cellular integration capacity determine whether cells migrate or not. In some instances, biochemical signals in the cellular microenvironment even determine cell fate by inducing apoptosis.[30] Remarkable research progress has been made on the molecular mechanisms and signaling pathways involved in cell navigation, but important open questions remain for processes like adhesion, cell retraction and polymerization.[16] As with most biological systems, some of the biomolecules involved in cell migration pathways may be redundant, making it hard to elucidate their specific functions and specific contributions to cell migration processes.

2.1.3. Netrin-1 guidance in neuronal development

Netrins are neuronal guidance cues and members of the laminin superfamily.[31] There are six of these secreted proteins in mammals, namely netrin 1 – 4 and netrin G1 – G2. Netrin-1 has about 600 amino acids and a molecular weight of 75 kDa. Netrin-1 is a bifunctional cue, where cellular responses are dictated by receptors expressed by neurites. For example, spinal commissural neurons express deleted in colorectal carcinoma (DCC) receptors, which lead to chemoattraction, while trochlear neurons express uncoordinated-5 (UNC-5) receptors, which result in chemo-repulsion towards netrin-1.[31,32] DCC and UNC-5, both transmembrane proteins of the immunoglobulin superfamily, are the major receptors, but not the only ones. Cellular studies performed in our research project utilized C2C12 cells, a mouse muscle myoblast cell line expressing the DCC paralogue neogenin,[33,34] which results in chemoattractive responses towards netrin-1.

Substrate-bound guidance cues help direct axonal outgrowth during embryogenesis via haptotaxis.[21] During neuronal development, growth cones (axon tips) decipher and integrate signals from several guidance cues to orient axons towards the correct synaptic targets. Axon pathfinding is critical for neural circuit wiring during development as incorrect wiring of the nervous system has disastrous effects on the health and overall well-being of organisms.[35] The growth cone's lamellipodia and filopodia, the latter being spike-like projections at the edge of the growth cone, act as sensors that probe the micro-environment to establish a surface concentration gradient initiating contact-mediated responses. Neuronal guidance cues like netrins, slits, ephrins and semaphorins, together with morphogens and growth factors like nerve growth factor (NGF), dictate the polarity of growth cones leading to their outgrowth or collapse. When growth cones encounter attractive cues, focal adhesions form at the filopodia, leading to actin polymerization and retrograde flow, and eventually axon migration.

An example of haptotaxis is the guidance of spinal commissural neurons towards the ventral midline by a gradient of netrin-1 that is bound onto the neural tube.[36] Commissural neurons are pushed out of the roof plate (RP) by repellent guidance cues like the dorsally secreted bone morphogenic proteins (BMPs) and draxin, and are synergistically attracted to the floor plate (FP) by netrin-1 and sonic hedgehog (Shh) gradients.[5,37,38] Figure 2 below shows the graded distribution of netrin-1 *in vivo* from immunoreactivity fluorescent stains. Notice the netrin-1 gradient, with an increasing surface concentration towards the FP. A schematic from Sloan *et al.* shows a low and high fractional change density zone for netrin-1 and Shh. The different fractional changes influence axonal turning at different degrees while netrin-1 and Shh both attract developing commissural neurons towards the FP.[5]

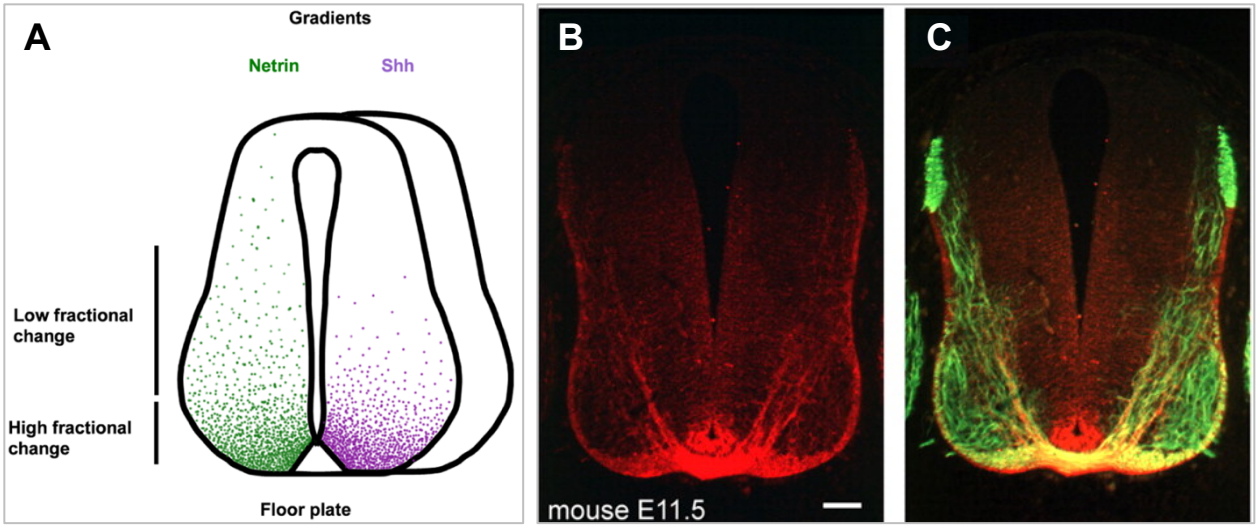

Figure 2: The distribution of the neuronal guidance cue, netrin-1. **A)** A schematic representation of the distribution of netrin-1 and sonic hedgehog (Shh) *in vivo* showing an increasing netrin-1 density adjacent to the floor plate (FP). **B)** Distribution of netrin-1 (red) in the developing mouse spinal cord visualized from tissue slices using immunoreactivity, *i.e.*, using netrin specific fluorescently-tagged antibodies. **C)** Neurofilaments (green) tracking in the direction of increasing netrin-1. At this stage, most of the commissural neurons have crossed the ventral midline. [A) is reprinted from PLOS BIOLOGY (Sloan *et al.* (2015)[5] under the Creative Commons Attribution License. B) and C) are reprinted with permission from The Journal of Neuroscience (Kennedy *et al.* (2006)[36]].

Netrin-1 guidance is a topic of intense research and open debate. Recently, Dominici *et al.* challenged the classical netrin-1 guidance model in the spinal cord.[39] The Nature manuscript makes three claims that challenge and contradict previous understanding: (1) FP-derived netrin-1 is dispensable for spinal commissural axon guidance, contrary to the belief that netrin-1 from the FP is key in orienting commissures to the ventral midline. (2) Netrin-1 from the ventricular zone (VZ) is responsible for commissural axons guidance. (3) Netrin-1 is a short-range cue, which is contradictory to previous knowledge. To validate these claims, the authors inhibited netrin-1 secretion by the floor plate cells in knockout mice and observed that commissural neurons develop normally. Varadarajan *et al.* independently reported in the Neuron journal similar claims, adding that commissural guidance is due to the netrin-1 produced by neural progenitors and deposited on the pial surface not the FP-derived netrin-1.[40] A critical review of the netrin-1 mediated axonal

guidance quickly followed these two publications.[41] This review highlights that these papers are not the first to claim that the absence of floor plate derived netrin-1 prevents commissural neurons from reaching the floor plate. Charron and Tessier Lavigne previously showed that in the absence of netrin-1, sonic hedgehog (Shh) is sufficient to direct the commissures.[42] Morales, in a another minireview states that "floor plate attractants are there as a redundant, or, more exactly as a degenerate system" that successfully attracts commissural axons.[43] An interesting question posed here is why commissural axons stop following netrin-1 on the pial surface and turn towards the floor plate in the FP netrin-1 null subjects. Ducuing *et al*. also recently reviewed a handful of repulsive guidance cues guiding commissural axons on the neural tube, highlighting the complexity of the environment navigated by commissural axons during the pathfinding process, and the ongoing discussion about various mechanisms at play.[38]

The argument in support of the netrin-1 classical guidance model is outside the scope of this thesis. Hopefully, novel and optimized immunohistochemistry protocols for netrin-1 in neural tissues[44] will elucidate more information and enhance our understanding of netrin-1 in axon pathfinding. Unchallenged in the recent publications, is that netrin-1 attracts spinal commissural neurons via haptotaxis as previously verified by Moore *et al.*[45]

2.2. Haptotaxis assays

A review of stripes and gradient assays is provided along with the different techniques used to generate these surface patterns. To better understand the protein patterning techniques discussed below, we will first introduce microfabrication and prototyping processes.

2.2.1. Relevant microfabrication processes

Soft lithography is the standard technique to replicate micro- and nano(fluidic) devices. Once silicon (Si) master molds have been developed using microfabrication processes in cleanroom facilities, soft lithography provides a simple, rapid and affordable prototyping method to replicate the master mold features to make useable micro(fluidic) devices. Soft lithography uses 'soft' elastomeric stamps typically made of poly(dimethylsiloxane) (PDMS) capable of replicating

features up to a resolution of 30 nm.[46] PDMS prepolymers constitute an elastomer base (Sylgard 184) and a curing agent which is a platinum based catalyst, both in liquid form.[47] Upon mixing at 10:1 (w/w), these polymers are poured onto master molds and crosslink via hydrosilylation reaction, forming solid 'rubber-like' elastomers at temperatures in the 60°C to 80°C range.[9] PDMS stamps are then cut and peeled from the cured PDMS resins. This procedure is termed cast molding. For flow microfluidic assays, the PDMS replicas are bonded onto glass slides to create enclosed microchannels. PDMS molds are inexpensive, elastic, chemically inert, easy to peel from master molds, provide excellent sealing properties and are optically clear, making them user friendly and versatile.[48] Applications of soft lithography include microcontact printing (μCP), microtransfer molding (μTM), micromolding in capillarics (MIMIC), and solvent-assisted micromolding (SAMIM).[46,49] Soft lithography has been used to pattern biomolecules and cells for approximately two decades now.[50,51]

Feature micromachining processes utilizing Si wafers can be classified into three categories, namely, (1) patterning (photolithography), (2) subtractive processes (etching) and, (3) additive processes (thin film deposition, oxidation and wafer bonding). This section will review the first two processes, which are most relevant to molds employed in generating surface-bound protein patterns.

Photolithography: The process of making a Si mold commences with sketching the desired patterns in a 2D drawing using layout editors like L-Edit or CleWin. The 2D patterns are then copied onto a chrome or transparent mask. A mask aligner in the cleanroom is used to position the mask directly on top of a Si wafer spin-coated with a photoresist layer. Ultraviolet (UV) light emitted through the mask cures the photoresist. The wafer is then developed – submerged in a solvent that selectively dissolves the cured (or uncured) resist. Two kinds of photoresists are used: negative and positive photoresists. UV-exposed areas dissolve in the developer solvent when positive photoresists are used, and the opposite occurs for negative photoresists. SU-8 is an epoxy-based negative photoresist widely used for patterning micron-sized features.[48] After development, the features of interest remain intact on the Si wafer as raised ridges or posts. To complete the microfabrication process, the wafer undergoes a flood UV exposure step followed by hard baking at elevated temperatures. At this point, the silicon mold is ready for soft lithography. To prevent

PDMS sticking onto Si wafer surfaces, the wafer is silanized with trichlorosilane via vapor deposition prior to soft lithography prototyping.

Electron Beam Lithography (EBL): The resolution threshold of photolithography is the diffraction limit of light, therefore, electron beam (e-beam) lithography (EBL) is an alternative for fabricating high resolution nano-sized features. EBL is capable of producing sub-10 nm features with a 30 nm pitch.[52,53] The highest resolution to date, resulting from the use of aberration-corrected scanning transmission electron microscopes, is 2 nm with a 5 nm half-pitch.[54] Similar to photolithography, patterns are sketched on 2D layout editors in preparation for the nanofabrication process. The Si wafer is coated with a thin layer of photoresist via spin coating. EBL uses both negative and positive photoresists as well. The extensively used resist is polymethylmethacrylate (PMMA), a positive photoresist. EBL is a maskless lithography technique, drawing its basis from the scanning electron microscopes technology, where a beam of electrons raster scans and directly writes (exposes) the desired patterns pixel per pixel onto the photoresist.[55] After development, the e-beam-exposed areas dissolve exposing the Si wafer in positive photoresists like PMMA. The wafer is then submerged in an etching solution for a specified time dictated by the etch rate and desired depth. The etchant diffuses into the wafer surface, reacts and corrodes the exposed Si, leading to nanoholes on the wafer. The remaining photoresist on the wafer surface acts as an etch mask, protecting the Si layer from the reactive species of the etchant. Photolithography can also be used to create the etch mask. There are three kinds of etchants: wet, dry and plasma etchants, and work in isotropic and anisotropic etch modes. Anisotropic etchants are generally preferred as they result in edges with vertical walls. Dissolving Si as a micromachining technique is termed reactive ion etching (RIE), and a subtractive lithography process.[56] For features requiring micron-sized depths, deep reactive ion etching (DRIE) is applied. To complete the nanofabrication process, the etch mask is stripped away once etching is complete. In our study, the final Si mold was then silanized and replicated via soft lithography.

Recent mold fabrication techniques have been developed to enable mold fabrication without the need for the cleanroom facility, as it is an expensive facility to assemble and involves high operation costs. Alternative techniques include 3D printing[57], cutting plotters (xurography)[58], thermal scribing[59] and micromilling[60] to mention a few. Unfortunately, the resolution of these rapid

prototyping techniques is yet to exceed the submicron threshold. Therefore, cleanroom fabrication processes still dominates for features requiring high resolutions and high aspect ratios like the digital nanodot gradients (DNGs).[61]

2.2.2. Classical stripe assays

Different protein patterns have been used in haptotaxis assays to facilitate the understanding of cellular and neuronal tactile signal integration of surface-bound guidance cues. Stripe assays have been widely used due to the ease in pattern generation. The three dominant stripe patterning techniques are discussed below.

2.2.3. Techniques to engineer classical protein stripes

Microfluidic networks (µFN), are self-filling devices where microchannels localize small volumes of aqueous solutions over substrates, and are primarily used to generate protein patterns for bioassays.[62] This patterning technique results in active placement of bioactive proteins using PDMS conduits to spatially localize protein solutions on a substrate. Delamarche *et al.* used µFNs to pattern immunoglobulin-G (IgG) onto Au, glass and Si-SiO_2 surfaces using chemical coupling of amino groups on proteins to hydroxylsuccinimidyl esters on the three different substrates.[63] Chemical reactions or electrostatic interactions results in protein immobilization on these confined areas producing the desired protein patterns thereafter. The µFN patterning process is summarized in figure 3 below. Briefly, a PDMS replica with channels is brought into conformal contact with a flat substrate, creating closed capillary channels. The microchannels have to be hydrophilic to enable the flow of the liquid from the inlet into the channels via capillary forces. As such, the PDMS was plasma-treated to make it hydrophilic. However, this results in protein adsorptions onto the walls of the PDMS and not only on the intended substrate. As such, Papra *et el.* fabricated µFNs using Si, Au and PDMS coated with polyethylene glycol to prevent protein attachment onto µFN walls, and successfully patterned proteins onto PDMS substrates.[62]

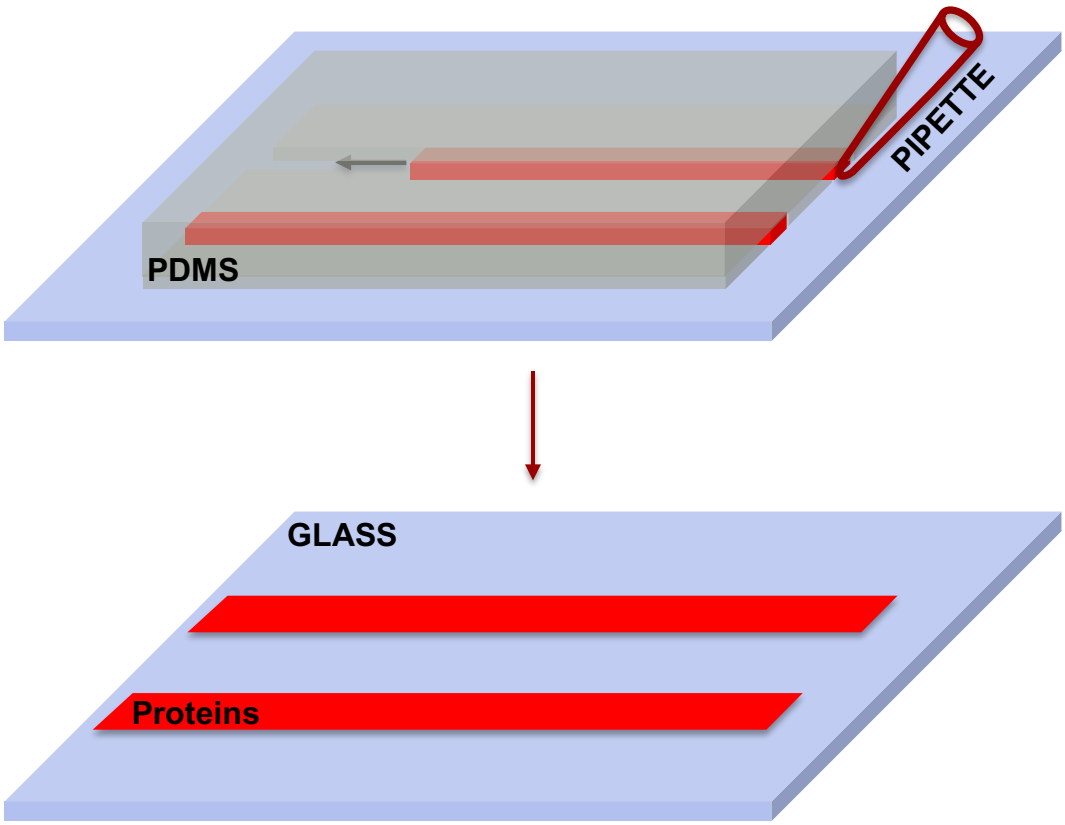

Figure 3: Printing using microfluidic networks (μFNs). A hydrophilic PDMS stamp with channels is placed on a functionalized glass slide. An aqueous solution with the proteins of interest is pipetted into the channels where filling is driven by capillary forces. After incubating for a few minutes, the PDMS and glass slide are separated living protein stripes on the glass substrate.

Microcontact printing (μCP), was developed at the Whitesides lab in 1993 to pattern thiols for bio-sensing applications.[64] μCP was later altered to generate surface patterns of proteins and antibodies,[65-67] and subsequently utilized to spatially pattern guidance cues for neuronal migration studies.[3,68] The μCP technique (figure 4) uses a soft elastomeric stamp, usually a hydrophobic PDMS stamp, with relief features to print protein patterns onto substrates. First, the stamp is incubated with a protein solution. During incubation, proteins adsorb onto the stamp forming a quasi-monolayer under saturating conditions. The inked stamp is then rinsed and briefly dried under a stream of nitrogen, and quickly brought into contact with a plasma-treated glass slide. Proteins on the relief features, in contact with the substrate, are transferred to the glass, while proteins in the recesses remain on the stamp. Proteins physisorbed on the PDMS stamp are

transferred onto the glass substrate due to the high surface energy of the hydrophilic glass, that is, from low free energy PDMS to the high free energy surface (on the glass).[67,69] The soft elastomeric stamp is essential as it allows for conformal contact of the stamp and the rigid glass substrate. When appropriate printing protocols are followed, the transfer efficiency can exceed 99%, producing biologically active proteins on the substrates.[1,67]

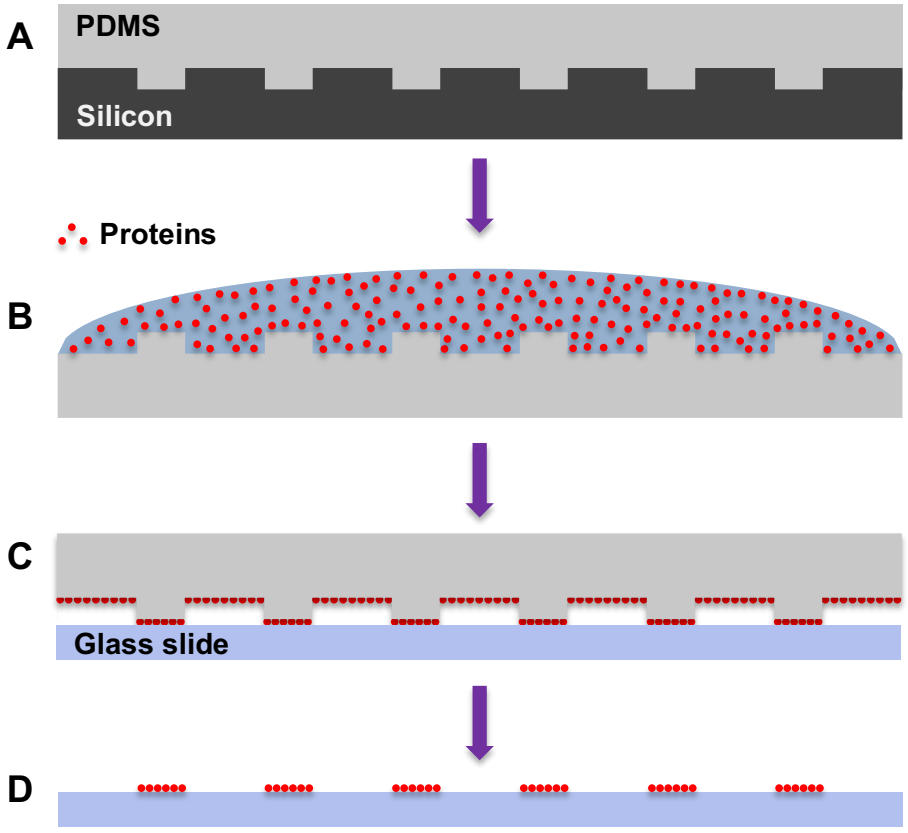

Figure 4: Microcontact printing (μCP) casting method. **A)** A PDMS stamp is replicated from a silicon mold. **B)** Proteins are incubated on the PDMS stamp, and physio-adsorb onto the hydrophobic PDMS surface. The stamp is rinsed and briefly dried, leaving a monolayer of proteins on the stamp surface. **C)** The inked stamp is then brought into contact with a hydrophilic glass substrate, and (**D)** proteins on relief features are transferred onto the glass substrate.

Membrane filters were among the early adopted protein surface patterning techniques used – where proteins were sucked through a filter or porous membrane onto a substrate (figure 5f). The filter acted as a physical mask and protein carpets were patterned in between the mask.[4] Reported

protein carpets with 100 μm widths were utilized in stripe assays to study axonal guidance.[2] Patterning using silicon matrices instead of the membrane mask – which gave the assay its name: membrane stripe assay – was first described by Bonhoeffer and colleagues in 1987.[70] This modified stripe assay generates stripes of two alternating cues presenting axons with a binary choice to study differential cellular responses. Later a silicone matrix, PDMS with parallel microchannels was used to pattern the first protein.[4,71] Once the PDMS and substrate are separated, the second protein (in solution) is added and adheres onto areas not blocked by the first protein. Recently, a receptor/ligand stripe assay has been introduced as a follow up to the membrane stripe assay. The receptor/ligand stripe assay combines microcontact printing to pattern the first protein and microfluidic networks to pattern the second protein, by flowing the second protein in the channels of the PDMS stamp while it is in contact with the substrate being patterned.[72]

Stripe assays essentially challenge cells with patterned and non-patterned areas. An alternate coating is also possible (for all patterning methods discussed above), that is, coating the area between the stripes. This can be achieved in two ways. 1) By patterning stripes on glass substrates already functionalized with proteins like polylysine (PLL). In this case, PLL will act as the secondary stripe. 2) Alternatively, once stripes have been patterned onto the substrates, the second protein is added and incubated onto the substrate, only adhering to protein-free areas.

The Kania lab used stripe assays to demonstrate that (i) netrin-1 repels and attracts specific motor column axons depending on the netrin receptors expressed by these neuron subsets, and that (ii) motor axons are synergistically guided by attractive netrin and repulsive ephrin cues.[2] These stripes were printed using microfluidic networks. Yamagishi *et al.* used the stripe assay, printed using silicon matrices, to show that the ectodomain of fibronectin and leucine-rich transmembrane protein-2 has strong aversion for hippocampal neurons.[73] Previously, our group used stripe assays to observe the haptotaxis behavior of Rat2 fibroblasts, C2C12 myoblasts and commissural neurons towards fibronectin, polylysine and netrin-1 protein cues.[1] Stripe patterns of 10 μm width and a pitch of 100 μm were generated on glass substrates using microcontact printing.

Stripes are comparatively easy to generate and provide cell migration results relatively fast. However, stripe assays result in protein distributions of either 0% or 100% protein coverages, which present only one aspect of *in vivo* protein distributions. As such, haptotaxis results from stripe assays are limited to 'on' and 'off' stripes, where cells choose to migrate onto proteins on the stripes or avoid the proteins in the case of repulsive cues. Though informative, classical stripe assays do not challenge cells with different protein densities, that are between 0% and 100% coverages, leaving a gap regarding cell choices in this range.

2.2.4. Methods for generating surface-bound protein gradients

To circumvent the limitations of stripe assays, *in vitro* protein gradient assays have been developed to produce protein distributions that are more physiologically relevant. Protein immobilization techniques for patterning gradient arrays were developed with different advantages, limitations and feature resolutions.

Hydrogel stamp diffusion is one of the techniques used to modulate the surface distribution of proteins (figure 5c). Here embedded channels in a hydrogel are filled with a protein solution, and the proteins diffuse through the gel and adsorb onto the substrate, at a decreasing concentration from the source (the channels). Hydrogel stamps are replicated from silicon molds fabricated via standard lithography processes. Mai *et al.* utilized this technique using an agarose stamp to pattern netrin-1 and brain-derived neurotrophic factor (BDNF) gradients onto glass substrates.[74] The stamp was bonded to a polylysine coated glass slide resulting in 350 × 100 µm channels with a channel-to-channel gap of 4 mm. The protein solution was pipetted into the resulting channels, and proteins diffused through the hydrogel and adhered onto the spacing between the channels. As this process is fully governed by diffusion, the expected surface gradient profile can be simulated. Obviously, proteins also adhere onto the glass they are in direct contact with (in the channels), saturating the surface. The process is highly dependent on the gel and protein properties limiting the usability of the method.

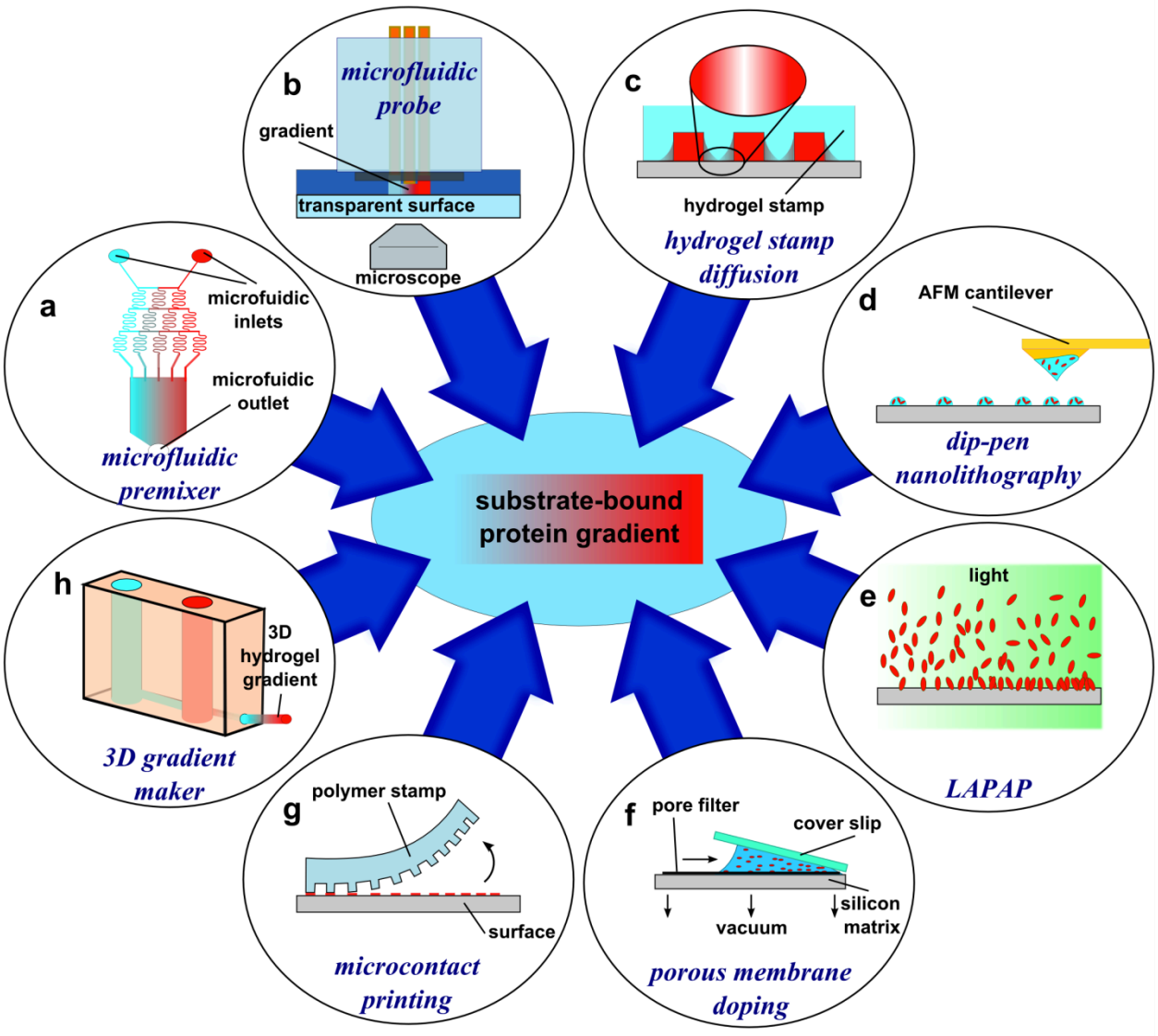

Figure 5: Graphical representation of eight different methods used to generate *in vitro* surface-bound protein patterns, using **(a)** microfluidic gradient generator, **(b)** microfluidic probes, **(c)** diffusion in hydrogel stamps, **(d)** dip-pen nanolithography, **(e)** laser-assisted protein patterning via photobleaching (LAPAP), **(f)** porous membrane filter, **(g)** microcontact printing and a **(h)** 3D hydrogel maker. [Reprinted with permission from McGill University (Ricoult *et al.* (2014)[75]]

3D protein gradients provide *in vitro* assays closely resembling complex 3D systems in living organisms. Cells in 3D scaffolds were confirmed to be more physiologically relevant than those of 2D cell cultures.[76] A **3D hydrogel gradient maker** is made of two interconnected vertical chambers, namely, a stock and mixing chamber.[77] The stock chamber and mixing chamber

contains solution 1 and solution 2 respectively. As solution 2 from the mixing chamber is drawn out, solution 1 continuously replenishes the mixing chamber. The solution in the mixing chamber is mixed using a magnetic stirring bar. The outflowing liquid stream is dominated by solution 2 at first and gradually becomes saturated by solution 1 as more of solution 1 is mixed into the mixing chamber solution, as shown in figure 5h with the blue and red solutions. The mold chamber, into which the affluent is drawn, is then UV cured to conserve the established gradient. Cubes of the mold are then cut and introduced into well-plates. Cells are then added into the wells with the cubes for cell migration assays. The concept was demonstrated with 20% poly(ethylene glycol) dimethacrylate (PEGDM) and 5% PEGDM solutions as solutions 1 and 2 respectively. Irgacure 2959 was added as the photoinitiator. Though the 3D gradient maker concept is practical, 3D cell migration assays are limited by the complexity of tracking cells in this 3D architecture.[76] Additionally, the poor optical properties of the hydrogels also hinder the usage of this technique.

Gradient generators (figure 5a) are widely used in chemotaxis, but can also be used in haptotaxis to generate surface-bound protein gradients. A gradient generator comprises of a microfluidic premixer, called a serial dilutor, that mixes two or more solutions using a series of split and mix steps until a graded protein gradient is formed in solution.[78] The concentration across the final solution is location dependent, that is, the protein concentration increases from one edge of the microfluidic channel to the other. The proteins from this final solution adsorb onto the surface while conserving the protein concentration distribution in the solution. This creates a continuous gradient of surface-bound proteins across the surface. Sloan *et al.* utilized a linear gradient generator with a wider gradient chamber, named *le Massif*, to pattern gradients of netrin-1 and sonic hedgehog (Shh) for axonal pathfinding experiments.[5] The gradient generator was adjusted to create surface densities with a low fractional change claimed to be closer to the minimum value of shallow gradients that can elicit an axonal response to guidance cues.

The **inkjet bio-printing** method is another widely used technique to engineer spatial protein patterns, generally for microarrays. It is a simple non-contact technique where ink droplets are ejected at a specific location onto a surface via a nozzle. The nozzle size and droplet volumes directly dictate the size of the printed spots, therefore smaller nozzle diameters and droplet volumes yield high resolution prints. Currently, the smallest droplets are 10–20 picoliters and

nozzle diameters are 20–30 microns, resulting in printing resolutions of ~60 μm.[79] At the moment, the technique is not suitable for generating nano-features yet.

A **microfluidic probe** (MFP) (figure 5b) is a microfluidic platform that creates a local reaction microchamber using wall-less hydrodynamic flow confinement (HFC).[80-82] MFPs exploit the principles of both microfluidics and scanning probes, and as such, can cover large surface areas. The MFP has a flat tip with two apertures, an injection and aspiration aperture. Proteins to be patterned are added in the injection micro-stream whose size is controlled by the flow rates, and leakage to the surrounding area is prevented by the HFC. Similar to inkjet printing, MFP writes protein spots onto surfaces where proteins in the injection micro-stream adsorb onto the substrate underneath. The MFP is mobile, and can be interfaced with an automated (microscope) stage for better spatial control and tip positioning, hence the ability to generate complex surface density gradients.[80] Juncker *et al.* further demonstrated that the MFP can pattern two proteins on the same substrate, a feat difficult to achieve with standard patterning methods.[81] Drawbacks for MFPs are the need of trained personnel to operate the platform and expensive equipment. MFPs also suffer from air bubbles that interfere with streams and the quality of the printed spots.[83]

Laser-assisted protein adsorption by photobleaching (LAPAP) (figure 5e) is a versatile technique developed by Costantino and colleagues in 2008.[84-86] Here fluorescein conjugated to biotin is photobleached using a laser, making it react with a BSA passivated substrate. Biomolecules are then grafted onto the biotin via biotin-streptavidin chemistries. The resolution depends on the laser-diffraction limit, and submicron features can be generated. LAPAP uses readily available lab reagents and equipment, making it easy to adopt the system. Additionally, LAPAP is capable of generating complex patterns and anchoring multiple proteins onto the substrate. LAPAPs major drawback is that the chemistries applied to bind proteins to the surface do not work for all proteins.

Dip-pen nanolithography (DPN), (figure 5d) is a scanning probe lithography that employs (atomic force microscopy) AFM techniques to generate the surface nanopatterns. The AFM tip deposits bioink onto the final substrate with a resolution of up to 50 nm for biomolecules.[87]

Massive tip parallelization modules as high as 55000 cantilevers were designed to account for the technique's low throughput but these are generally not practical for lab use. The resolution of DPN is impressive but the use of DPNs remains relatively low, probably due to the need for specialized cantilevers and the technique's low throughput.

2.2.5. Nano-contact printing for patterning biomolecules

The standard microcontact printing (μCP) technique described previously, also known as the casting method, is not ideal to pattern nanometer-sized features, primarily due to the mechanical properties of the elastomeric PDMS stamps. PDMS is ideal for patterning rigid substrates as its softness allows for conformal contact with rigid substrates requiring only light pressures to establish contact. However, the PDMS' low mechanical stability results in lateral collapse or sagging when printing sparse features, or buckling of features with high aspect ratios (Figure 6).[88] As a result, it is not possible to faithfully print small and/or sparse features with conventional PDMS stamps because the collapsing features will result in undesired protein transfer between the features. The **Lift-off microcontact printing**, an alternative to the casting method, circumvents these soft PDMS-related issues and enables sub-micron features to be efficiently patterned, with a resolution exceeding 100 nm. Herein, the terms lift-off microcontact printing and nanocontact printing will be used interchangeably from here onwards.

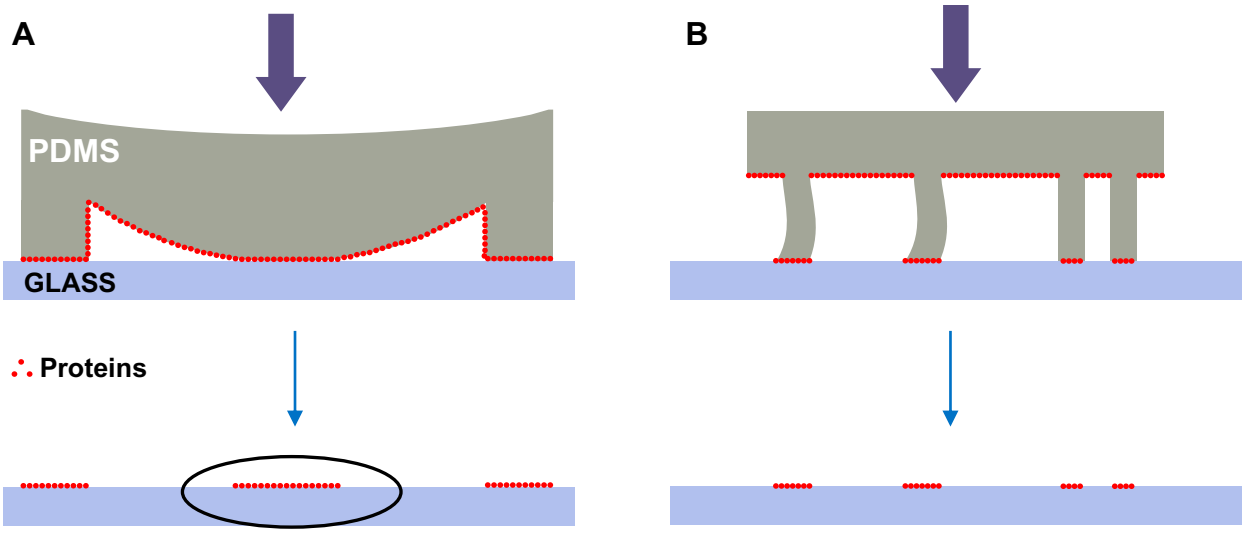

Figure 6: PDMS stamp deformation reduces pattern fidelity. **A)** Sagging of PDMS stamps during the stamping step in microcontact printing leads to patterning proteins in between PDMS relief features (marked with black circle). **B)** Buckling of PDMS posts results in protein patterns that are much longer than the desired widths.

Nanocontact printing offers more flexibility with regard to feature geometry and aspect ratio as features are only defined on the rigid mold. In this approach, a flat PDMS stamp is inked and briefly dried, leaving a monolayer of proteins on the PDMS surface. A rigid silicon (Si) mold with features of interest defined as holes or trenches, referred to as a 'nanotemplate' by Coyer *et al.*,[66] is then used to lift-off the inverse of the desired pattern from the inked stamp. The desired pattern, left on the PDMS stamp, is then transferred onto the final substrate by conformal contact of the stamp with the substrate. The Delamarche group first demonstrated protein patterning with flat PDMS stamps by patterning five micron wide immunoglobulin-G (IgG) stripes onto glass.[89] Here the PDMS stamp was inked using silicon microfluidic networks, before transferring the stripes onto the hydrophilic glass substrate. The same group was also the first to pattern sub-100 nm features (~90 nm) using the lift-off microcontact printing technique.[66] The lift-off technique required no surface chemistries to bind proteins to substrates and was completed in 32 min – showcasing its ease and effectiveness. Using Si nanotemplates rendered the technique quite expensive and fragile. Molds were re-used, for a limited number of times, after a thorough cleaning process with oxygen plasma, which is also an expensive equipment to own and utilize.

Owing to these limitations, our lab developed a cheaper alternative resulting in a modified protocol called the double-mold replication lift-off nanocontact printing.[61] This replication and printing procedure is summarized in figure 7 below where the technique was used to generate a gradient pattern from 200 × 200 nm^2 nanodots. Briefly, an inverse of the Si mold replica is replicated onto a PDMS (polydimethylsiloxane) mold. The PDMS mold is then used as the master mold for patterning a UV-curable polymer, NOA-63 (Norland Optical Adhesive), producing an identical replica to the original Si mold. Hydrophilic NOA stamps are used for the protein lift-off step (figure 7H) instead of the master Si molds. To print proteins, a flat PDMS stamp is inked with the protein solution and incubated for a few minutes (5 – 10 min), and then briefly dried leaving a protein monolayer on the surface. The PDMS stamp is then brought into contact with a plasma-activated NOA stamp which subtracts the unwanted protein pattern from the PDMS stamp, leaving the patterns of interest which are then transferred onto a plasma-activated glass by contacting the glass. In this approach, a single PDMS replication from the fragile Si mold leads to an intermediary PDMS mold that can be used multiple times to make hundreds of NOA stamps, thereby prolonging the Si wafer's lifetime and offsetting manufacturing costs significantly.

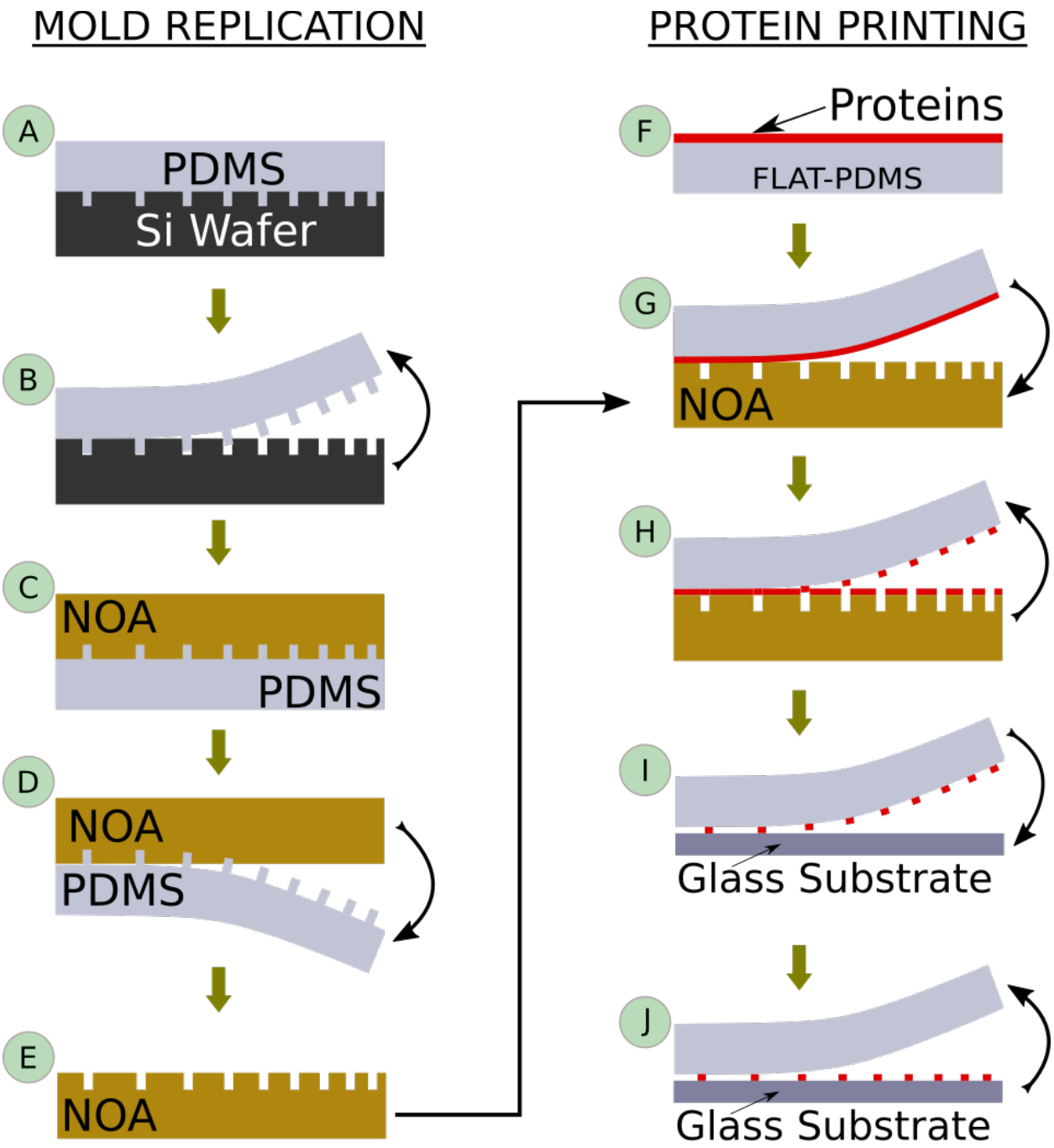

Figure 7: Schematics of the double mold replication and lift-off nanocontact printing protocol. Patterns are first etched onto a silicon wafer, then replicated onto a PDMS master mold **(A – B)**. A UV-curable NOA stamp is made from the PDMS mold **(C – E)**. To print the protein, a flat PDMS stamp is inked with the protein solution **(F)** and the inverse of the desired patterns are lifted off using the plasma-treated NOA stamp **(G – H)**. The remaining pattern is transferred onto the plasma-treated glass substrate **(I – J)**. [Adapted from figure 2 of Ricoult *et al.* (2013)[61]]

2.2.6. Continuous, graded and digital *in vitro* gradient assays

Gradients can be classified into two categories: 1) continuous and 2) non-continuous surface gradients. Continuous gradients are dominated by randomly distributed protein gradients generated through diffusive mixing or serial dilution using a microfluidic gradient generator, though other techniques like patterning using hydrogel stamps can be used as well. Dertinger *et al.* used the gradient generator to pattern a continuous surface gradient of laminin and uncovered that rat hippocampal neurons were oriented in the direction of increasing laminin coverages only at steep laminin slopes.[90] In a separate study, rat epithelial cells migrated up laminin gradients independent of the magnitude of the slope.[91] Later, Rhoads *et al.* studied haptotaxis behaviors towards fibronectin continuous gradients.[7] Here, a correlation between the epithelial (CHO) cells net migration and the increase in fibronectin slopes was observed, with increased migration velocities on steeper gradients. Additionally, the authors concluded that higher local fibronectin concentrations minimized cell haptotaxis responses, potentially due to receptor saturation. In all the three examples discussed above, the reference surface (RS) was passivated using bovine serum albumin (BSA).

Non-continuous gradients are typically made of disconnected (sub-micron) features and the protein surface density is modulated by the distributions of these features. Lang *et al.* and Philipsborn *et al.* investigated the repulsive behavior of temporal retinal ganglion (RGC) axons towards graded and discontinuous ephrinA5 gradients, with orders of magnitude (OM) of up to 1.8.[68,92] RGC axons innervated the repulsive ephrins and stopped at a specific stop zone dictated by the steepness of the slope and the local concentration of ephrinA5 ligands. A few years thereafter, our lab designed monotonic non-continuous and step-wise digital gradients made of 200 × 200 nm^2 dots with impressive OM up to 3.8.[61] Digital protein gradients are of interest as they provide spatial control of the immobilized proteins making it easy to understand cellular contact-mediated interactions.[93] Later, Ongo *et al.* designed a set of 100 different digital nanodot gradients (DNGs) with surface coverages ranging from 0.02 to 44.4% with up to 3.86 OM.[6] The DNGs incorporated randomness (randomly distributed nanodots) with different slopes and further incorporated noise in some gradient designs to match noise signals encountered by cells in their *in vivo* microenvironments

while transducing migratory signals. These DNGs were developed in silicon and printed onto glass substrates using the lift-off nanocontact printing technique. Recently, our lab went a step further to pattern these DNGs onto soft substrates (E < 10kPa) – physiologically representative of *in vivo* stiffness – and studied netrin-1 signaling.[94,95]

2.2.7. Indirect microcontact printing methods

Direct printing of biomolecules onto surfaces using microcontact printing methods, though proven to work, has a few limitations. Firstly, biomolecules can de-adsorb from the final substrates. Secondly, proteins are briefly dried during the printing process potentially impacting their biofunctionality. This intermittent step is very transient but can lead to unfolding and/or denaturation of proteins, thus reducing their bioactivity due to the exposure to nonphysiological conditions. Philipsborn and colleagues, for example, claimed that the protein fibronectin was not suitable for microcontact printing as it lost bioactivity in the process.[3] Several other studies have successfully printed proteins (including fibronectin) and shown strong surface adhesion and biofunctionality.[1,3,61,66] Recently, Sathish *et al.*, concerned about proteins de-adsorbing from surfaces after patterning, printed amine-NH_2 terminated silanes and covalently bound antibodies and proteins to them.[96] Covalent binding ensures that biomolecules are firmly fastened to surfaces, therefore withstanding high shear forces. Additionally, biomolecules were added in solution form, with no partial dehydration, thus no denaturing and loss of bio-functionality occured. Sathish *et al.* successfully generated microarrays down to 200 × 200 nm^2 protein dots. The approach taken in this study required the use of cross-linking chemistries like EDC-NHS and BS3 to graft proteins to silane prints, which are not just lengthy processes, but also very expensive.

In another recent publication, Hu and colleagues showed that depending on the traction forces exerted by cells onto the ECM proteins, microcontactly printed proteins delaminate.[97] They demonstrated this by seeding vascular smooth muscle cells (VSMCs), with 6–10 kN/m^2 rating of traction forces onto microcontactly printed fibronectin circles. When fibronectin is covalently bound to the surface, via 4% (v/v) 3-mercaptopropyl trimethoxysilane (MPTMS) to glass and then via N-γ-maleimidobutyryloxy succinimide ester (GMBS) to fibronectin, it does not delaminate. Notably, for a while, the transfer of proteins was only from low to high free energy surfaces, thus limiting the range of proteins applicable to microcontact printing. To circumvent this limitation,

our group in 2014 engineered a 'universal microcontact printing' technique where protein transfer was independent of the surface energy of the substrates.[69]

Our lab, and others, have managed to minimize the aforementioned microcontact printing limitations associated with migration assays by meticulously applying the appropriate protocols. For instance, limiting protein dehydration to short times, incubating stamps in humidified environments, and being especially careful with our prints. As such, patterned proteins remain bioactive and protein delamination from substrates is limited. The bio-functionality of printed netrin-1 was demonstrated in stripe assays[1] using function blocking antibodies, and recently in a study where netrin-1 demonstrated signal transduction in neurons.[98]

2.2.8. The reference surface (RS) in haptotaxis assays

A key feature in haptotaxis assays is the coexistence of surface-attached proteins and the area between the patterned protein cues. This non-patterned area or area in-between the printed protein ligands is defined as the reference surface (RS).[1] In immunoassays, this is the background which is typically blocked or passivated to prevent non-specific binding of biomolecules, thereby guaranteeing that any surface binding is specific to the desired domains. Likewise, the adhesive levels of the RS have to be controlled to ensure that all observed haptotaxis responses are specific to the patterned protein cues, as migratory cells interact with both the proteins and RS. The term RS was introduced by Ricoult *et al.*[1] along with the term 'cell-surface affinity' to replace the use of 'surface adhesive strength' (low or higher adhesive) with regard to cell migration assays. The old nomenclature is more general and notably incorporates the scenario where cells prefer a less adhesive surface versus a more adhesive one. For instance, cells preferentially migrated onto laminin-1 patterns over fibronectin, even though laminin-1 is less adhesive than fibronectin.[99] Imperatively, cell choices are mainly dependent on specific biochemical signal transduction pathways effected by signals from specific surface protein cues, and not by how adhesive the surface proteins are. Several migration studies are beginning to adopt the introduced nomenclature,[93,100,101] though there are a few publications still using cell-substrate adhesiveness.[22,102,103]

In surface gradients, concentrations of the RS and surface proteins are inversely related (figure 8). This schematic representation shows a monotonic gradient made of immobilized protein nanodots (in green) with the RS (in yellow). The impact of the RS is more critical in gradient patterns as the RS and the protein cues are not binary as is the case with stripes. For simplicity, the schematic shows a surface gradient with a constant increasing linear slope for the cue, in the horizontal axis. The RS has a complementary slope to that of the cue, that is, a linear decreasing slope with the same magnitude. The effect of the RS's fractional change on cell signaling, characterized by the relative change plot shown in figure 8 below, is position dependent. The configuration is such that at the high end of the gradient, there is a high relative change in RS. Therefore, if the RS influences cell responses, it could dominate the response and overshadow the cell response towards the cue at the high end of the gradient. For example, on the higher end of the gradient (right), the RS coverage changes from, for instance, 2% to 1%. This is a 100% change as the density is halved. On the higher end of the gradient, a change from 99% to 98% RS coverage equates to a 0.010% which is insignificant. Yet, these extreme positions on the gradient are both expected to work effectively with a RS of the same composition and cell affinity, a remarkably hard feat to achieve.

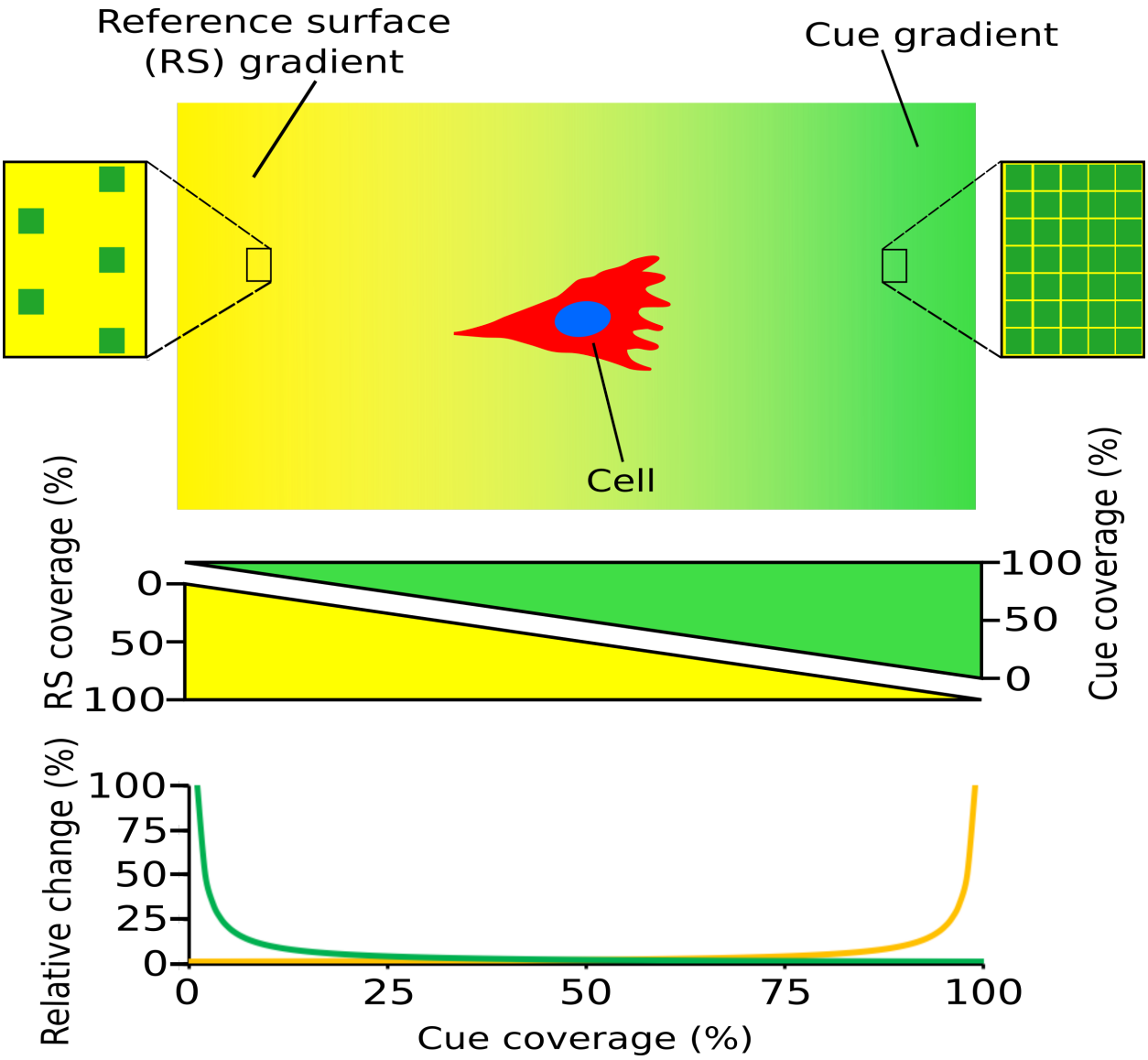

Figure 8: The co-existence of the RS and patterned cues in gradient assays both influence haptotaxis behaviors. This schematic shows that the RS surface coverage (in yellow) increases inversely to that of the printed protein cue (in green). The cue is patterned in the form of nanodots at an increasing surface coverage from 0% to 100% from left to right. Inserts show the cue coverage at 10% and 90% on the left and right, respectively. The lower plot shows the absolute relative (fractional) change of the cue and RS affinity. Notice that the rates of change of the cue and RS are significantly larger at the lower and higher end of the gradient, respectively, and consequently the effect of the cue and RS on cell responses on these regions will be relatively high.

2.2.9. Effect of the RS on cellular responses

The cell-surface affinity of the RS must be tuned to maximize the desired cellular response, and to reflect cell responses in *in vivo* conditions. Ricoult and Thompson-Steckel investigated the effect of the RS on haptotaxis and showed that a RS with either a low or high cell-surface affinity significantly alters cell migration results, as indicated in figure 9 with fibroblast cells cultured on fibronectin stripes.[1] Here, the cell-surface affinity of the RS is modulated by adjusting the ratio of polyethylene glycol (PEG) to poly-D-lysine (PDL), which have a low and high cell-surface affinity, respectively. The results show that a low cell-surface affinity RS 'pushes' the cells onto the cue, whereas a high cell-surface affinity RS restrains cell attraction to the printed fibronectin. Essentially, a RS with a high cell-surface affinity masks the attraction (presence) of the guidance cues. Additionally, the authors concluded that cell responses in haptotaxis are dependent on the cell type (fibroblasts, myoblasts, etc.), the printed cue (fibronectin, polylysine, etc.), and the affinity of the RS.[1] In their publication they show that for the same printed cue and same RS, the migration response of Rat2 and C2C12 cells is different, alluding to cell specificity. Wen *et al.* recently reiterated that haptotaxis is cell-type specific and that cellular responses to ligand density gradients is mediated by the substrate 'adhesiveness' as well.[22]

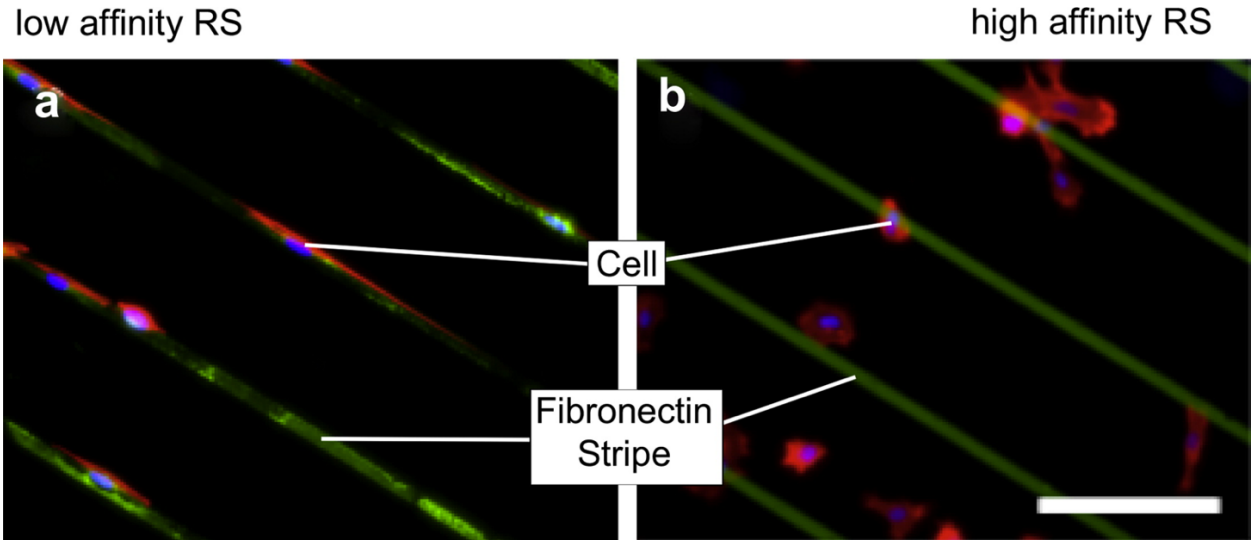

Figure 9: Rat2 fibroblasts migration responses to fibronectin stripes in the presence of a very low and very high cell-surface affinity reference surface (RS). Cells in **a)** migrated onto stripes due to the repulsion of the RS, while cells in **b)** ignored protein cues on the stripes due to the stickiness of the RS. Essentially, cell responses in both a) and b) are a result of the RS and not the patterned

cue (fibronectin). Scale bar is 100 µm [Reprinted with permission from Biomaterials (Ricoult and Thompson-Steckel, 2013)[1]].

2.2.10. Inconsistency and lack of standards for reference surfaces limit conclusions drawn from haptotaxis studies

Different scientists use different proteins or polymers to control the cell-surface affinity of the RS, or do not control it at all (Table 1). Generally, the relatively stable growth-permissive protein, poly-D-lysine (PDL), is used. The amount of PDL used in different studies varies significantly as well. Sloan *et al.* coated the RS with 0.1 µg/mL of PDL for an hour to provide an adhesive substrate for neurons in an axon turning assay towards netrin-1 and Shh gradients.[5] Joo *et al.*, while studying the migration and differentiation of stem cells to laminin stripes, utilized a RS created by flowing 0.1 mg/mL of PDL for 2 hours.[104] Notice the 3 orders of magnitude difference in PDL concentrations in these two assays. Philipsborn and colleagues used 20 µg/mL of laminin as the RS while studying the repulsive behavior of retinal ganglion axons to ephrin prints.[68] Laminin is a growth-permissive molecule, but also orients retinal ganglion (RGC) axons as an attractive guidance cue,[105] and thus provided a non-neutral cell-surface affinity for the RS. As a result, the RGC's were challenged with repulsive ephrins and attractive laminin. Therefore, the results cannot be specifically attributed to either, even though the study was to evaluate the repulsive behavior of RGC towards ephrins. Axonal growth cones possibly ended up on the laminin because they were attracted to it, not because they were repelled by the ephrin prints. Alternatively, the response might have been synergetic. A RS with a moderate affinity would be more meaningful in this migration assay as the response can clearly be attributed to one specific cue. Hu *et al.* studying how protein-substrate adhesion regulates cell behavior, used a surfactant, 0.1% pluronic F127, as a RS incubated for 15 min on fibronectin prints "to prevent unexpected cell-substrate attachment".[97] As expected, a surfactant results in a low cell-surface affinity, and possibly impacted the obtained results. Even worse, the authors also compared the migration results to those of fibronectin patterned via the 'bath' application where the uncoated glass surface was taken as the RS. Fricke *et al.* studied neurite growth to poly-L-lysine and laminin gradients or both using rat cortical neurons.[106] Here, the ECM proteins were patterned using microcontact printing onto pre-hydrophilized glass coverslips, implying that the pre-hydrophilized non-patterned areas dictated the cell-surface affinity of the RS. Here, the RS's cell-surface affinity was not controlled at all, and most likely was very 'adhesive' due to the glass pre-hydrophilization.

These discussed examples highlight the lack of a 'gold standard' procedure to control the cell-surface affinity of the RS. As a result, our lab dedicated efforts to not only demonstrate the need to control the RS and show the negative effects of an uncontrolled RS cell-surface affinity, but also to provide the ideal RS for different patterns and cell types. Our lab introduced, characterized and have extensively utilized a mixture of PEG and PDL to backfill the RS. Ricoult *et al.* showed that the optimal RS for neuronal navigation on netrin-1 prints is 75:25 %PEG:%PDL.[1] PEG, a non-cell affinity molecule that is devoid of cell binding domains, is a copolymer with polyethylene glycol side chains grafted onto polylysine backbone, and correctly abbreviated as PLL-g-PEG. PDL is a synthetic protein similar to poly-L-lysine, the extracellular matrix protein, but cannot be degraded by enzymes hence its stability. PDL is relatively positively charged and provides electrostatic attachments to cells.[107,108] Tuning the ratios of the PEG and PDL result in RSs with neither high nor low cell-surface affinities, and in turn yield optimal cell responses.[1]

RSs with optimized cell-surface affinities ought to be growth permissive but not instructive, that is, they allow cells to grow and respond to biochemical cues in their microenvironment, but ideally do not dictate or interfere with the degree of cellular attraction and repulsion to cues. As such, cell navigation responses and migration choices are only a result of attraction (or repulsion) towards the printed protein cues. Assays without properly adjusted RSs present questionable results as the observed cell behaviors could be significantly impacted by the cell-surface affinity of the RS. Therefore, cell migration responses to a particular cue should always be interpreted relative to the cell-surface affinity of the RS. Furthermore, the lack of specified and characterized RSs in cell navigation studies implies that haptotaxis results cannot be compared across different cues, cell types and experiments.

Table 1: Haptotaxis assays with stripes and gradient patterns emphasizing different feature sizes and the different references surfaces (RS) applied (if any).

Pattern configura-tion	Feature sizes	Coverage (%)	Surface-anchored cue(s)	Reference surface (RS)	Cell type studied	Citation Reference	Additional comments
Stripes	20 µm	0, 100	Fibronectin or BMP-2	PEG[a]	C2C12 Myoblasts	Hauff *et al.* (2006)[109]	-
Stripes	10 µm	0, 100	Fibronectin or netrin-1	PEG:PDL[b] (10 µg/mL)	Neurons, Myoblasts	Ricoult, Thompson-Steckel (2014)[1]	-
Stripes	100 µm	100	Netrin-1 & ephrinB2	-	Motor neurons	Poliak *et al.* (2015)[2]	Two alternating cues
Stripes	30 µm	0, 100	Laminin	PDL[c]	Astrocytes, neurons	Joo *et al.* (2015)[104]	-
Continuous gradient[d]	-	0 – 100	Laminin	BSA	Hippocam-pal neurons	Dertinger *et al.* (2002)[90]	Gradient width = 1.25 mm
Continuous gradient	-	0 – 100	Laminin	BSA	Epithelial cells (IEC-6)	Gunawan *et al.* (2006)[91]	Gradient width = 0.75 mm
Continuous gradient	-	0 – 100	Fibronectin	BSA	Epithelial cells (CHO)	Rhoads *et al.* (2007)[7]	Gradient width = 0.75 mm
Continuous gradient	-	0 – 100[e]	Netrin-1, *Shh*	PDL[c]	Neurons	Sloan *et al.* (2015)[5]	Gradient width = 3.65 mm
Discontinu-ous gradient	0.9 × 2 µm^2	n.a.	PLL, laminin	None	Cortical neurons	Fricke *et al.* (2011)[106]	No RS coating reported
Graded gradient	2 µm^2	n.a.	EphrinA5	Laminin (20 µg/mL)	Retinal neurons	Philipsborn *et al.* (2006)[68]	-
Digital gradient	100^2 nm^2	0.17 – 44.4	RGD, netrin-1	PEG:PDL	Myoblasts	Ricoult *et al.* (2013)[61]	Haptotaxis on 200^2 nm^2
Digital gradient	200^2 nm^2	0.02 – 44.4	Netrin-1	PEG:PDL	Myoblasts	Ongo *et al.* (2014)[6], MacNearney (2016)[94]	MacNeaarn-ey used soft substrates (E < 10 kPa)

[a] PEG refers to PLL grafted onto PEG [PLL(20kDa)-g(3.5)-PEG(2kDa)]

[b] Different ratios of PEG and PDL were used

[c] PDL was flown in solution

[d] All continuous gradients highlighted here have linear concentration slopes

[e] The fractional change ranged from 0.3 – 2.2%

Abbreviations:

Shh: Sonic hedgehog

PLL: Polylysine

PDL: Poly-D-lysine

RGD: Peptide sequence Arg-Gly-Asp

BSA: Bovine Serum Albumin

n.a.: Not available

2.2.11. Limitations of haptotaxis gradient assays

Preceding haptotaxis, cells establish peripheral interactions specifically, integrin-ligand mediated adhesions linking the cell to the substrate. Thus, stable cell-surface adhesions require a minimum number of active protein receptor-ligand connections. Geiger *et al.* claim that for melanoma cells, stable receptor-ligand complexes are only formed when individual surface proteins are less than 73 nm apart.[14] Consequently, they claimed that integrin nano-clustering is a prerequisite for haptotaxis. It was later reported that the minimum effective nanocluster for fibroblasts is 0.11 μm^2 (where they used rectangular spots with dimensions of 333 × 333 nm^2) establishing a lower threshold for cell sensitivity.[10] However, other studies have demonstrated cell responses towards smaller nanodots of the same protein, fibronectin, with dimensions of 200 nm diameters.[110] As highlighted here, the effect of nanodot sizes on haptotaxis remains to be thoroughly investigated.

For gradients to trigger cell motility, the protein concentration difference between the leading and the trailing edges must be sufficiently large, and higher than the noise signals from the

environment. At high surface protein densities, all cell receptors bind to protein ligands, resulting in cell receptor saturation. High ligand densities can easily lead to 'equal' cell adhesions at the leading and trailing edges, and no cell polarity, even when the actual protein coverage at the leading edge is higher. The ligand density difference merely cannot be dictated by the saturated receptors. At this point, no directional cell migration will be observed. Mathematical models for axonal outgrowth have been generated and validated experimentally to demonstrate this concept.[111,112] Sloan *et al.*[5] reported that commissural axons responded to steep but not towards shallow netrin-1 and Shh gradients, suggesting the existence of cases where the growth cone cannot differentiate the stimuli concentration between its leading and trailing edge. As a result, axons did not turn in the expected directions during the turning assay experiments, possibly due to receptor saturation on the higher end of the gradient. Gradient array configurations do not provide definitive results with regard to receptor saturation, therefore novel designs are required to probe this effect.

Migration results from gradient assays also mask receptor sensitization which arises due to the plasticity of guidance responses.[113] For example, levels of cyclic adenosine monophosphate (cAMP) in cortical neurons has been reported to change as growth cones track on netrin-1 towards the optic nerve, and consequently this alters the affinity of axons to netrin ligands.[114] Likewise, as cells traverse from the lower end of the gradient, receptor-ligand complexes are repeatedly assembled and disassembled leading to activation of signaling pathways that upregulates the receptors sensitivity to the cues. Cells that would otherwise stop on gradient arrays with small changes in protein concentration thereafter are able to sense these small differences and continue tracking towards the higher end of the gradient due to the enhanced receptor sensitivity. Unfortunately, the is no reporter mechanism to alert on the cellular receptor sensitization process. Alternatively, cells tracking on protein gradients could possibly continue on their established migration trajectories due to their migration directional persistence. For instance, neurons tracking on repulsive ephrins continue migrating into ephrin prints for quite some time and distance, before they eventually stop and retreat.[68,92] In another study, fibroblasts directional persistence increased proportionally to the ligand density of surface-attached fibronectin.[115] It was also reported that epidermal growth factor (EGF) stimulated cells demonstrated long-timescales of directional persistence on fibronectin substratum in a concentration dependent manner.[116]

Directional persistence – continued cell migration in a direction preset by previous cell signaling events – is a consequence of the cell's intrinsic polarity modulated by intracellular short positive feedback loops between the small GTPase RAC and actin polymerization effectors such as actin-related proteins (ARP 2/3).[8] This feedback regulator mechanism leads to continuous actin polymerization where it was previously activated (at the active leading edge) for some time, without re-calibrating the cell migration polarity as per the local external cues. Eventually, negative feedback is triggered by Arpin, an inhibitor of ARP 2/3, which is activated slowly by RAC, and restores the cell's homeostasis. Up to that moment, the cell's direction is independent of the protein concentration differences across its leading and trailing edges, implying that the final cell position is not indicative of the underlying gradient steepness. In effect, migration directional persistence most likely masks 'true' cell responses on the higher end of gradient arrays, an area cells reach after migrating from the lower end of the gradient. As such, persistence-free haptotaxis platforms that cover the full density range of protein distributions *in vivo* are required to unravel key information regarding cell-to-protein ligand sensing and signal transduction mechanisms.

2.3. Project rationale

Protein patterns for haptotaxis assays are primarily conducted in the form of alternating stripes with (100% coverage) and without the cue (0% coverage), which does not adequately mimic the distribution of proteins *in vivo*. Continuous or digital gradients covering a large dynamic range of protein densities are also used, but as discussed above, they complicate the extraction of local cell decisions and suffer from (i) receptor sensitization, (ii) receptor saturation and (iii) directional persistence effects. Therefore, we set out to develop the nanodot stripe assay (NSA) made of binary arrays covering the full range of protein concentrations to allow for clear cell migration choices when cells are challenged with different concentration steps at the leading and trailing edges. The NSA is a combinatorial choice assay consisting of binary combinations of stripes, with 0% and 100% coverages, and digital nanodot arrays following a 3-fold increase and spanning two orders of magnitude in surface densities. Our approach aimed at finding (i) the least surface concentration that cells can sense, (ii) the concentration difference (or step) in leading and trailing edges of the cell that can evoke cell migration, and (iii) to explore cell choices free from directional persistence which influences cell migration responses. We included arrays made of 200 × 200, 400 × 400 and 800 × 800 nm^2 nanodots to investigate the effect of the nanodot dimensions on cell migration.

Additionally, we utilized the NSA platform to investigate and optimize the cell-surface affinity of the RS with regard to cell migration responses towards protein nanodots. Cell choices on the NSA platform were studied by observing the chemoattraction responses of neogenin-expressing C2C12 myoblasts towards immobilized netrin-1 proteins.

3. REFERENCE SURFACE OPTIMIZATION

We investigated the cell-surface affinity produced by different reference surface (RS) compositions using the classical stripe assay and performed cell adhesion experiments, preliminary to the NSA development.

3.1. Cell migration on classical netrin-1 stripes

We used the standard stripe assay to examine C2C12 myoblasts haptotaxis responses towards a surface-attached netrin-1 cue. Netrin-1 stripes with 15 μm widths and a 75 μm pitch were printed on glass substrates using the standard microcontact printing method. The replication, patterning and cell culture protocols were explained in detail elsewhere.[1] Fluorescent Immunoglobulin-G (IgG) antibodies were mixed with netrin-1 proteins at a 4:1 concentration ratio for visualization purposes, and IgG alone was printed for the negative control assay. The patterned glass coverslips were backfilled with different ratios of %PEG:%PDL to tune the cell-surface affinity of the RS.

Four different RSs corresponding to four different cell-surface affinities were tested (Figure 10). The ratio of cells on stripes versus cells on the RS demonstrates the cell's choices when challenged with netrin-1 and a RS. C2C12 cells cultured on low cell-surface affinity substrates (*e.g.* 100:0 %PEG:%PDL) made similar choices where they migrated onto stripes when presented with the attractive netrin-1 cue, and when presented with the non-affinity IgG which is devoid of cell binding domains or charges. Therefore, we concluded that this non-permissive RS composition dictates cell choices making cells migrate onto the stripes even in the absence of attractive cues. On the other hand, high cell-surface affinity substrates, given by a ratio of 75:25 %PEG:%PDL, result in non-responsive cells (Figure 10). On the 75:25 %PEG:%PDL RS, only 21% of the cells

preferred netrin-1 stripes which corresponds to the total surface area of stripes to that of the RS (15:60), thus cells located on netrin-1 stripes were positioned there purely by chance. The high cell-surface affinity RS masks the presence of the attractive cue and impedes cell responses towards the netrin-1. In the control assay with the 75:25 %PEG:%PDL RS, about 4% of the cells preferred the IgG stripes which is less than the 20% we expected based on stripes:RS area. This data shows that the C2C12 myoblasts preferred the PDL on the RS over the patterned IgG stripes. The cell choices in the control assay are justifiable considering that cells were challenged with IgG (without cell binding affinities) and significant amounts of PDL (2.5 um/mL) in the PEG:PDL making the RS composition. Similarly, in the test assay, the PDL on the RS acted as an attractive cue competing with the attractive netrin-1 cue. This result clearly shows a case where the cell affinity of the RS interferes with cell migration towards the cue under investigation.

The 90:10 %PEG:%PDL RS results in the highest cellular response to netrin-1 (94%) and no directed response towards IgG in the negative control (16%). Confidently, we conclude that this cell response is netrin-1 specific. Culturing cells on surfaces covered with this RS, as presented below (figure 11), indicated that cells can thrive and also make migration choices when presented with attractive guidance cues. As such, the 90:10 %PEG:%PDL RS is justified as 'optimal' for studying haptotaxis of C2C12 myoblasts towards netrin-1 stripes. Previously, our group reported that the optimal RS for neurons in a netrin-1 stripe assay was produced by backfilling with 75:25 %PEG:%PDL. Notably, they showed that different cells produced different response curves even to the same cue, highlighting that the response is unique to each cell type – protein pair. Therefore, the optimal RS is specific to each cell – protein combination. Consequently, we investigated the RS affinity producing optimal cell response with the C2C12 myoblasts and netrin-1 pair. Nevertheless, subtle differences in cell responses could still occur even between researchers within the same lab. Potentially these differences emanate from the protein bioactivity levels which may vary from batch to batch, and from slight differences in protocols like number of rinsing steps, incubation on or off motorized shakers (that ensure solutions are uniformly mixed), and etc. Thus, the RS should be tested and optimized (verified) prior to any experimental set.

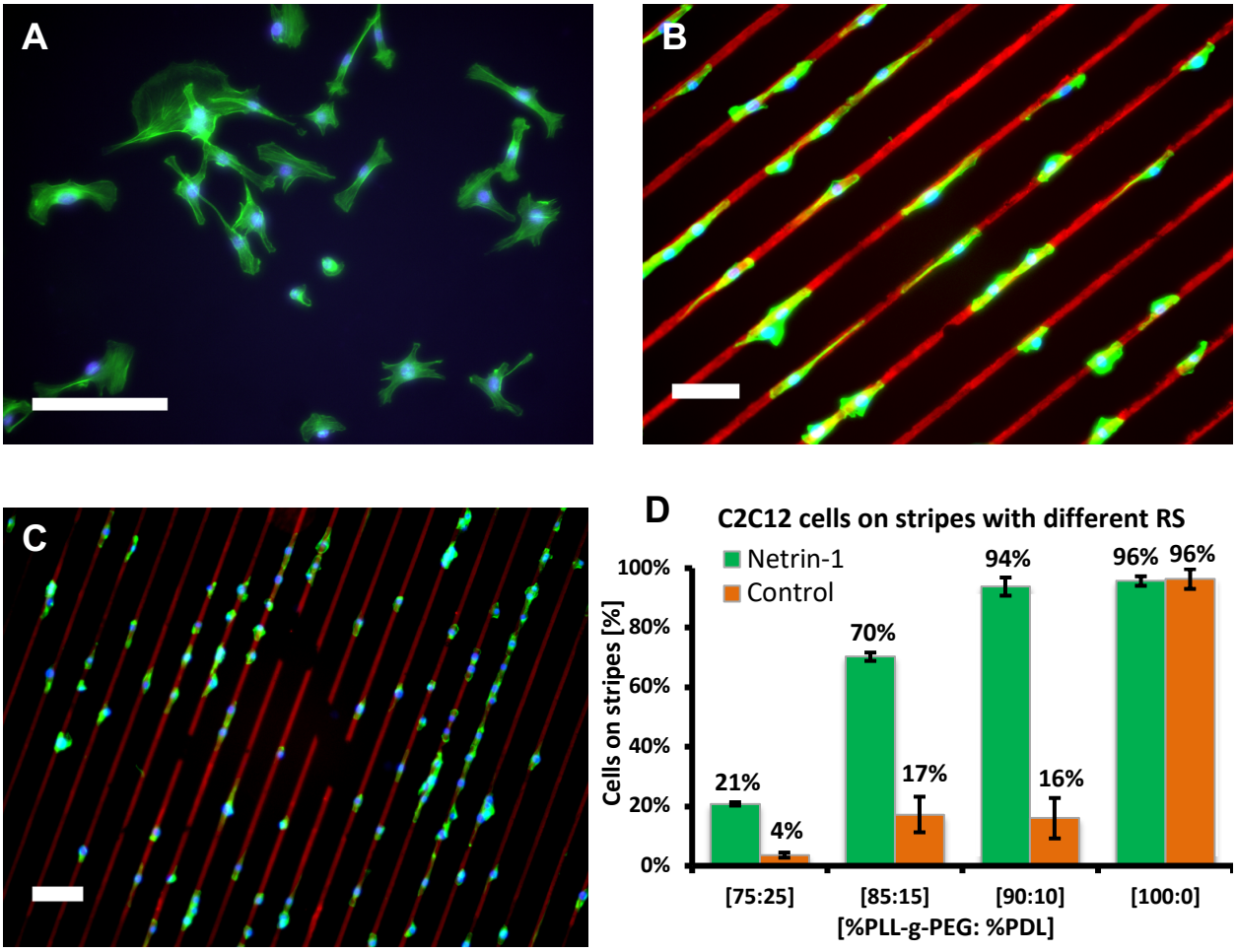

Figure 10: C2C12 myoblasts haptotaxis preferences on netrin-1 stripes. **A)** Cells randomly distribute in the absence of netrin-1 stripes. **B) – C):** With a RS of 90:10 %PEG:%PDL, cells are chemotropically attracted to the netrin-1 cues. **D)** A high cell-surface affinity RS made of 75:25 %PEG:%PDL masks the presence of the netrin-1 cues, while a RS with a low cell-surface affinity dominates the response as seen in the 100:0 %PEG:%PDL case. A netrin-1 specific chemoattraction response is observed at the intermediate RSs with 90:10 %PEG:%PDL resulting in optimal cell responses. Error bars indicate standard deviation (N = 5). Scale bar for **a)** – **c)** is 100 μm.

3.2. Cell adhesion and proliferation on substrates with adjusted cell affinities

To improve our understanding of cell-substrate interactions, specifically between cells and the RS, we investigated cell survival on glass surfaces coated with different ratios of %PEG:%PDL (figure 11). The aim was to find the range of RSs with cell-surface affinities that permit cell adhesion and proliferation. C2C12 myoblasts perish in the absence of cell-surface adhesions, that is, when the substrate is completely non-permissive. On the other hand, high cell-surface affinity substrates, though boasting with high growth permissive levels, impede cell migration as the trailing edge of a migrating cell cannot detach from the substrate and allow the migrating cell to crawl forward.[16]

Myoblasts adhesion and proliferation behaviors were investigated on six different compositions of %PEG:%PDL. Substrates coated with netrin-1 were included to provide a better understanding of how its cell-surface affinity compares to the rest of the RSs affinities. Coverslips were first plasma treated (PlasmaEtch PE-50, Carson City, NV, USA) for 1 min and then inserted into a 12 well plate. The different substrate solutions were added and incubated for 1 h at 4°C, employing the same procedures utilized for our stripe cell migration assays. The RS was aspirated followed by two PBS (1X) rinses. Right after passaging cells, 2600 cells/cm^2 were seeded in well plates, cultured for 18 h then fixed and stained with Hoechst (nucleus) and phalloidin (actin). Images measuring 3.7 × 2.7 mm^2 were captured using a fluorescence microscopy (TE2000, Nikon) and analyzed using Fiji.

Expectedly, the population of adherent cells on the substrates increased with an increase of the cell-surface affinity of the substrate. This trend is apparent in figure 11D from the 100:0 to 75:25 %PEG:%PDL surface coatings. Approximately, ten-fold cells were counted in the 75:25 %PEG:%PDL condition compared to 100:0 %PEG:%PDL. The remarkable difference between the two extreme conditions tested demonstrated the effectiveness of the cell-surface affinity, not just to cell migration behavior, but to cell survival as well. Clearly, cells thrive on surfaces with PDL and barely stay alive on surfaces with only PEG. Our observed results, are in agreement with previous cell studies on similar cell-surface affinity micro-environments.[1] Netrin-

1 coated surfaces show that netrin-1 is an adhesion and growth permissive biomolecule, which is in agreement with other publications.[117]

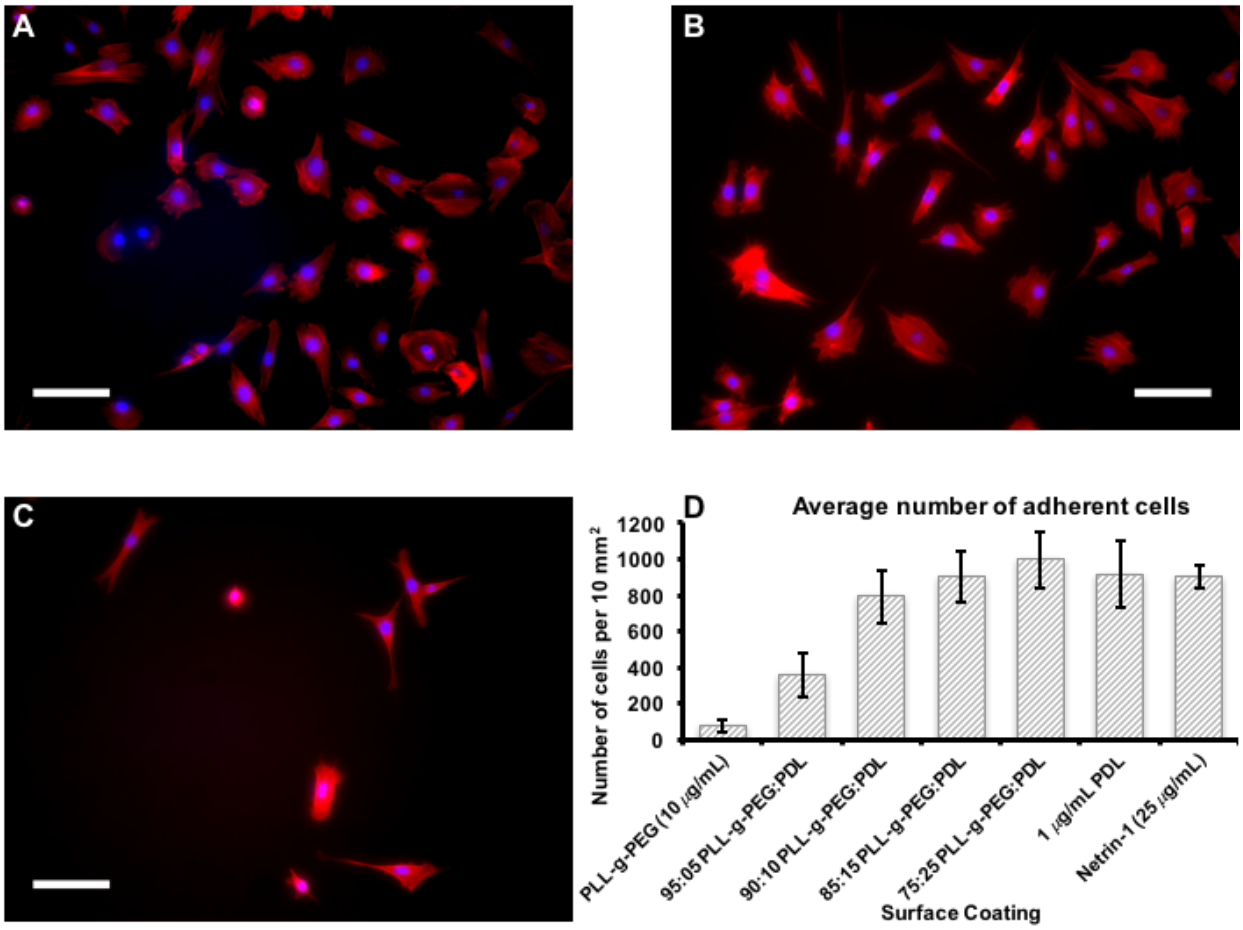

Figure 11: Cell densities on RSs of different cell-surface affinities quantifies the substrate's degree of growth permissiveness. **A) – C)** shows images of adherent cells on different surface coatings: A) 1 µg/mL PDL, B) 90:10 %PEG:%PDL and C) 100:0 %PEG:%PDL. **D)** A plot showing the number of adherent cells on the glass substrates coated with different RS mixtures. Different ratios of %PEG:%PDL yield different cell-surface affinities hence varying the permissiveness of the surface. The least cell-surface affinity condition (PEG, 10 µg/mL) has the least cells. The number of cells increases with an increase in PDL concentrations (decrease in PEG concentration), matching the direction of increasing cell-surface affinity. Scale bars are 100 µm. Error bars indicate standard deviation (N = 3).

4. COMBINATORIAL NANODOT STRIPE ASSAY FOR HAPTOTAXIS STUDIES

This chapter takes the form of a manuscript. Once its internal review process is complete, the manuscript will be submitted to a journal for publication.

COMBINATORIAL NANODOT STRIPE ASSAY TO STUDY CELL HAPTOTAXIS

Mcolisi Dlamini[1,2], Timothy E. Kennedy[3] and David Juncker[1,2*]

[1]Biological and Biomedical Engineering Department, McGill University, Montreal, QC, Canada

[2]McGill University and Genome Quebec Innovation Centre (MUGQIC), Montreal, QC, Canada

[3]Department of Neurology and Neurosurgery, McGill University, Montreal, QC, Canada

*email: david.juncker@mcgill.ca

4.1. Abstract

Haptotaxis is cell migration in response to surface cues and has been reported for many critical processes including neuronal development, wound repair and immune response. Numerous *in vitro* haptotaxis assays have been developed, however they often take the form of a binary choice between a complete coverage by the cue (usually a protein) and a surface without any cue. As such, these assays only test the extremes and do not reflect the *in vivo* conditions where cells navigate through gradients with different steepness and extending across the entire density range, not just the extremes. Gradients have been used *in vitro*, but receptor saturation and cell migration history may mask the immediate cell response. Here, we introduce the nanodot stripe assay (NSA), a combinatorial array of stripes that covers the full range of density steps and average density. Protein guidance cues are patterned as 40 × 400 μm^2 stripes made of arrays of 200 × 200, 400 × 400 or 800 × 800 nm^2 nanodots, with surface coverages of 0, 1, 3, 10, 30, 100%; the concentrations follow an approximately threefold increase, while a stripe of 44% was added as it constitutes the highest concentration achievable using nanodots. The choice and migration of C2C12 myoblasts expressing neogenin were probed on netrin-1 NSA for every binary combination. The reference surface (RS) between the nanodots was backfilled with a mixture of polyethylene glycol (PEG) and poly-D-lysine (PDL) with a low and high cell-surface affinity, respectively, at the ratios of 100:0, 90:10 and 75:25 of %PEG:%PDL. Cell response was found to be maximal for 90:10 %PEG:%PDL and independent of the nanodot size. A cell choice was observed for most combinations, except for the intermediate ratios of 30% vs. 44% and 44% vs. 100% suggesting a threshold for cell response to density ratios > 2.5 at high average density. The NSA constitutes a powerful haptotaxis platform to systematically and quantitatively study cell navigation and signaling in response to surface-bound cues.

4.2. Introduction

Cell migration is essential for life processes including angiogenesis,[12] immune response,[118] tissue repair,[22] cancer metastasis,[19] and embryonic development.[11] Cells migrate directionally in response to motile signals transduced from soluble and surface bound (protein) cues that are present in their microenvironment via chemotaxis[18] and haptotaxis,[24,25] respectively. For instance, fibroblasts navigate on surface-bound gradients of extracellular molecules at the interface of healthy and fibrotic tissues,[22] and during embryogenesis, a netrin-1 surface gradient directs growing commissural axons towards the floor plate en route to their specific synaptic targets,[21,31,36] which are both examples of haptotaxis.

Haptotaxis signaling studies *in vitro* observe cellular responses to proteins patterned as either stripes or surface gradients. Surface-bound protein patterns can be formed using multiple different techniques including microfluidic premixers, microfluidic probes, hydrogel stamp diffusion, dip-pen nanolithography, laser-assisted protein adsorption by photobleaching (LAPAP), membrane filters, and microcontact printing.[83] Stripe assays are widely used for haptotaxis experiments as they are relatively easy to generate and provide cell distribution results rapidly.[1,2] Ricoult and Thompson–Steckel used the classical stripe assay to demonstrate that haptotaxis results must be interpreted in the context of the cell-surface affinity of the references surface (RS) – the area between patterned protein cues.[1] Previously, the impact of the RS on cell migration was overlooked and not standardized, which casted doubt on published results, and these surfaces were not even characterized. Here a method to systematically adjust the cell affinity of the RS was introduced and examined, leading to the conclusion that cell response to the RS is a function of the cell-protein pair and type of patterns under investigation.

Migration results from stripe assays are limited to ‘on’ and ‘off’ protein stripes, that is, 0% and 100% densities only. Therefore, the classical stripe configuration does not encompass the full dynamic range that is found for *in vivo* protein distributions, hence gradient assays. Lang *et al.* and Philipsborn *et al.* developed and used digital gradient patterns to uncover surface concentrations required to trigger repulsion.[68,92] Microscale dot and line gradient patterns of ephrinA5 were patterned while using laminin as RS, and the repulsion of growth cones of temporal retinal ganglion cells were studied. Ongo and Ricoult *et al*. designed a set of 100 different digital nanodot

(200 × 200 nm^2) gradients (DNGs)[6,61] that provided a significantly greater diversity of slopes and a remarkably higher dynamic range of up to 3.86 orders of magnitude for haptotaxis signaling, with designs incorporating noise as encountered by cells while transducing migratory signals *in vivo*.[36] Notably, haptotaxis gradient designs reported in the literature are made of nanodots of varying sizes from 0.01 μm^2 to 2 μm^2, a relatively wide range.[61,68] It was stated that single surface RGD integrins ought to be no more than 60 nm apart to support cell adhesion, cell spreading and the formation of stable focal adhesions.[14,119,120] Ligand spacing >73 nm led to erratic filopodia protrusions or even cell apoptosis, strongly suggesting that integrin nanoclustering is crucial for cell signaling. These ligand-receptor point contacts lead to protein complexes called focal adhesions which are necessary to evoke cell migration processes. Coyer *et al.* identified the minimal integrin-ligand complexes area for fibronectin at 333 × 333 nm^2, suggesting that nanodots smaller than this threshold are not sufficient to support cell migration.[10] However, other experiments have observed normal cell responses towards smaller dots of 200 nm diameter for instance.[110] Up to date, the effect of the nanodot cluster sizes on haptotaxis navigation behavior has not been thoroughly explored.

Gradient assays complicate the extraction of the choices that cells make locally while traversing on gradient patterns. Without cell tracking platforms which are complicated and less accessible, the final haptotaxis results are simply a readout of global cell distributions on the gradient array. Therefore, the final cell positions do not inform on the cell's initial position, migration trajectory, and protein resolution difference required to evoke cell migration responses and to halt an already motile cell. As such, gradients mask the migration choices that cells make locally on different protein densities. Additionally, migration results from gradient assays may not be accurate indicators of cell preferences, especially on the higher end of the gradient, due to migration directional persistence[8] which has been reported on fibroblasts haptotaxing on continuous fibronectin gradients.[7]

Herein, we introduce the digital nanodot stripe assay (NSA) to challenge cells to different discrete protein concentration steps, and to easily acquire precise cell migration choices. The NSA configuration, made of combinations of nanodot stripes from seven protein coverages covering the full range of physiological densities, challenges cells to make a binary choice between lower versus

higher protein densities. This platform provides accurate information about the relationship between cell migration decisions with respect to the protein concentration step or difference across the cell relative to the local protein concentration. Therefore, the NSA allows for the examination of the local sensitivity, the minimum surface ligand concentration required to trigger haptotaxis responses, and saturation limits for cell's transmembrane receptor-ligand induced haptotaxis responses, which are key parameters for directing motile cells. We tested the effect of protein ligand nanoclustering on cell migration responses by varying the dimensions of the nanodots in the NSA. Additionally, the NSA was used as a calibration platform to optimize the cell-surface affinity of the RS for surface-anchored protein nanodots. To probe cell choices, we studied haptotaxis responses of C2C12 myoblasts towards the widely studied neuronal guidance cue, netrin-1.[121] C2C12 cells express neogenin, a transmembrane receptor for netrin-1,[33] which has been verified to trigger chemoattractive haptotaxis responses when bound to netrin-1 ligands.[1]

4.3. Materials and methods

4.3.1. NSA design and Si mold fabrication:

The nanodot stripes were designed and sketched using L-edit from Tanner design tools. The design file from L-edit was exported to a .gds file in preparation for the fabrication process. The NSA were fabricated onto a silicon (Si) wafer at the Institut National de la Recherche Scientifique (INRS) using electron beam lithography and direct UV laser writing for the nano- and micron-sized stripe features respectively. In brief, the designs were developed using the fabrication process flow summarized in figure S2. A two-step lithography process was employed to 1) pattern the nanodot features, and to 2) pattern the 40 × 400 μm^2 stripes. The Si wafer was first spin-coated with a 200 nm layer of positive ZEP520a resist. Nanodots were then patterned using electron beam lithography (EBL) onto the ZEP520a resist layer. After development, dry etching into Si using a SF6/C4F8 plasma generated the 200 nm deep nanoholes in silicon. Prior to fabricating the stripes, the wafer was spin coated with positive Shipley 1813 resist generating a 2 µm thick layer. The 40 × 400 μm^2 stripes were then aligned to the wafer with nanofeatures using fiducial markers, and patterned via direct UV laser writing. Nano-arrays, paired with the stripes, were designed to overlap with stripes to account for misalignment up to 4 µm in the horizontal and vertical

directions. Finally, dry etching into Si using a Bosch process was employed to make 5 µm deep channels. The remaining photoresist was stripped away to complete the fabrication process.

4.3.2. PDMS and NOA mold replication:

The low-cost lift-off nanocontact printing procedure pioneered and published by Ricoult *et al.*[61] was utilized to generate secondary molds and to pattern netrin-1 nanodot stripes. The process steps are summarized in Figure S4. Briefly, features from the Si mold were first replicated onto a polydimethylsiloxane (PDMS) elastomer. The Si was coated with trichloro(1H,1H,2H,2H-perfluorooctyl)silane (Sigma-Aldrich, Oakville, ON, Canada) via vapor deposition to prevent PDMS sticking. PDMS base, Sylgard 184 (Dow Corning, Midland, Michigan, USA) was mixed with its curing agent at 10:1 (v/v), degassed and cured on Si in an oven (VWR, Montreal, QC, Canada) at 60°C for at least 12 h. To prevent PDMS leaching, uncured oligomers were extracted by submerging PDMS in 70% ethanol overnight, then dried at 60°C for 6 h. A UV-curable NOA-63 (Norland Optical Adhesive, Norland Products, Cranberry, NJ, USA) stamp was then replicated from the PDMS mold. NOA-63 stamps had identical features to the original Si mold.

4.3.3. Protein patterning:

To print proteins (Figure S4), a ~1 × 1 cm^2 planar PDMS stamp was sonicated in 70% ethanol for 30 min and dried using a strong nitrogen stream. Thereafter, the stamp was inked with 15 µL of netrin-1 at 25 µg/mL, covered with a cover slip to evenly spread the protein solution, and incubated for 10 min. Fluorescent goat-anti-rabbit immunoglobulin–G (IgG) conjugated with Alexa Fluor 546 (Invitrogen, Burlington, ON, Canada) was mixed with netrin-1 at 4:1 concentration ratios to visualize the printed spots. The stamp was then dried with nitrogen gas and contacted to a plasma-treated (PlasmaEtch PE-50, Carson City, NV, USA) NOA stamp to lift-off the unwanted pattern. The desired pattern, left on PDMS stamp, were then printed onto a plasma-treated (1 min) cover slip, left at conformational contact for 10 s. Cover slips with netrin-1 prints were quickly inserted into a well plates, then backfilled with the desired RS and incubated in a cold room for one h.

4.3.4. Reference surface (RS) solution preparation:

The RS solutions were made by mixing a poly(L-lysine)-graft-poly(ethylene glycol) copolymer, PLL(20)-g[3.5]-PEG(2), (Surface Solutions, Dubendorf, Switzerland) and referred to as PEG (for short) with poly-D-lysine (PDL, 70-150 kDa, Sigma-Aldrich, St. Louis, MO, USA) at the desired volume ratios. PDL is an enzyme degradation resistant synthetic polylysine. PEG has a very low cell-surface affinity while PDL has a very high cell-surface affinity. Stocks of PEG and PDL were diluted in phosphate buffered saline (PBS) to 10 µg/mL prior to mixing them at desired volume ratios. RS incubation was 1 h followed by aspiration using a pipette, and a (3x) rinse with 1X PBS.

4.3.5. Cell culture procedures:

C2C12 cells (ATCC, Manassas, VA, USA), a mouse myoblast muscle cell line expressing neogenin, a transmembrane receptor for netrin-1 and a DCC paralogue[33], were cultured following standard cell culture procedures. Briefly, cells were cultured in high glucose DMEM (Dulbecco's modified media), supplemented with 10% fetal bovine serum and 5% penicillin/streptomycin (all from Invitrogen, Burlington, ON, Canada). Cells were passaged every 2 – 3 days and re-seeded at a $1 \times 10^5 cells$ in 25 cm^2 cell culture flasks and cultured in an incubator at 37°C and 5% carbon dioxide. A fraction of the passaged cells was seeded onto the wells with cover slips patterned with netrin-1 nanodot stripes and desired RS at a surface density of 2.8×10^3 cells/cm^2 – estimated from hemocytometer counts.

4.3.6. Cell staining and imaging:

After 18 h of cell culture in an incubator at 37°C and 5% carbon dioxide, cells on netrin-1 prints were fixed with 4% paraformaldehyde and 0.2% (v/v) glutaraldehyde (Sigma-Aldrich, Oakville, ON, Canada) for 4 min. Cells were then permeabilized with 0.15% triton X-100 in PBS for 4 min, and then blocked with 3% Horse Serum for at least one h. Thereafter, cells were stained for 30 min with Hoechst (1:10000) and phalloidin conjugated with Alexa Fluor 488 (1:250) to label the nucleus and actin filaments, respectively (all from Invitrogen, Burlington, ON, Canada), rinsed with 1X-PBS 3× and then imaged along with the prints using a fluorescence microscope (TE2000, Nikon). A multi-position and multi-channel NIS Elements script was used to capture images for

the netrin-1 patterns and cells. Images were overlaid to determine location of cells on the netrin-1 nanopatterns with the center of cell's nucleus taken as the cell's location.

4.3.7. Data extraction and analysis:

Image J (Fiji) was used to overlay fluorescent images of the netrin-1 prints and the cells. A region of interest (ROI) was selected based on the boundaries of the netrin-1 print, and the particle analysis tab was used to find cell locations relative to the netrin-1 patterns (Figure S5). A MATLAB script was used to identify which design and density arrays the cells were located on. Each design consists of two alternating arrays, say array A and array B, and cells could either be on A or B. This configuration reduces the cell migration test to an 'ON' or 'OFF' binary test, specifically, on B or off B. As such, a Wilson statistical test was utilized to calculate the 95% confidence intervals for the cell navigation choices. The Wilson score interval is an improvement of the normal approximation interval[122] and yields reliable margin of error values.

4.4. Results and discussion

4.4.1. NSA design and fabrication

The NSA we introduce consists of arrays of seven different ordered nanodot arrays arranged according to a square lattice with coverages of 0%, 1%, 3%, 10%, 30%, 44% and 100% (Figure 12A). Each array measures 40 μm × 400 μm, with nanodots of the same size equally spaced apart. Each design consists of a pair of alternating arrays with a lower and a higher density array, repeated five times, rendering each design footprint at 400 × 400 μm^2 (Figure 12B). To test the effect of the nanodot sizes on cell migration, we included nanodots with three different dimensions of 200 × 200 nm^2, 400 × 400 nm^2 or 800 × 800 nm^2 in the NSA. As such, we designed three sets of 21 unique binary combinations while conserving the nanodot size per design, totaling 63 nanodot stripe designs.

The array width for NSA designs was chosen based on the size of C2C12 myoblasts right after surface adhesion, with an average diameter of approximately 20 μm. An array width of 40 μm was chosen (i) to minimize the cell populations that could be positioned only on one array as these cells will experience one surface density and provide no useful information about cell migration choices, and (ii) to prevent a single cell from overlapping and presenting its leading and trailing edges with the same protein concentrations which will prevent clear cell choices. As such 20 μm was the minimum array width possible, and 40 μm satisfied both criteria.

Designs are referred to as C:A–B where C is the nanodot size, A is the lower density array and B is the higher density array, as shown in figure 12 and figure S1. For example, 200:3–30 refers to a 200 × 200 nm^2 nanodot size design with alternating arrays of 3% and 30% densities. The NSA design resembles a stripes design format, except it is made of nanodots of different surface coverages to modulate the local surface protein density, and include intermediate coverages within the extremes of 0% and 100% coverages. To enable studying migration across the different surface coverage densities, three step gradient designs made by stair-casing the five nanodot stripes with 1, 3, 10, 30 and 44% coverages were added to the NSA platform. The nanodot size was kept constant in each gradient array. In overall, the NSA provide a systematic and direct comparison of haptotaxis responses towards different nanodot stripes combinations, ranging from low to high surface densities with 66 different designs from a single print (Figure S3).

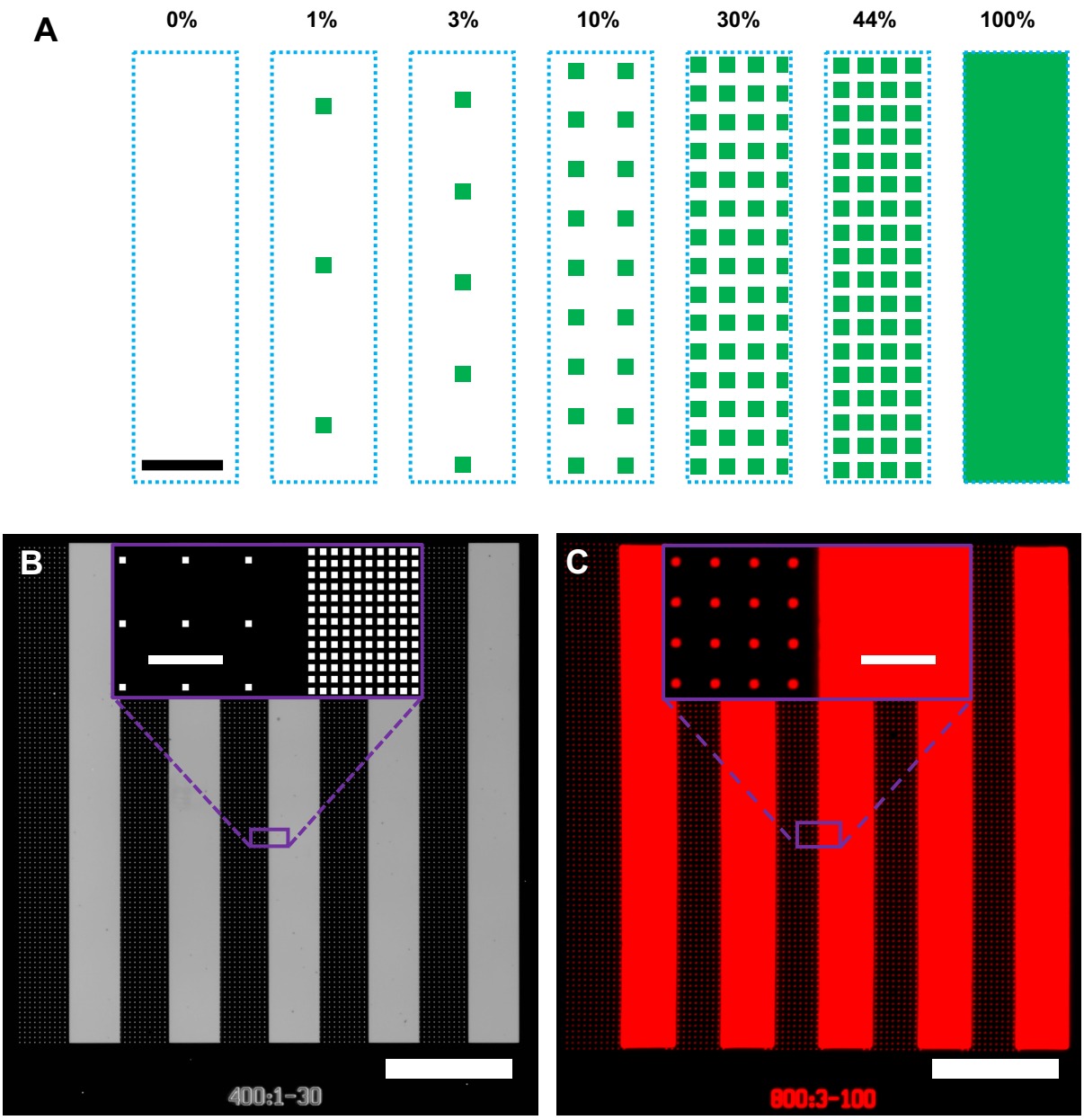

Figure 12: **A)** Schematic visualizations of the seven different nanodot stripes showing the different surface coverages utilized in designing the NSA. These representative arrays are made of 200 × 200 nm^2 nanodots. **B)** 400:1-30 NSA design, made of 400 × 400 nm^2 nanodots with 1% and 30% alternating arrays, etched onto the silicon mold. Insert shows 400 × 400 nm^2 nanodots highlighting the density step at the interface of the 1% and 30% arrays. **C)** Arrays of surface-anchored fluorescent netrin-1 proteins, patterned via nanocontact printing, showing design 800:3–100 with nanodot arrays of 3% and 100% (stripe) coverages. Scale bars: A) 1 µm, B) 100 µm, C) 100 µm (10 µm for inserts).

4.4.2. Cell migration choices on the netrin-1 NSA

Cell migration processes commence with cell transmembrane receptors binding to surface-attached protein ligands via cell adhesion molecules such as integrins. These receptor-ligand junctions establish macromolecular protein complexes called focal adhesions.[10,14,15] Ligand concentration differences between the leading and trailing edges determine the cell's migration polarity.[13] When a cell is presented with a chemoattractive protein surface cue, like netrin-1, the leading edge undergoes actin polymerization which trigger membrane protrusions in the front and actin retrograde flow, process involved in cell migration.[16,17,123] In this study, we used the NSA to examine contact-mediated cell navigation choices of C2C12 myoblasts towards different density nanodot stripes of netrin-1. C2C12 cells scan the surrounding microenvironment resulting in neogenin receptors binding to netrin-1 ligands anchored on the surface. Based on the surface ligand density, C2C12 myoblasts establish a migration polarity and preferentially migrate onto nanodot stripes with the density of choice, resulting in cells accumulating on the preferred stripes. Figure 13 shows preferentially migrated myoblasts on fluorescent netrin-1 prints at the end of the migration assay. To ensure that cellular haptotaxis choices were not by chance, we compared migration results on netrin-1 NSA to negative control assay results, where we printed fluorescent Immunoglobulin-G (IgG), devoid of ligands to bind cells and no affinity for cell domains.

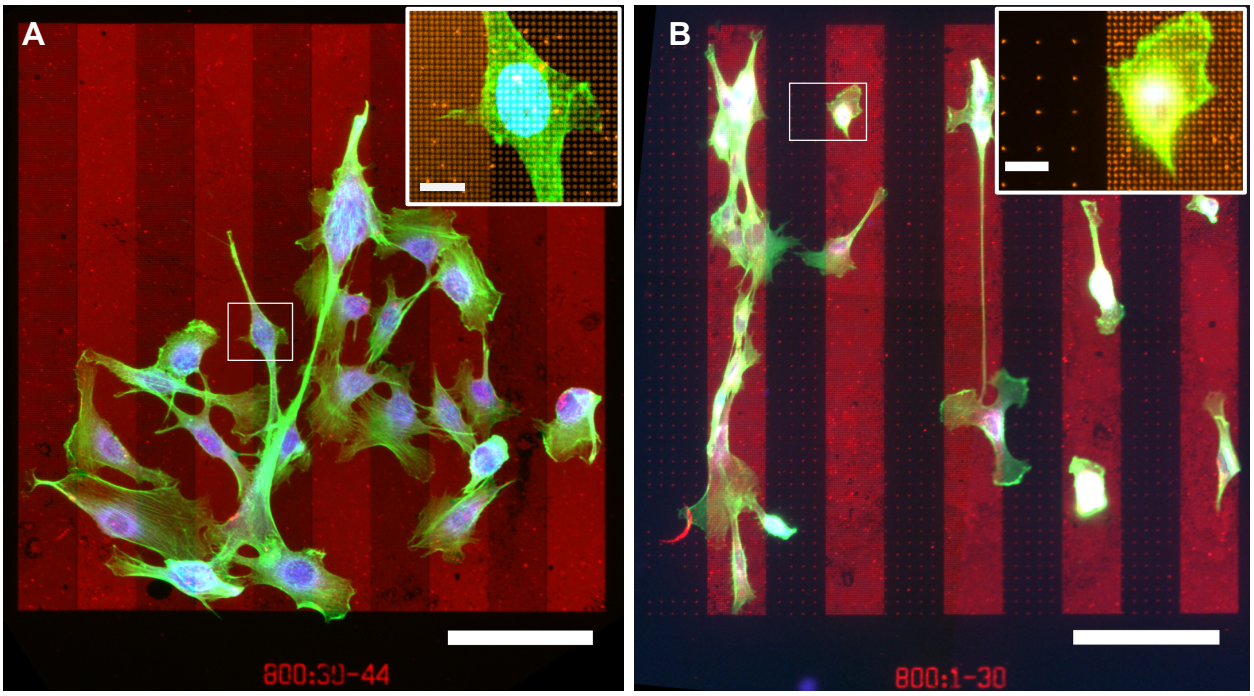

Figure 13: NSA haptotaxis responses of C2C12 myoblasts on surface-anchored netrin-1 where the RS was backfilled with 90:10 %PEG:%PDL. Cells were fixed and stained 18 h after seeding. **A)** Composite image of netrin-1 (red), cells (green) and nucleus (blue) for cell distribution on design 800:30–44 showing no cell preferences for either netrin-1 arrays. **B)** A composite image for netrin-1 and cells on design 800:1–30 showing that cells preferentially migrate onto higher density arrays. Scale bar is 100 µm (10 µm for inserts).

Myoblasts haptotaxis choice results were analyzed for each design by calculating the ratio of cells on each of the alternated arrays relative to the total cells. We computed the relative cell distribution percentage using equation 1.

$$Higher\ density\ preference\ ratio\ = \frac{Number\ of\ cells\ on\ B}{Number\ of\ cells\ on\ A\ and\ B} \qquad [1]$$

where *A* and *B* are the coverage densities of alternated arrays per design, and *B* has a higher density than *A*. For instance, in the design 800:3–100, A = 3% and B = 100%.

Cell migration choices are independent of protein nanodot sizes: We examined the effects of nanodot sizes on cell migration choices by observing myoblasts haptotaxis responses on the NSA with three different nanodot sizes. Each nanodot accommodates (nano)clusters of netrin-1 proteins. Cell choice results were compared on three nanodot sizes across the 21 different NSA designs (Figure 14). We verified our printed nanodots matched the design dimensions, but also the efficacy of nanocontact printing, which has previously been shown to retain the size of the nanodots from design sketches to final patterns on substrates.[61,94] Contrary to several publications,[10,14,15,112,119] our results show that cell navigation choices are independent of the size of the nanodots (or protein nanoclusters). Therefore, we concluded that it is the overall surface ligand density that dictates cell migration preferences. Coyer and colleagues claimed that fibronectin nanoislands with an area of 0.11 μm^2, from 333 × 333 nm^2 nanodots, were not sufficient for focal adhesions maturation.[10] Our netrin-1 nanosquares with 200 × 200 nm^2 (64% smaller than the above limit of 0.11 μm^2), perform just as well as the 400 × 400 nm^2 and 800 × 800 nm^2 netrin-1 nanodots. To obtain quantitative molecular data from nanodot arrays, we would require focal adhesions size measurements across the three different nanodot sizes and cell migration velocities to inform on the ease of focal adhesion formation with regard to the dimensions of protein clusters.

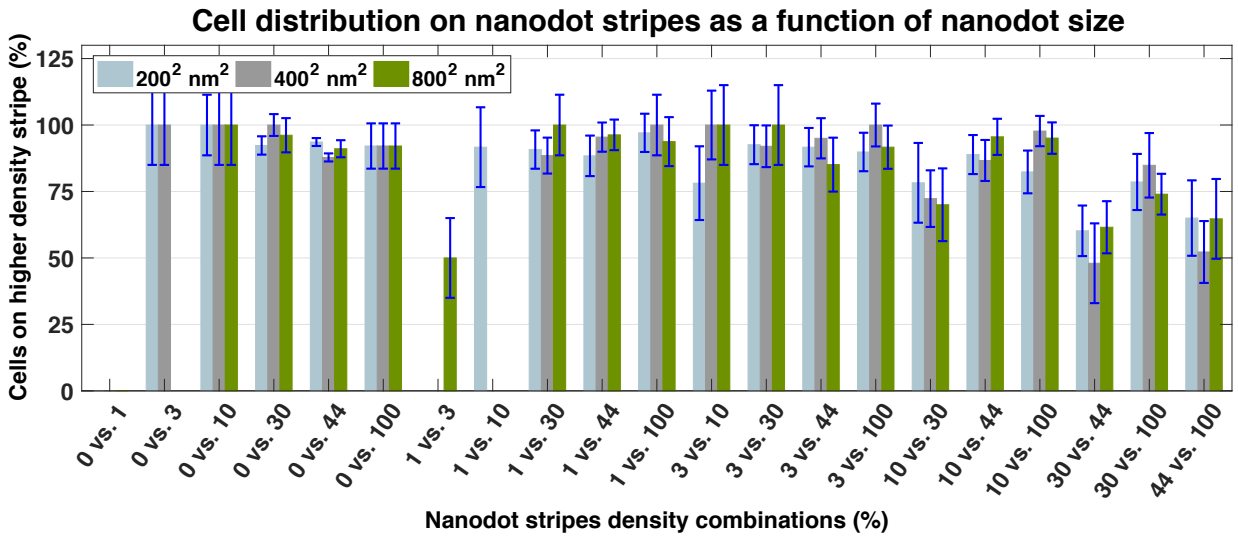

Figure 14: NSA cell migration results on netrin-1 nanodot stripes with different sizes, backfilled with the appropriate reference surface (shown below). The different sized nanodots do not alter cell migration behaviors. The legend shows a shortened notation for 200 × 200 nm^2, 400 × 400 nm^2 and 800 × 800 nm^2 nanodots. Error bars indicate 95% confidence intervals.

Cell preferentially choose higher netrin-1 density arrays, in the proper RS context: Controlling the cell-surface affinity levels of the RS is a must as it was previously shown to significantly interfere with haptotaxis results when not properly adjusted.[1] Different scientists use different extracellular matrix proteins or polymers at different concentrations to control the cell-surface affinity of the RS, or do not control it at all. For example, Sloan *et al.* studied chemoattraction to netrin-1 and sonic hedgehog and backfilled the RS with 0.1 μg/mL of PDL for an hour while Joo *et al.* backfilled with 0.1 mg/mL of PDL for two hours for his stem cell migration experiments,[5,104] a three orders of magnitude difference in PDL concentrations. Some experiments used laminin to backfill the RS despite the fact that laminin is an attractive cue itself,[68,105] and others let pre-hydrophylized surfaces dictate the surface affinity of the RS.[106] Uncontrolled RSs undermine the validity of the obtained results while a non-interfering or neutral RS guarantees cellular responses are specific to the protein cues under investigation. With this information in mind, it is surprising that most haptotaxis results are not defined in the context of the RS.

In this study, we demonstrate the need for carefully choosing the RS for haptotaxis assays involving nanodots, and show migration interferences as a consequence of using either a low or a high cell-surface affinity RS. We tested cell choices on netrin-1 and IgG (control) nanodot stripes, backfilled with three different volume ratios of PEG and PDL (%PEG:%PDL) to modulate the cell-surface affinity of the RS. These three different RS affinities resulted in remarkably different cell migration choices with two cases highlighting the RS interference on cellular migration behaviors. Notice that after demonstrating that NSA cell responses are independent of the size of the nanodots, we compiled and summarized the cell migration choices across different nanodot sizes in the next figures.

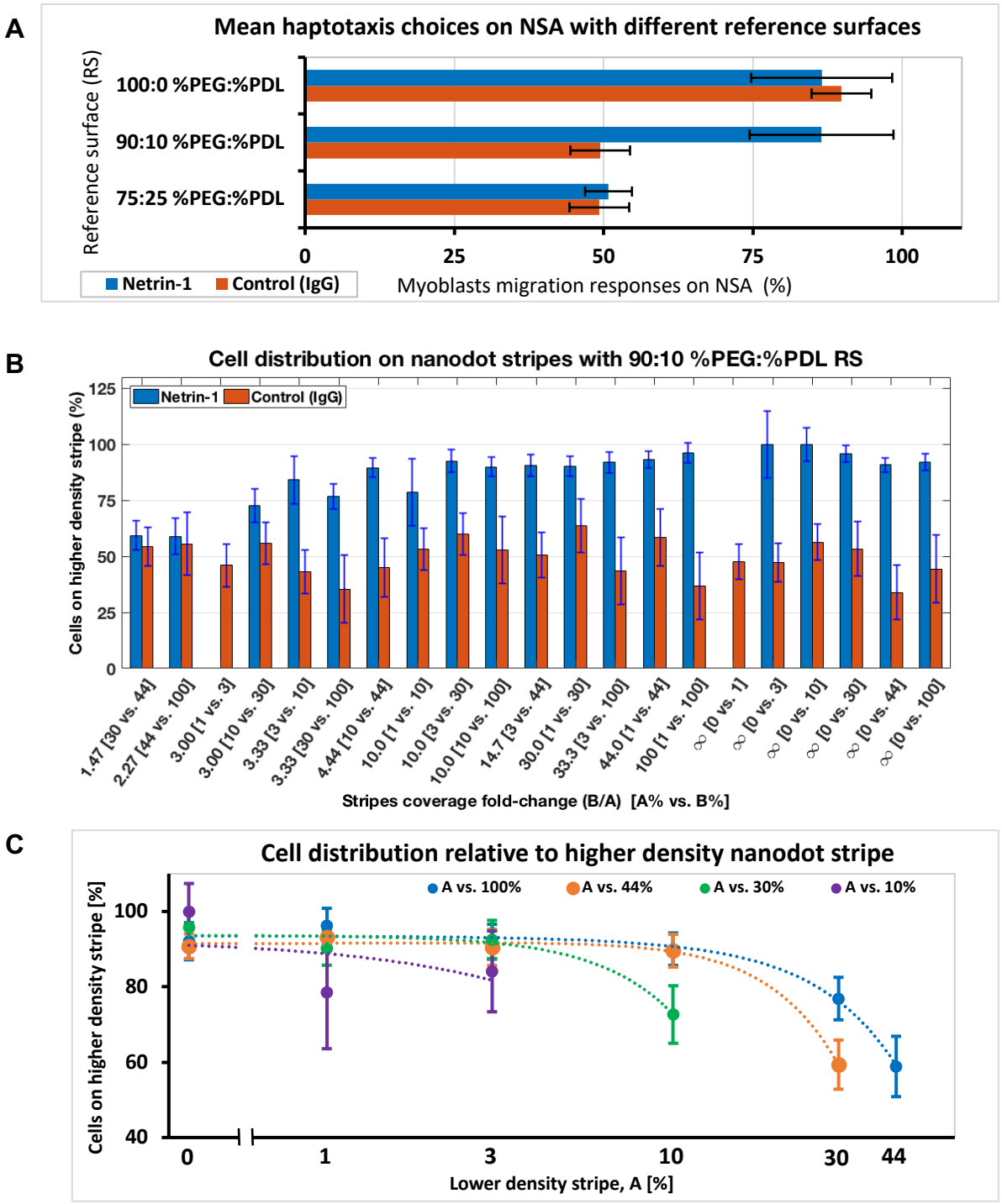

Figure 15: C2C12 myoblasts migration choices on netrin-1 and control NSAs. **A)** A summary of migration choices across different RS showing specific cell migration only for the 90:10 %PEG:%PDL RS. Essentially, a low cell-surface affinity (*i.e.* 100% PEG) RS pushes cells onto nanoarrays with higher surface coverage densities while a high cell-surface affinity

(75:25 %PEG:%PDL) masks the presence of netrin-1 and impedes migration preferences. Error bars indicate standard deviations from the 21 NSA designs. **B)** Comparison of cell response to netrin-1 vs. IgG on 90:10 %PEG:%PDL surface. Cell distribution on NSAs is in order of increasing ratio of high to low density stripe (B/A). **C)** Cell distribution plots indicative of haptotaxis choices on NSAs with constant high density stripe versus increasing lower density stripe. Here cell preferences strength for higher density stripe decreases as the fold-change between the two nanodot stripes decreases. Error bars in B) and C) indicate 95% confidence intervals.

A low cell-surface affinity of the RS was achieved by backfilling with 100:0 %PEG:%PDL, essentially 10 μm/mL PEG. In 16 out of 17 (>94%) designs, C2C12 myoblasts preferentially migrated onto arrays of higher surface densities in both the netrin-1 NSA and the control NSA (Figure 15A). The identical migration responses observed for netrin-1 and the IgG control, suggests that the cells' response is not netrin-1 specific, that is, the cells are attracted to either molecules. Therefore, we attribute this cellular response to the PEG that makes up the RS, as it is the only other parameter interacting with the cells. This was observed across different nanodot sizes (Figure S7). This result emphasizes the need to correctly adjust the cell-surface affinity of the RS in haptotaxis assays. Cell adhesion experiments on this RS, showed that a very small number of cells can thrive on this surface (Figure S11). This result suggests that PEG reduces the cell-surface affinity to below the threshold required to support cell attachment and survival for adhesive cells such as the myoblasts studied here. Notably, cell adhesion tests indicated that, as low as 10% of cell attractive molecules (such as PDL present in the RS (*i.e.*, a RS of 90:10 %PEG:%PDL), show that cell adhesion and survival is fully supported (Figure 11). PDL is a growth permissive biomolecule widely used for adherent cells in cell culture studies. The cell-to-PDL interaction is mediated by electrostatic interactions where PDL's positively charged chains bind to negatively charged cell membrane domains.[107,108]

A higher cell-surface affinity RS prevents chemoattraction of cells towards netrin-1. When a RS of 75:25 %PEG:%PDL was utilized in this study, cells on netrin-1 and IgG NSAs were randomly distributed demonstrating a lack of preferential migration and no cellular choices towards higher density arrays (Figure 15A). The absence of a response to netrin-1 suggests that the cell-surface affinity of the RS masks the chemoattractive netrin-1 cue, thus preventing cells from preferentially

migrating onto netrin-1 stripes and netrin-1 nanodot stripes of higher densities. Expectedly, this was observed across different nanodot sizes (Figure S8). The netrin-1 concentration was kept constant in all our assays, thus the cell-affinity of the RS is relatively high in this condition, and effectively preventing directional cell migration. The RS contains PDL at higher concentrations (2.5 μg/mL of PDL), than the previous two conditions, making the RS compete with netrin-1 signals resulting in 50:50 cell navigation choices. Substrates coated with high PDL concentrations have been shown to slow down cell migration velocities.[1] Here, consistent with previous observations, the C2C12 myoblasts migration is completely prevented.

The ideal cell-surface affinity of the RS should permit maximal netrin-1-specific chemoattraction cell responses. As observed in 17 out of 19 (~89%) NSA designs, C2C12 myoblasts migrated preferentially onto higher netrin-1 density nanodot stripes when the RS was backfilled with 90:10 %PEG:%PDL (Figure 15). The same migration choices were observed when cells were presented with nanodots versus stripes, where cells prefer the stripes as they have higher surface concentrations (100%) of netrin-1. The negative control of IgG on this RS led to random cell distributions on the nanodot stripes, confirming that this RS results in netrin-1 specific cellular responses. Cell preferences for individual nanodot sizes are presented in Figure S9 and show no significant differences. The NSA cell choice results in figure 15B are arranged in order of increasing protein density fold change between the two alternating arrays, characterized by the ratio of the higher density array to the lower density per design combination. Here, the percentage of cells choosing higher density nanodot stripes increases with an increase in the coverage fold change. Therefore, cell haptotaxis choices are a function of the coverage fold change, and not just the concentration step size in the two alternating arrays. For instance, the design 30% vs. 44% has a netrin-1 concentration difference of 14% but no cell preferences, while the design 3% vs. 10% (with 7% concentration difference) results in significant cell preferences. All NSAs feature a 3-fold or a 3.3-fold increase between the low and high densities, with the exception of the stripe at 44% coverage (which is the highest density achievable with 200^2 nm^2 nanodots), and which represents a change of only 1.47 relative to 30%, while 100% constitutes an increase of only 2.27, respectively. For both the 30% vs. 44% and the 44% vs. 100% arrays, cells show no preferences, indicating that cells could not differentiate a density increase of 2.27 or lower (at high local density), but can differentiate for density increase of 3 or higher for all arrays with surface coverages $\geq$ 3%.

Cell migration on step gradient arrays: The NSA can differentiate cell responses that are otherwise masked on gradient assays. The step-gradient assay (Figure 16) shows that cells migrate from 30% to 44% netrin-1 coverages, which based on the other experiments is not an actual response, but simply the extension of the cell migration trajectory. Expectedly in the step gradient assay, C2C12 myoblasts migrated from lower density nanodot stripes of 1%, 3% and 10% to higher density stripes with 30% and 44% netrin-1 coverages. Approximately 6% of the C2C12 myoblasts preferred arrays with 1%, 3%, and 10%, with the majority (~94%) choosing 30% and 44% coverages. Contrary to the absence of cell choices in NSAs with high density stripes, here there is a significant difference of ~21% between cell preferences on the 30% and 44% nanodot stripes, the latter with a high cell preference. We hypothesize that in the step-gradient designs, the already motile cells from the lower density arrays (1, 3 and 10%) continued tracking past the 30% and 44% stripes interface because the already motile and polarized cells have acquired elevated levels of migration directional persistence. Long-timescales of directional persistence have been reported to occur on stimulated cells leading to directional persistence times in the order of minutes.[116] Signaling pathways involving the small GTPase Rac and Arp2/3 are known to prolong positive feedback loops that maintain actin polymerization at the cell's leading edge and sustain the cell's direction based on initial events.[8] Here the cell continues migrating in a predetermined direction without re-calibrating its migration axis and locomotion based on the local cues. As such, the final cell distributions are not indicative of the cell choices dictated by the protein gradient. Notably, not all cells cross over to the 44% nanodot stripe as some cells are originally on the 30% array and remain there as they never attain a cell polarity, and acquire the migration directional persistence state. Directional persistence most likely masks saturation effects that would otherwise be observed if the cell was still actively integrating signals from the high density surface ligands. The combined results of the NSA and the step gradient assays suggest that in gradient-type experiments, it may not be possible to differentiate between cell choice, and continuation of cell migration owing to previous polarization and signaling inputs.

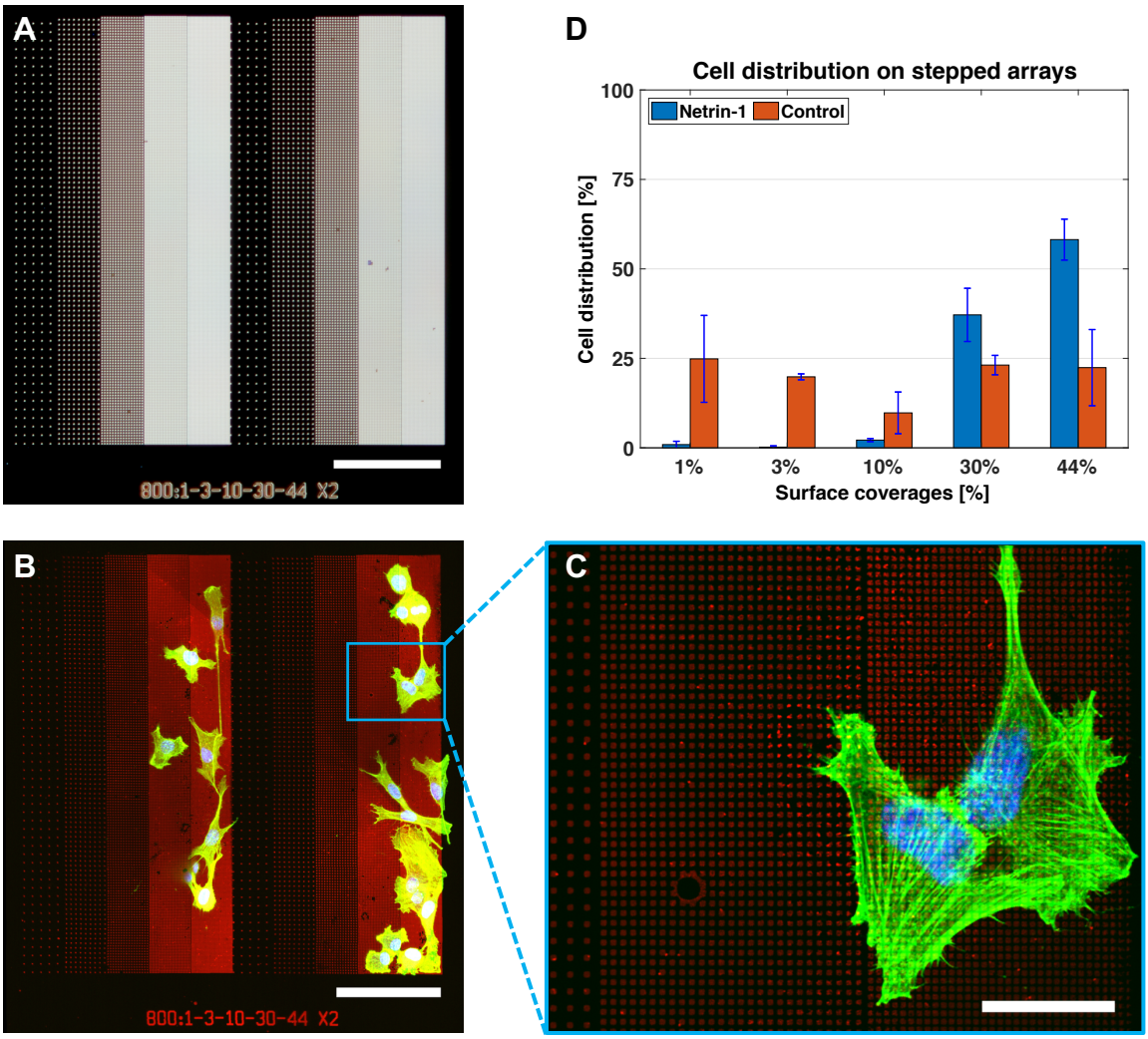

Figure 16: Cell migration on stepped designs backfilled with 90:10 %PEG:%PDL as the RS. **A)** Stepped gradient arrays on a silicon mold showing 1, 3, 10, 30 and 44% arrays, repeated twice in the x-direction, made of 800 × 800 nm^2 nanodots. **B)** A composite image of myoblasts on the stepped patterns showing that cells preferentially migrated onto the 30% and 44% density arrays. **C)** An insert showing a close view of C2C12 myoblasts on netrin-1 nanodots. **D)** Haptotaxis results on stepped arrays clearly show that cells accumulate on the 30% and 44% netrin-1 density arrays and are randomly distributed on the control (IgG) arrays. Scale bar is 100 µm and 20 µm for insert. Error bars indicate 95% confidence intervals.

4.5. Conclusions

The NSA allows for the systematic study of cellular haptotaxis choices between low and high protein surface densities across seven different coverages and three nanodot sizes resulting in 63 different concentration steps. Unlike classical stripes that only offer 0% and 100% densities, providing limited haptotaxis information, and gradients that complicate extraction of local migration choices, the NSA provide finer and richer information on cellular haptotaxis choices. The combined NSA and gradient assay results reported here showed that gradient assays suffer from directional persistence effects which temper with the final cell distributions especially on the higher end of the gradient. Essentially, with the NSA we observe cell responses which cannot be discovered in gradient assays due to cell migration directional persistence. Therefore, the NSA we introduce, provide accurate and clear migration results to inform on the true initial and final cell decisions which have been masked previously.

The NSA cell migration responses reported herein revealed that (i) the minimum cell recognizable netrin-1 surface concentration is ~3% coverage, and (ii) that cell migration choices are a function of the protein concentration coverage fold-change across a cell's leading and trailing edges. We demonstrated that with the appropriate reference surface (RS) affinities, provided by 90:10 %PEG:%PDL, C2C12 myoblasts preferentially migrated onto higher netrin-1 nanodot stripes only when the protein coverage concentration step was at least three-fold. Additionally, we showed that cell choices are independent of the size of protein nanodots which mediate ligand cluster dimensions, but cell haptotaxis decisions are dictated by the overall protein surface concentrations experienced by the entire cell body. We studied nanodot sizes from 0.04 μm^2 to 0.64 μm^2 where each nanodot consists of hundreds of netrin-1 ligands. To thoroughly assess the influence of ligand cluster sizes, patterns with single protein (ligand) distributions, as already pursued by other investigators,[119,124] would provide more conclusive results, especially when combined with quantitative focal adhesion dynamics.[15]

Future studies will use the NSA for colocalization experiments where receptor–ligand (*e.g.* neogenin–netrin-1) complexes will be investigated using fluorescent colocalization microscopy[98] or FRET imaging[125] techniques to explore receptor inhibition or sensitization, and receptor saturation in haptotaxing cells and neurons. Patterned guidance cues in the NSA can also be varied

from extracellular matrix proteins like fibronectin, laminin and vitronectin to neuronal guidance cues like slits, ephrins and semaphorins to investigate cell choices for different cell types towards chemoattractive and chemorepellent stimuli. To mimic *in vivo* physiological conditions, these future NSA experiments will utilize soft substrates as previously introduced by our group[36] and others.[126] The accrued knowledge can not only be used to accelerate tissue repair and direct regenerating axons, but understanding haptotaxis pathways would also help orient neurons for implant purposes resulting in improved device-to-body interfaces.[127]

Acknowledgements: *The authors would like to thank Mr. Grant Ongo, Dr. Sebastien Ricoult and Mr. Donald MacNearney for their advice on this project. We are grateful to Dr. Andy Ng and Dr. Christopher Corkery for their help editing this manuscript. M.D. received funding from the NeuroEngineering NSERC-CREATE. T.E.K. holds a Killam Foundation Scholar award. D.J. acknowledges a Canada Research Chair.*

Conflict of interest: *The authors declare no competing financial interest.*

4.6. Supplementary information

4.6.1. NSA coverage combinations and design equations

The number of discrete coverage densities to choose for the NSA was limited to seven between 0% and 100% inclusive. A 100% array is a stripe pattern, included here to provide a direct cell choice comparison to nanodot designs. We settled on exponential surface coverages given by M^i where $M = 3$ and $i = [0,\ 1,\ 2,\ 3,\ 4,\ 5, \dots, n]$. For each nanodot square size from the list; $200 \times 200, 400 \times 400$ and 800×800 nm^2, we then calculated the horizontal (x) and vertical (y) spacing between the nanosquares. The spacing for the arrays is specific to each surface coverage density. For each array design $x = y = center - to - center\ spacing$. The spacing was calculated using the equations:

$$x = y = k + s \qquad [2]$$

$$D = \frac{k^2}{(k+s)^2} \qquad [3]$$

$$s = \frac{-2kD \pm \sqrt{2kD^2 - 4D(Dk^2 - k^2)}}{2D} \qquad [4]$$

where, k is the nanodot width, s is the nanodot-to-nanodot gap size and D is the desired surface coverage density. Ultimately, the final densities were slightly adjusted for even distribution and the maximum nanodots coverage that can be achieved with the electron-beam lithography technique, which limits the spacing between features to ~100 nm producing a surface density of ~44%.

Squares of the desired nanodots were sketched as instances on L-Edit and arrayed to match different densities producing 40 µm × 400 µm arrays. Each design consists of two arrays with five alternating repeats covering a total area of 400 × 400 µm^2. Arrays were then paired and repeated accordingly. The number of possible different pairs from these coverages is a combination calculation, aC_b, where $a = 7\ and\ b = 2$ producing 21 different pairs, across three different nanodot sizes, totaling 63 designs. We added three stepped gradient arrays made by stair-casing the different density nanodot stripes in increasing order.

Table S1: The 21 different stripe density combinations used in the NSA showing the differences, fold change and dynamic ranges that exist between them.

Density A [%]	Density B [%]	Average density [%]	Density Difference [%]	Fold change [B/A]	Dynamic range [O.M.]
0	**1**	0.5	1	∞	-
0	**3**	1.5	3	∞	-
0	**10**	5	10	∞	-
0	**30**	15	30	∞	-
0	**44**	22	44	∞	-
0	**100**	50	100	∞	-
1	**3**	2	2	**3.0**	0.477
1	**10**	5.5	9	**10.0**	1.000
1	**30**	15.5	29	**30.0**	1.477
1	**44**	22.5	43	**44.0**	1.643
1	**100**	50.5	99	**100.0**	2.000
3	**10**	6.5	7	**3.3**	0.523
3	**30**	16.5	27	**10.0**	1.000
3	**44**	23.5	41	**14.7**	1.166
3	**100**	51.5	97	**33.3**	1.523
10	**30**	20	20	**3.0**	0.477
10	**44**	27	34	**4.4**	0.643
10	**100**	55	90	**10.0**	1.000
30	**44**	37	14	**1.5**	0.166
30	**100**	65	70	**3.3**	0.523
44	**100**	72	56	**2.3**	0.357

800:1-100	800:3-100	800:10-100	800:30-100	800:44-100	400:44-100	400:30-100	400:10-100	400:3-100	400:1-100
200:1-100	200:3-100	200:10-100	*400:1-0	*200:1-0	*200:10-0	*200:44-0	0:100	200:30-100	200:44-100
800:3-44	800:10-0	800:10-30	800:10-44	800:30-0	800:30-44	800:44-0	800-stepped	*200-stepped	*400-stepped
400-stepped	400:44-0	800:1-0	800:1-3	800:1-10	800:1-30	800:1-44	800:3-0	800:3-10	800:3-30
400:1-0	400:1-3	400:1-10	400:1-30	400:1-44	400:10-0	400:10-30	400:10-44	400:30-0	400:30-44
200:10-0	200:10-30	200:10-44	200:30-0	200:30-44	200-stepped	400:3-0	400:3-10	400:3-30	400:3-44
200:1-0	200:1-3	200:1-10	200:1-30	200:1-44	200:3-0	200:3-10	200:3-30	200:3-44	200:44-0

Figure S1: The 63 different combinations for the NSA designs plus three stepped arrays, as they were arranged on the mask. An asterisk denotes a design that was repeated to fit the seven by ten mask set-up.

4.6.2. NSA fabrication process flow

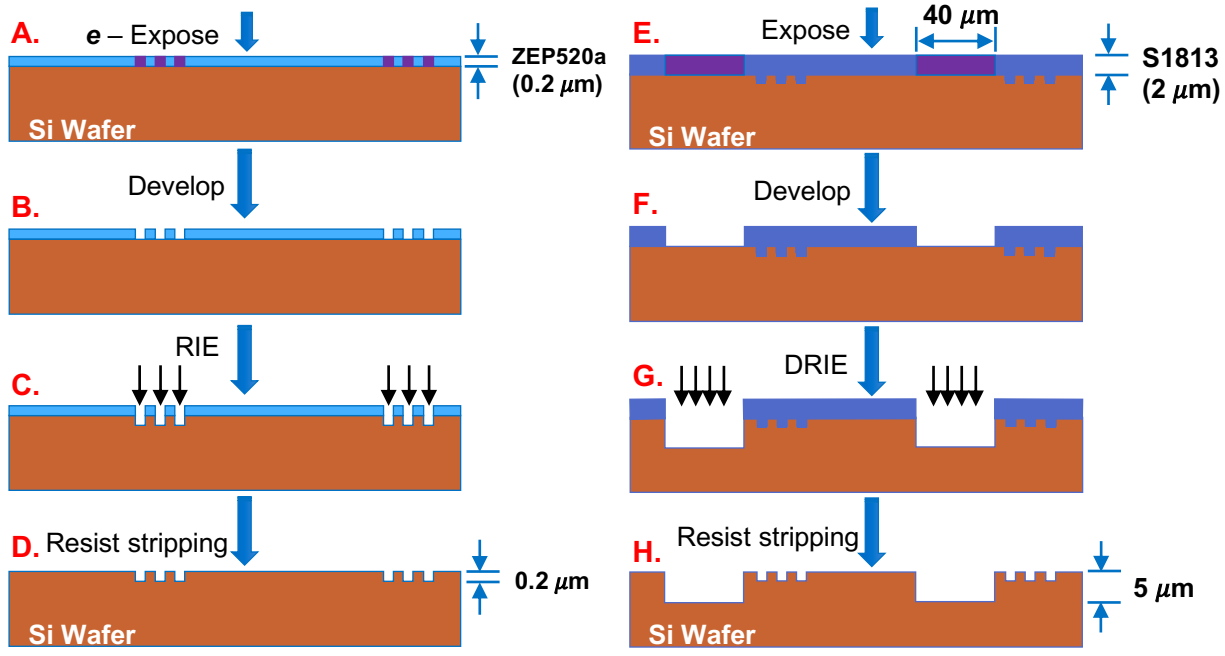

Figure S2: The fabrication process flow for the nanodot stripe assay (NSA) wafer. **A–D:** Nanodots are patterned using e-beam lithography generating 200 nm holes in silicon after reactive ion etching with SF6/C4F8 plasma. **E–H:** Stripes are patterned on a positive Shipley resist using UV direct writing, and then channels were etched using the Bosch process, a deep reactive ion etching process.

4.6.3. NSA designs overview on Si mold

Below are images of the designs showing an overview of the different NSA designs on the silicon mold with a few zoomed in designs for nanodots visualizations.

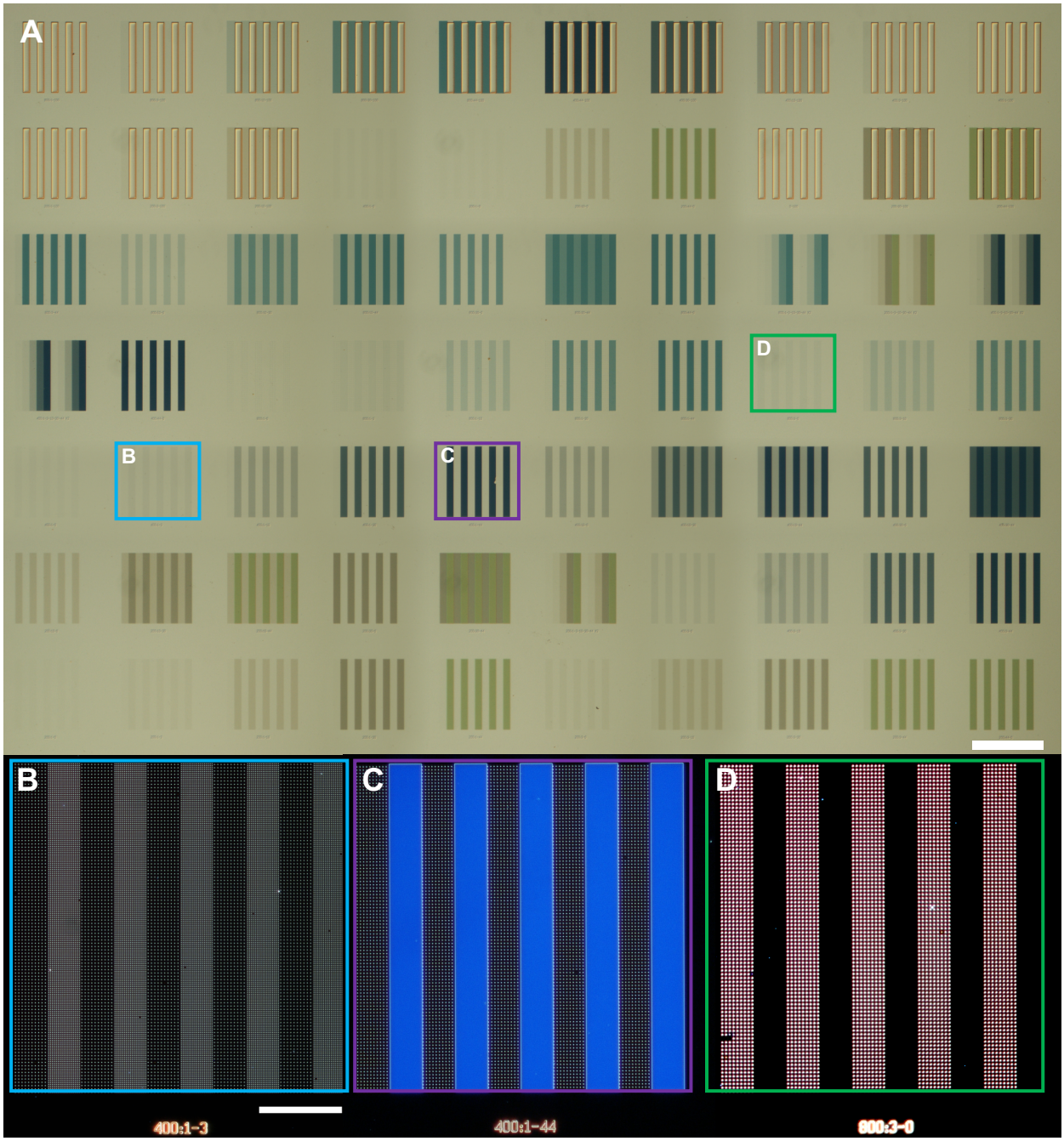

Figure S3: The NSA designs on the silicon mold. An overview of all the designs is shown in **A)**. **B)** through **D)** shows examples of some of the designs showing the nanodot features. Densely packed nanodots appear as stripes at 10X magnification. Additionally, the observed colors are due to structural coloration as the wafer was not colored. Scale bar: A is 400 µm and B is 100 µm.

4.6.4. Mold replication and protein patterning procedure

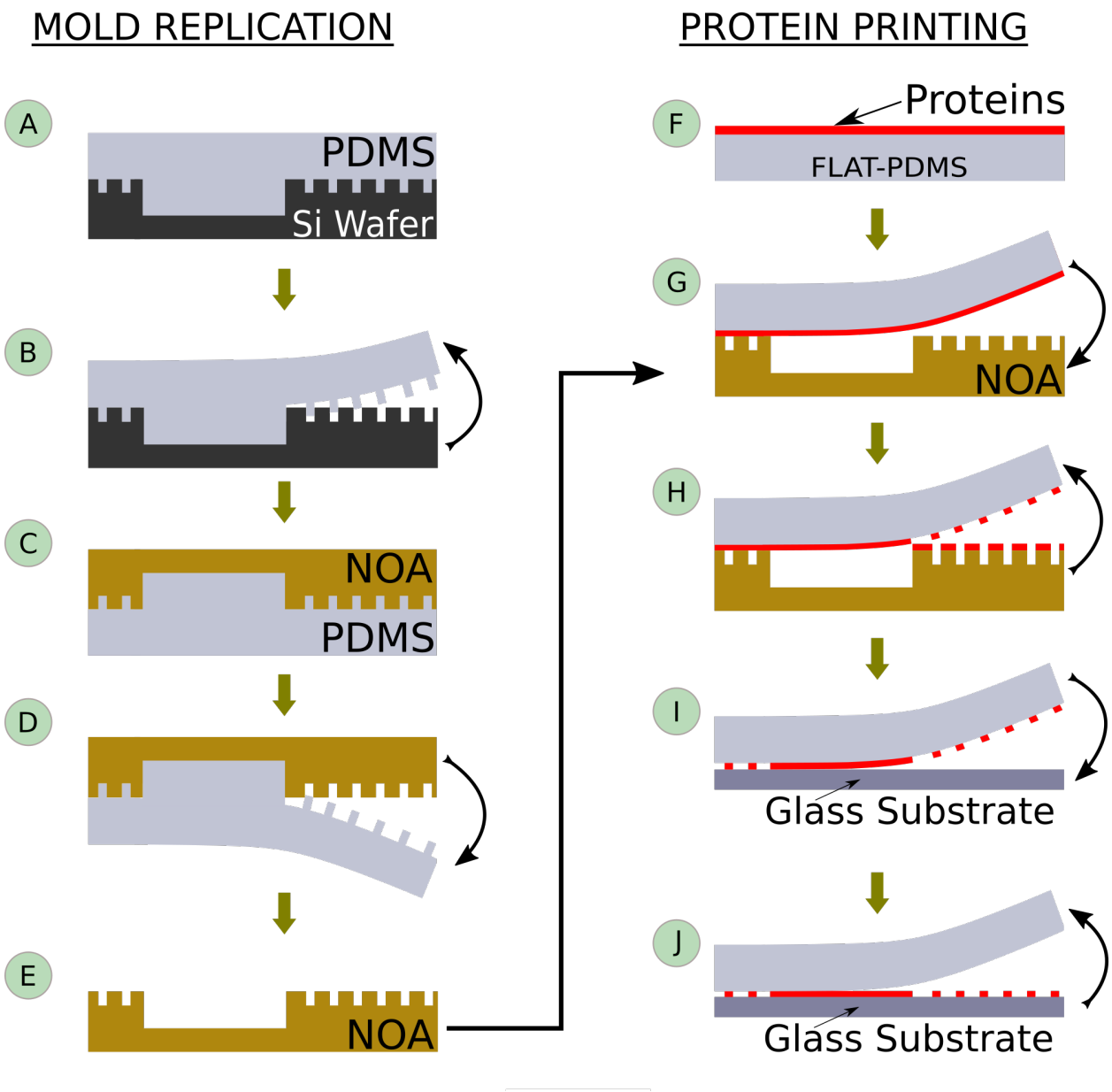

Figure S4: Schematic showing the lift-off nanocontact printing and protein patterning technique steps. Stamp replication from the original silicon master to PDMS and to NOA-63 **[A–E]**. Proteins are then inked in **[F]**, lifted-off in **[G–H]** with the plasm-activated NOA stamp and finally transferred onto the plasma-treated glass cover slip **[I–J]**.

4.6.5. NSA data extraction procedure

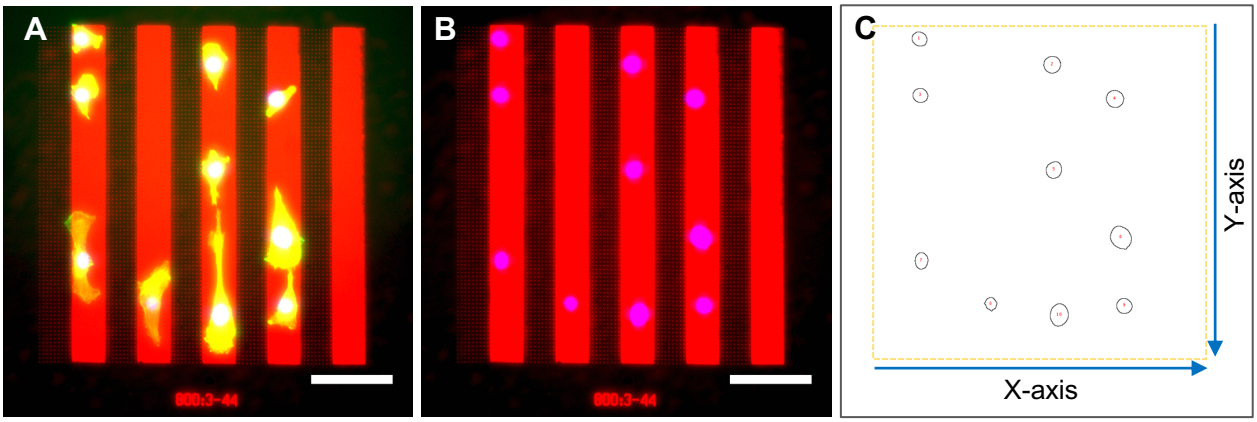

Figure S5: Data extraction procedure. **A)** Shows a composite image for netrin-1 prints and cells on design 800:3–44 after performing the 18 h cell migration assay. **B)** The nucleus was considered as the cell position and overlayed on prints. **C)** Image J was used to extract the x and y coordinates of the nuclei in the identified region of interest. Scale bar is 100 µm.

4.6.6. Cell migration images

The following are representative images of cells on the NSA migration platform after performing the haptotaxis assay.

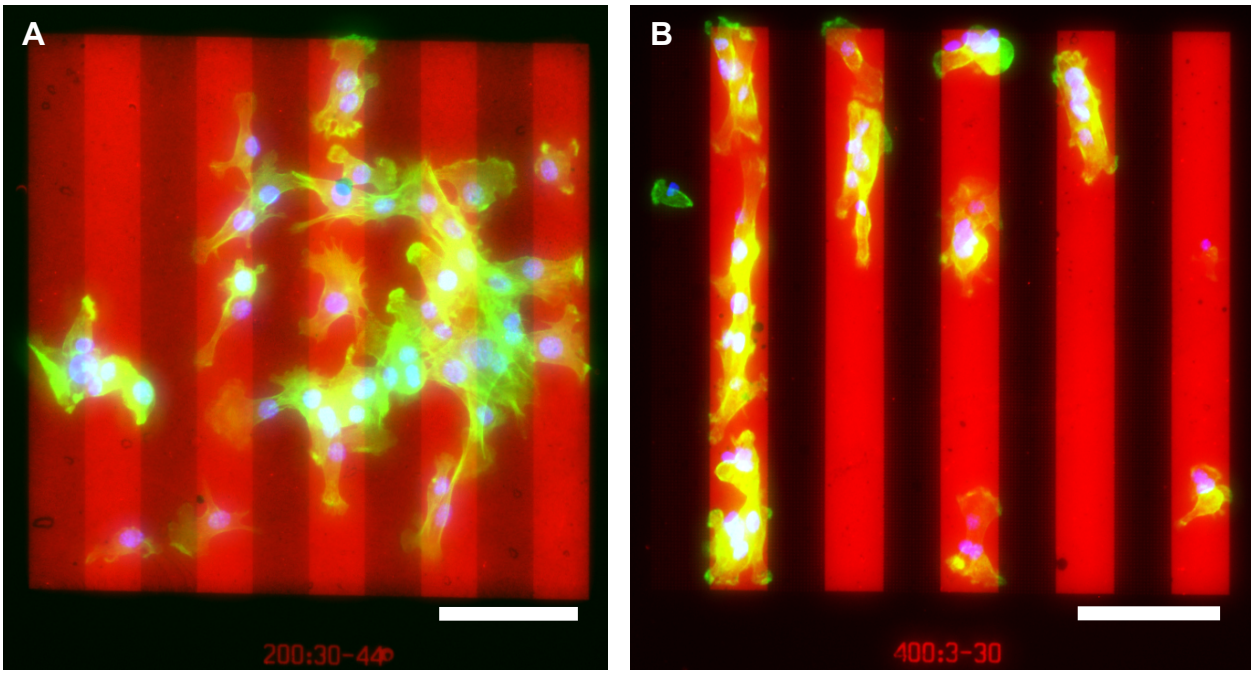

Figure S6: Cell migration images for netrin-1 on 200:30-44 and 400:3-30 NSA designs backfilled with 90:10 %PEG:%PDL as the reference surface. In **A)** cells are randomly distributed on the 30% and 44% arrays while in **B)** cells preferentially choose 30% over 3% netrin-1 surface density. Scale bar is 100 μm.

4.6.7. Complementary cell migration data

The following plots show cell navigation choices on different RSs and on different-sized nanodots. The fraction of cells (percentage) on the higher density array on the NSA designs is presented for each design pair. No cells were found on designs without a bar.

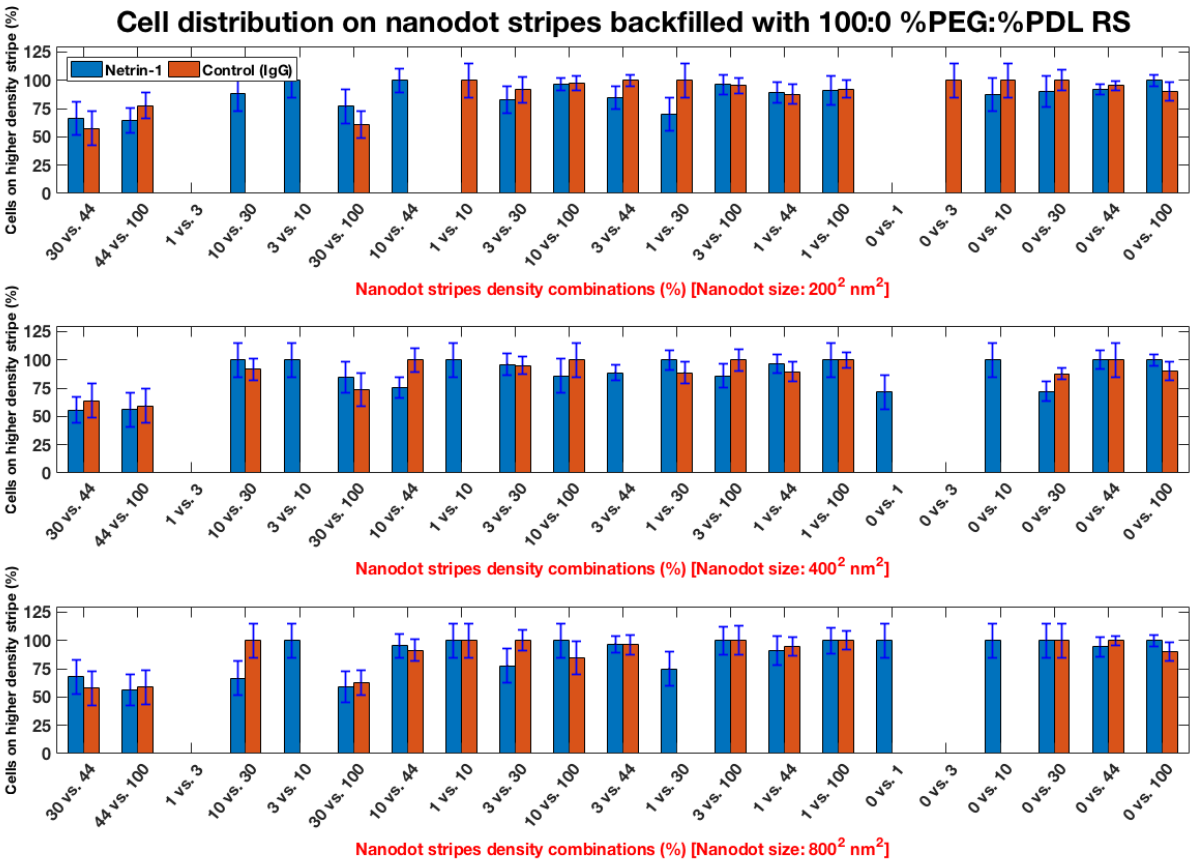

Figure S7: NSA migration choices of C2C12 myoblasts on netrin-1 nanodot stripes backfilled with 100:0 %PEG:%PDL as the RS. In this condition, the RS is dominated by PEG which has a low cell-surface affinity, therefore, cells are repelled onto the printed cue and even onto the non-cell binding IgG. The observed response, therefore, is due to the repellent RS, not the netrin-1 cue. This migration result interference applies to all the designs across the different nanodot sizes. Error bars indicate 95% confidence intervals.

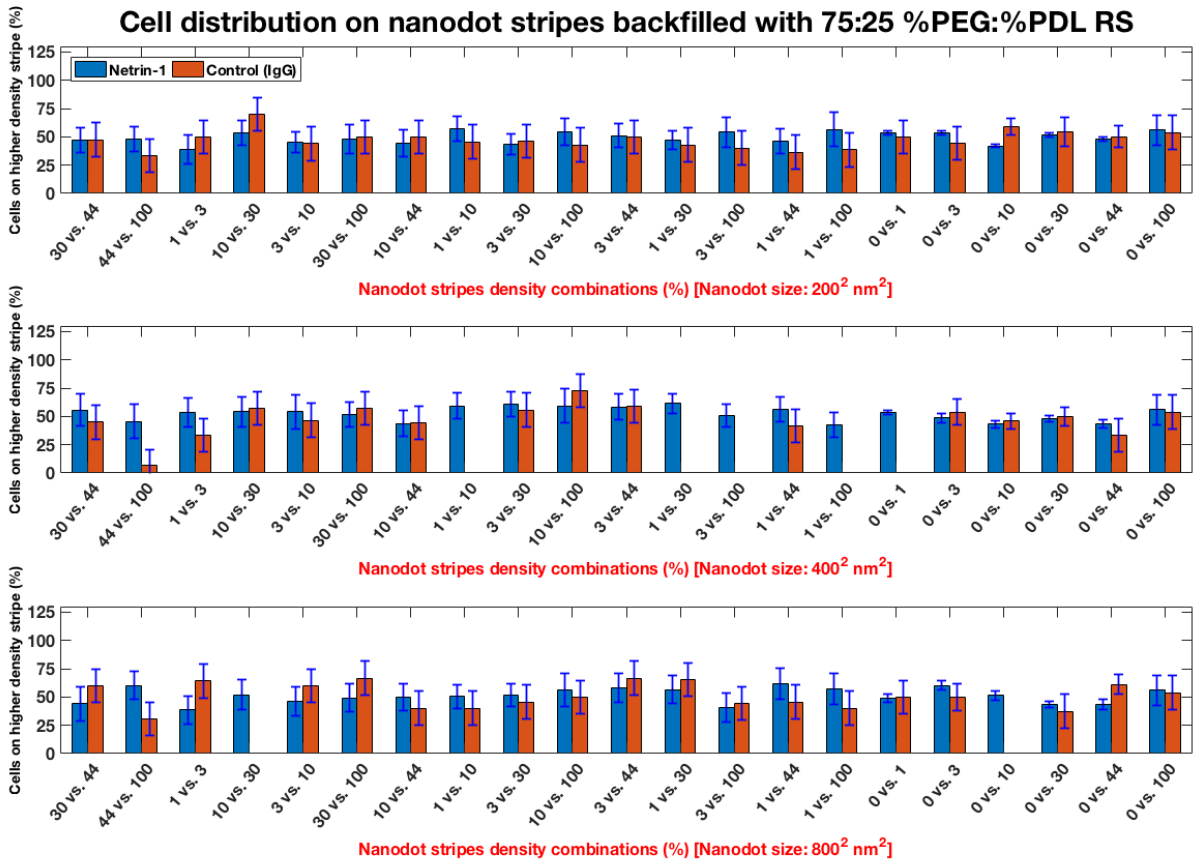

Figure S8: NSA migration choices of C2C12 myoblasts on netrin-1 nanodot stripes backfilled with 75:25 %PEG:%PDL as the RS. Cells are randomly distributed in the presence of netrin-1 or IgG prints. As such, we conclude that cell choices are nullified by the high cell-surface affinity of the RS. The same migration behavior is observed across the different nanodot sizes. Error bars indicate 95% confidence intervals.

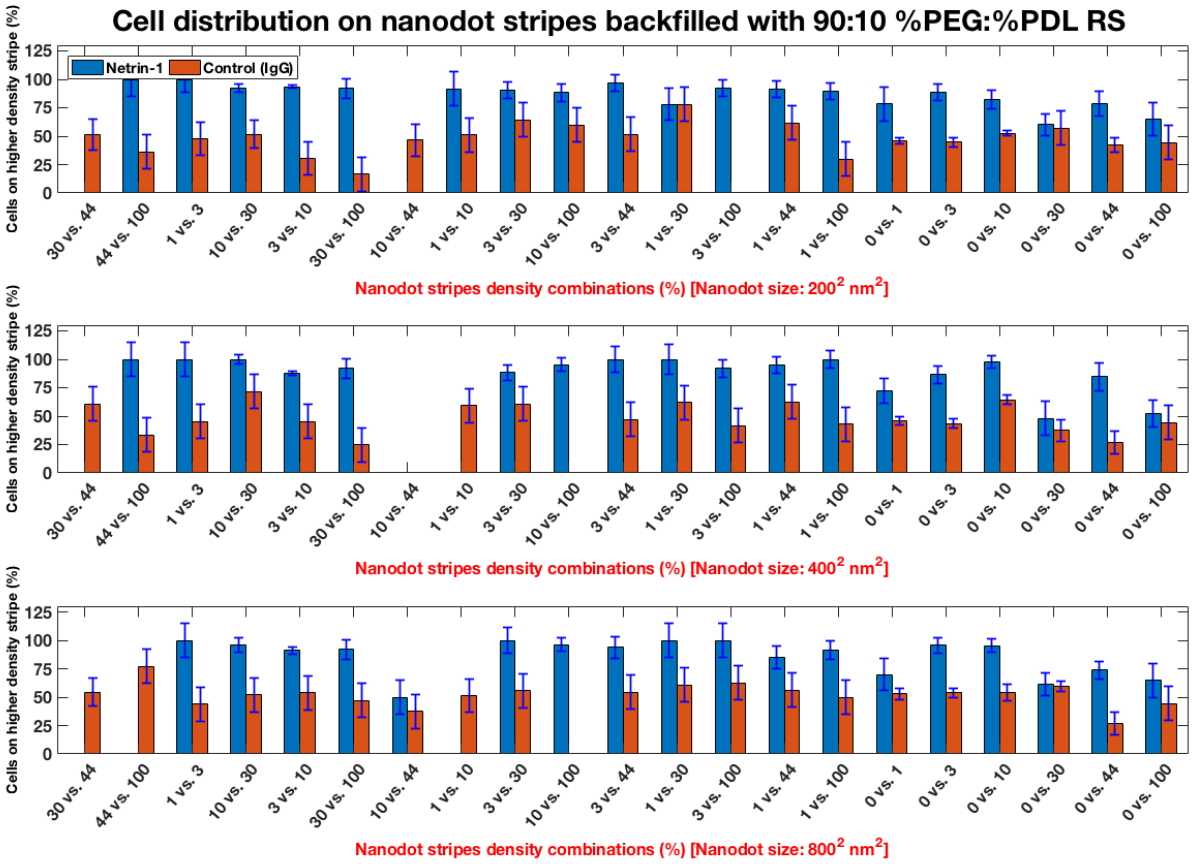

Figure S9: NSA migration choices of C2C12 myoblasts on netrin-1 nanodot stripes backfilled with 90:10 %PEG:%PDL as the RS. Generally, cells preferred the netrin-1 prints with higher densities while in the control groups, the cells are randomly distributed. Likewise, this applies to all designs regardless of the nanodot sizes. Error bars indicate 95% confidence intervals.

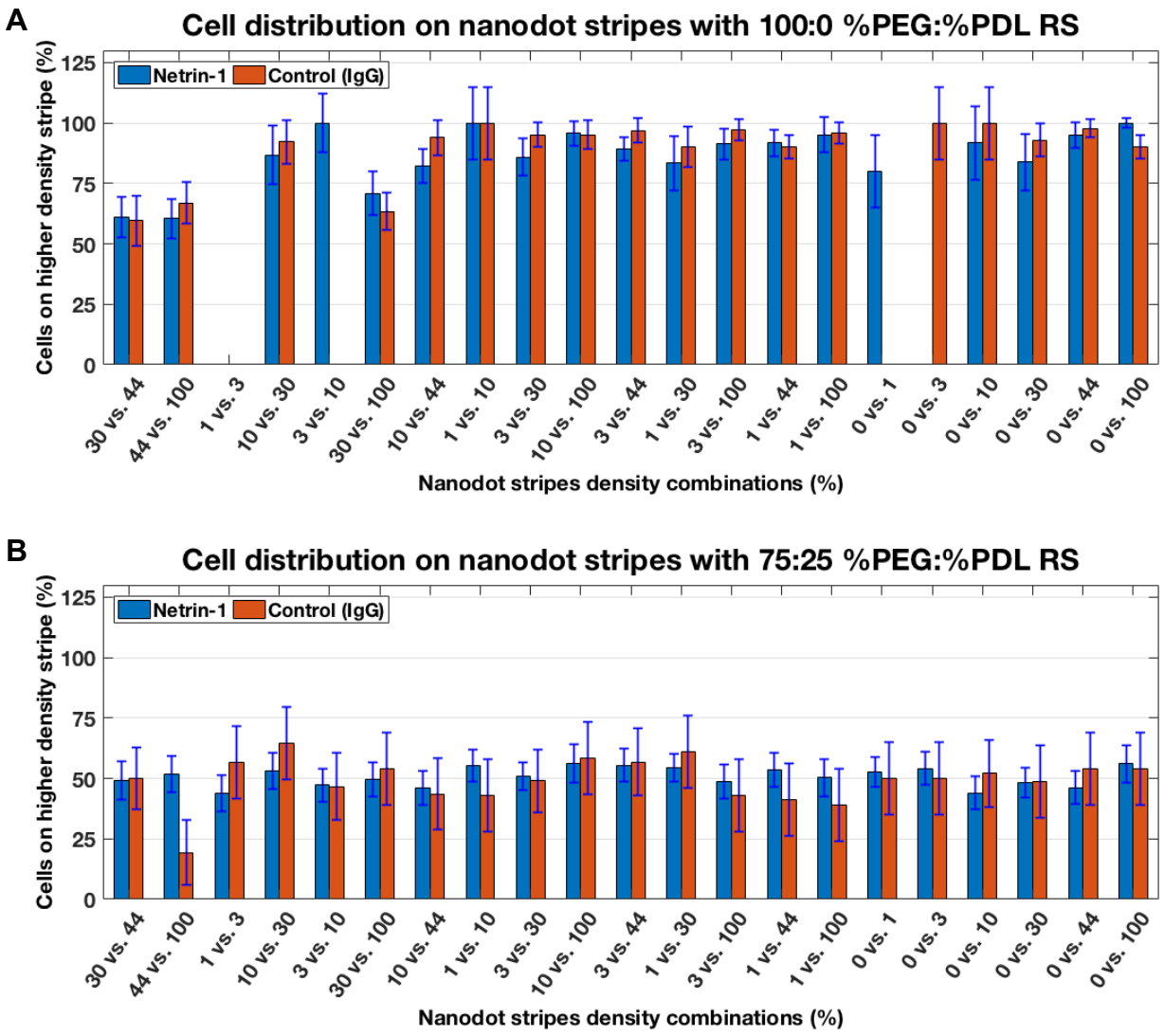

Figure S10: Haptotaxis choices on netrin-1 and control NSAs backfilled with low and high cell-surface affinity reference surfaces (RS). **A)** A RS with a low cell-surface affinity (*i.e.* 100% PEG) pushes cells onto nanoarrays with higher surface coverage densities. **B)** A RS with a high cell-surface affinity (75:25 %PEG:%PDL) impedes migration entirely by masking the presence of the attractive netrin-1 protein cue. These plots include migration on all the three different nanodot sizes. Error bars indicate 95% confidence intervals.

4.6.8. Cell migration data for analyzed cells

Table S2: The total number of cells observed and scored under the three different RS conditions.

	Reference Surface [%PEG: %PDL]					
	100:0		90:10		75:25	
NSA Design Pairs	Netrin-1	Control	Netrin-1	Control	Netrin-1	Control
0 vs. 01	10	0	2	147	241	8
1 vs. 03	3	0	2	102	162	23
0 vs. 03	0	2	5	127	194	34
3 vs. 10	12	0	44	95	195	45
1 vs. 10	4	6	14	109	217	21
0 vs. 10	12	4	22	142	209	46
30 vs. 44	131	84	214	125	147	54
10 vs. 30	30	38	128	104	173	17
3 vs. 30	78	81	108	100	271	53
1 vs. 30	42	51	165	58	307	36
0 vs. 30	37	57	121	60	244	39
10 vs. 44	113	49	192	51	189	39
3 vs. 44	159	63	147	89	209	44
1 vs. 44	97	142	189	53	194	34
0 vs. 44	77	88	304	56	195	37
44 vs. 100	139	115	141	45	166	31
30 vs. 100	96	145	212	31	189	24
10 vs. 100	71	61	190	17	144	24
3 vs. 100	80	70	137	23	189	14
1 vs. 100	41	94	79	19	157	18
0 vs. 100	99	153	201	27	150	39

5. CONCLUSION

5.1. Research summary

Herein, we optimized the cell-surface affinity of the reference surface (RS) for haptotaxis experiments by investigating different RSs in the range of 100:0 and 75:25 %PEG:%PDL using the classical stripe assay, and through cell-surface adhesion experiments. We found that a 90:10 %PEG:%PDL RS results in optimal chemoattraction cellular responses towards surface-anchored netrin-1 cues. Additionally, a RS of 90:10 %PEG:%PDL resulted in normal myoblast cell adhesion and proliferation rates. Using this RS composition, a nanodot stripe assay (NSA) was developed with 63 different binary nanodot stripe combinations, consisting of seven arrays of different densities made of three different nanodot sizes to examine cell haptotaxis responses. The NSA consists of nanodot stripes with 0, 1, 3, 10, 30, 44 and 100% coverages, where each stripe density is produced by orderly distributed 200 × 200 nm^2, 400 × 400 nm^2 or 800 × 800 nm^2 nanodots. The NSA design configuration is such that each design has a lower and a higher density nanodot stripe, made of nanodots of the same size.

NSA haptotaxis results show that C2C12 myoblasts preferentially migrated towards nanodot stripes with higher netrin-1 coverages only when the difference in netrin-1 concentration per nanodot stripe combination was at least three-fold. The NSA cell choice results presented here show that cell haptotaxis responses are independent of the size of the patterned netrin-1 nanodots of 200 × 200, 400 × 400 or 800 × 800 nm^2, but cell choices are governed by the overall netrin-1 surface coverages, regardless of the size of the protein clusters producing these densities. We found that our NSA permitted investigating cell responses on all different densities as cells do not suffer from migration directional persistence which masks cell responses at the higher end of gradient assays. In particular, while nanodot stripes of 30% vs. 44% coverages (lower than three-fold difference in netrin-1 concentration step) did not lead to haptotactic responses, an unexpected, yet statistically significant cell migration preference on these two nanodot stripes can be observed when they are part of a step gradient configuration (Figure 16). Therefore, the NSA as demonstrated herein, complements classical stripes and gradient arrays as it provides migration information that cannot be accessed in these other cell migration assays.

5.2. Future work

C2C12 myoblasts haptotaxis behaviors were similar on the three nanodot sizes tested in this research (Figure 14). Since these results contradict other studies pertaining cell migration dependence on the different dimensions of protein nanoclustsers,[10,14] further investigation with other cell types like fibroblasts and neurons is necessary to verify this effect. On that regard, the distribution and density of protein ligands within single nanodots (nanoclusters) has to be characterized to quantify the number of ligands per dot, which in turn, dictates the overall surface ligands density. The cell migration data presented in this document suggests that cell polarity and cell preferences between two surface densities is triggered by approximately three-fold surface concentration differences (Figure 15). In the future, this threshold ought to be verified for low density nanodot stripe combinations. Thereafter, more stripe combinations with fold changes between one- and three-fold (*e.g.* 1.5–fold) changes must be incorporated in the NSA and investigated. For instance, adding 15% and 20% nanodot stripes in the NSA could improve the accuracy of the threshold approximation. The lack of cell preferences in the 44% vs. 100% coverage design was attributed to a small fold change, but it is also likely that these high protein density stripes lead to neogenin receptors saturation. In the NSA, clear cell choices were observed with 30% vs. 100% stripe coverages while the 44% vs. 100% designs show no cell preferences, implying that the increase from 30% to 44% could have saturated the neogenin, the C2C12 myoblasts receptors. Beyond this saturation limit, cells are incapable of binding to more surface ligands and cannot detect an increase in cue concentration leading to no preferences when cells are challenged with higher density stripes. Further experimentation would be required to validate this possibility.

Comparing migration results from gradient assays and the NSA suggested that results from gradient assays are plagued with directional persistence effects. In the future, live experiments with tracking capabilities would be necessary to validate our hypothesis and provide quantifiable migration persistence values. Persistence could also be studied on its own, for example by forming step gradients that culminate in wide stripes, and the migration of cells followed with live imaging to monitor the shift from directional to random migrations in the absence of a surface concentration gradient or concentration step. The NSA, a directional persistence free platform, is also ideal for investigating cell signaling using inhibition (blocking) assays and fluorescent markers to monitor

and discover activated pathways and proteins in the cell haptotaxis transduction processes, in combination with different RS that may further modulate the sensitivity of cells.

5.2.1. Focal adhesions size measurements

The NSA introduced herein opens avenues to examine focal adhesion formation and maturation – which are prerequisites for cell migration – on different-sized protein nanodots. It was previously shown that for fibroblasts, cell migration velocities are a function of the size of focal adhesions.[128] Notably, small focal adhesions can increase cell migration velocities as these assemble and disassemble relatively fast. Additionally, small focal adhesions can only handle small forces which may also not be enough to facilitate cell migration. The size of the patterned nanodots in the NSA had no effect on the final cell choices in our migration assay. However, it is possible that cell response rates were different, and that the focal adhesions dynamics (size, stability and maturation efficiency) varied depending on the size of the protein nanodots. In the future, the NSA can be used to explore these hypotheses. Focal adhesion dynamics can be monitored by visualizing fluorescently tagged focal adhesion proteins like paxillin for example.

5.2.2. Investigating cell choices with other cell types and other guidance cues

Here we report on haptotaxis behaviors of C2C12 myoblasts towards netrin-1 protein cues. The NSA platform can be extended to study cell preferences using other cell types and other guidance cues. For instance, 1) in angiogenesis, endothelial cells migrate in response to signals – consisting mainly of vascular endothelial growth factors (VEGF) – secreted by the tissues they invade,[129,130] and 2) fibroblast cells which navigate on surface-attached fibronectin during the wound healing cascade.[131,132] Other cues of interest include extracellular matrix proteins like fibronectin, laminin and collagen and, neuronal guidance cues that are membrane-bound *in vivo* like sonic hedgehog (Shh), ephrins, and brain-derived neurotrophic factors (BDNF) to mention a few. Most importantly, repulsive guidance cues will provide information regarding the surface concentrations necessary to trigger actin de-polymerization.

5.2.3. Studying neuronal haptotaxis with the NSA

The most natural application of the NSA platform would be studying axonal navigation behaviors towards surface immobilized netrin-1 and/or other neuronal guidance cues. Commissural and cortical neurons are chemotropically attracted towards netrin-1, and their migration can be easily examined with the NSA by replacing the C2C12 myoblasts, studied here, with primary neurons. Optimal haptotaxis protocols with neurons on a stripe assay were previously published by our group.[1] Neuronal migration is slightly different from that of other cells, in that neurons anchor their cell bodies, and use their growth cones to sense their microenvironment. Depending on the signals encoded from the surface cues, the axons extend (or grow) enabling the growth cones to migrate in the preferred direction. In neuronal navigation, different scenarios on the NSA could be observed like (i) where the somas preferentially adhere, and (ii) the growth cones migration preferences, and (iii) the growth cones preferences relative to the soma location. Additionally, soft substrates which are more physiologically relevant to neurons' microenvironment,[133] could be used for the NSA. It was previously demonstrated that neuronal activity like growth, extension and migration is enhanced on matrix substrates with a low stiffness (rigidity).[134,135] Our lab pioneered a method to pattern DNGs on soft substrates (E<10 kPa)[94] which can be used to pattern nanodot stripes and investigate axonal haptotaxis on these soft substrates.

The knowledge accrued from NSA experiments will help advance our understanding of processes like wound healing and neuronal development, and to enhance axonal regeneration. For instance, fibroblasts migration towards fibrotic tissues can be enhanced once the key factors in the processes have been identified. Likewise, axon regeneration could be accelerated by supplementing affected sites with the right guidance cues.[136] Furthermore, information derived from the NSA might also be used to improve body-to-device interfaces in prosthetics like in cochlear implants by using the appropriate guidance cues to maximize the implants connectivity to auditory neurons.[137]

6. REFERENCES

1 Ricoult, S. G., Thompson-Steckel, G., Correia, J. P., Kennedy, T. E. & Juncker, D. Tuning cell–surface affinity to direct cell specific responses to patterned proteins. *Biomaterials* **35**(2), 727-736 (2014).

2 Poliak, S. *et al.* Synergistic integration of Netrin and ephrin axon guidance signals by spinal motor neurons. *eLife* **4**, e10841 (2015).

3 von Philipsborn, A. C. *et al.* Microcontact printing of axon guidance molecules for generation of graded patterns. *Nat. Protocols* **1**(3), 1322-1328 (2006).

4 Knöll, B., Weinl, C., Nordheim, A. & Bonhoeffer, F. Stripe assay to examine axonal guidance and cell migration. *Nature Protocols* **2**, 1216-1224 (2007).

5 Sloan, T. F. W., Qasaimeh, M. A., Juncker, D., Yam, P. T. & Charron, F. Integration of Shallow Gradients of Shh and Netrin-1 Guides Commissural Axons. *PLoS Biology* **13**(3), e1002119 (2015).

6 Ongo, G., Ricoult, S. G., Kennedy, T. E. & Juncker, D. Ordered, Random, Monotonic and Non-Monotonic Digital Nanodot Gradients. *PLoS ONE* **9**(9), e106541 (2014).

7 Rhoads, D. S. & Guan, J.-L. Analysis of directional cell migration on defined FN gradients: Role of intracellular signaling molecules. *Experimental Cell Research* **313**(18), 3859-3867 (2007).

8 Krause, M. & Gautreau, A. Steering cell migration: lamellipodium dynamics and the regulation of directional persistence. *Nature Reviews Molecular Cell Biology* **15**, 577-590 (2014).

9 Li Jeon, N. *et al.* Neutrophil chemotaxis in linear and complex gradients of interleukin-8 formed in a microfabricated device. *Nature Biotechnology* **20**, 826-830 (2002).

10 Coyer, S. R. *et al.* Nanopatterning reveals an ECM area threshold for focal adhesion assembly and force transmission that is regulated by integrin activation and cytoskeleton tension. *Journal of Cell Science* **125**(21), 5110-5123 (2012).

11 Lara Rodriguez, L. & Schneider, I. C. Directed cell migration in multi-cue environments. *Integrative Biology* **5**(11), 1306-1323 (2013).

12 Hsu, S., Thakar, R. & Li, S. Haptotaxis of Endothelial Cell Migration Under Flow. *Vascular Biology Protocols. Methods in Molecular Medicine.* **139**, 237-250 (2007).

13 Ridley, A. J. *et al.* Cell Migration: Integrating Signals from Front to Back. *Science* **302**(5651), 1704-1709 (2003).

14 Geiger, B., Spatz, J. P. & Bershadsky, A. D. Environmental sensing through focal adhesions. *Nat Rev Mol Cell Biol* **10**(1), 21-33 (2009).

15 Berginski, M. E., Vitriol, E. A., Hahn, K. M. & Gomez, S. M. High-Resolution Quantification of Focal Adhesion Spatiotemporal Dynamics in Living Cells. *PLOS ONE* **6**(7), e22025 (2011).

16 Ananthakrishnan, R. & Ehrlicher, A. The Forces Behind Cell Movement. *International Journal of Biological Sciences* **3**(5), 303-317 (2007).

17 Nichol, R. H., Hagen, K. M., Lumbard, D. C., Dent, E. W. & Gómez, T. M. Guidance of Axons by Local Coupling of Retrograde Flow to Point Contact Adhesions. *The Journal of Neuroscience* **36**(7), 2267-2282 (2016).

18 Van Haastert, P. J. M. & Devreotes, P. N. Chemotaxis: signalling the way forward. *Nat Rev Mol Cell Biol* **5**(8), 626-634 (2004).

19 Roussos, E. T., Condeelis, J. S. & Patsialou, A. Chemotaxis in cancer. *Nat Rev Cancer* **11**(8), 573-587 (2011).

20 Nuzzi, P. A., Lokuta, M. A. & Huttenlocher, A. in *Adhesion Protein Protocols* Vol. 370 (ed Amanda S. Coutts) 23-35 (Humana Press, 2007).

21 Tessier-Lavigne, M. & Goodman, C. S. The Molecular Biology of Axon Guidance. *Science* **274**(5290), 1123-1133 (1996).

22 Wen, J. H. *et al.* Haptotaxis is Cell Type Specific and Limited by Substrate Adhesiveness. *Cellular and Molecular Bioengineering* **8**(4), 530-542 (2015).

23 Taraboletti, G., Roberts, D. D. & Liotta, L. A. Thrombospondin-induced tumor cell migration: haptotaxis and chemotaxis are mediated by different molecular domains. *The Journal of Cell Biology* **105**(5), 2409-2415 (1987).

24 Carter, S. B. Principles of Cell Motility: The Direction of Cell Movement and Cancer Invasion. *Nature* **208**, 1183-1187 (1965).

25 Carter, S. B. Haptotaxis and the Mechanism of Cell Motility. *Nature* **213**, 256-260 (1967).

26 Keller, H. U., Wissler, J. H. & Ploem, J. Chemotaxis is not a special case of haptotaxis. *Experientia* **35**(12), 1669-1671 (1979).

27 Lo, C. M., Wang, H. B., Dembo, M. & Wang, Y. L. Cell movement is guided by the rigidity of the substrate. *Biophysical Journal* **79**(1), 144-152 (2000).

28 Chan, C. E. & Odde, D. J. Traction Dynamics of Filopodia on Compliant Substrates. *Science* **322**(5908), 1687-1691 (2008).

29 Koch, D., Rosoff, William J., Jiang, J., Geller, Herbert M. & Urbach, Jeffrey S. Strength in the Periphery: Growth Cone Biomechanics and Substrate Rigidity Response in Peripheral and Central Nervous System Neurons. *Biophysical Journal* **102**(3), 452-460 (2011).

30 Spill, F., Reynolds, D. S., Kamm, R. D. & Zaman, M. H. Impact of the physical microenvironment on tumor progression and metastasis. *Current Opinion in Biotechnology* **40**, 41-48 (2016).

31 Sun, K. L. W., Correia, J. P. & Kennedy, T. E. Netrins: versatile extracellular cues with diverse functions. *Development* **138**(11), 2153-2169 (2011).

32 Moore, S. W., Tessier-Lavigne, M. & Kennedy, T. E. in *Axon Growth and Guidance* Vol. 621 (ed Dominique Bagnard) 17-31 (Springer New York, 2007).

33 Kang, J.-S. *et al.* Netrins and neogenin promote myotube formation. *The Journal of Cell Biology* **167**(3), 493-504 (2004).

34 Wilson, N. H. & Key, B. Neogenin: One receptor, many functions. *The International Journal of Biochemistry & Cell Biology* **39**(5), 874-878 (2007).

35 Nugent, A. A., Kolpak, A. L. & Engle, E. C. Human disorders of axon guidance. *Current Opinion in Neurobiology* **22**(5), 837-843 (2012).

36 Kennedy, T. E., Wang, H., Marshall, W. & Tessier-Lavigne, M. Axon Guidance by Diffusible Chemoattractants: A Gradient of Netrin Protein in the Developing Spinal Cord. *The Journal of Neuroscience* **26**(34), 8866-8874 (2006).

37 Phan, K. D., Hazen, V. M., Frendo, M., Jia, Z. & Butler, S. J. The Bone Morphogenetic Protein Roof Plate Chemorepellent Regulates the Rate of Commissural Axonal Growth. *The Journal of Neuroscience* **30**(46), 15430-15440 (2010).

38 Ducuing, H., Gardette, T., Pignata, A., Tauszig-Delamasure, S. & Castellani, V. Commissural axon navigation in the spinal cord: A repertoire of repulsive forces is in command. *Seminars in Cell & Developmental Biology* (2018).

39 Dominici, C. *et al.* Floor-plate-derived netrin-1 is dispensable for commissural axon guidance. *Nature* **545**, 350-354 (2017).

40 Varadarajan, S. G. *et al.* Netrin1 Produced by Neural Progenitors, Not Floor Plate Cells, Is Required for Axon Guidance in the Spinal Cord. *Neuron* **94**(4), 790-799 (2017).

41 Hand, R. A. & Kolodkin, A. L. Netrin-Mediated Axon Guidance to the CNS Midline Revisited. *Neuron* **94**(4), 691-693 (2017).

42 Charron, F., Stein, E., Jeong, J., McMahon, A. P. & Tessier-Lavigne, M. The Morphogen Sonic Hedgehog Is an Axonal Chemoattractant that Collaborates with Netrin-1 in Midline Axon Guidance. *Cell* **113**(1), 11-23 (2003).

43 Morales, D. A new model for netrin1 in commissural axon guidance. *Journal of Neuroscience Research* **96**(2), 247-252 (2018).

44 Salameh, S., Nouel, D., Flores, C. & Hoops, D. An optimized immunohistochemistry protocol for detecting the guidance cue Netrin-1 in neural tissue. *MethodsX* **5**, 1-7 (2018).

45 Moore, S. W., Biais, N. & Sheetz, M. P. Traction on Immobilized Netrin-1 Is Sufficient to Reorient Axons. *Science* **325**(5937), 166 (2009).

46 Xia, Y. & Whitesides, G. M. SOFT LITHOGRAPHY. *Annual Review of Materials Science* **28**(1), 153-184 (1998).

47 Schmid, H. & Michel, B. Siloxane Polymers for High-Resolution, High-Accuracy Soft Lithography. *Macromolecules* **33**(8), 3042-3049 (2000).

48 Faustino, V., Catarino, S. O., Lima, R. & Minas, G. Biomedical microfluidic devices by using low-cost fabrication techniques: A review. *Journal of Biomechanics* **49**(11), 2280-2292 (2016).

49 Qin, D., Xia, Y. & Whitesides, G. M. Soft lithography for micro- and nanoscale patterning. *Nat. Protocols* **5**(3), 491-502 (2010).

50 Kane, R. S., Takayama, S., Ostuni, E., Ingber, D. E. & Whitesides, G. M. in *The Biomaterials: Silver Jubilee Compendium* 161-174 (Elsevier Science, 1999).

51 Whitesides, G. M., Ostuni, E., Takayama, S., Jiang, X. & Ingber, D. E. Soft Lithography in Biology and Biochemistry. *Annual Review of Biomedical Engineering* **3**(1), 335-373 (2001).

52 Chen, Y. Nanofabrication by electron beam lithography and its applications: A review. *Microelectronic Engineering* **135**, 57-72 (2015).

53 Vieu, C. *et al.* Electron beam lithography: resolution limits and applications. *Applied Surface Science* **164**(1), 111-117 (2000).

54 Manfrinato, V. R. *et al.* Resolution Limits of Electron-Beam Lithography toward the Atomic Scale. *Nano Letters* **13**(4), 1555-1558 (2013).

55 Tseng, A. A., Kuan, C., Chen, C. D. & Ma, K. J. Electron beam lithography in nanoscale fabrication: recent development. *IEEE Transactions on Electronics Packaging Manufacturing* **26**(2), 141-149 (2003).

56 Williams, K. R., Gupta, K. & Wasilik, M. Etch rates for micromachining processing-Part II. *Journal of Microelectromechanical Systems* **12**(6), 761-778 (2003).

57 Olanrewaju, A. O., Robillard, A., Dagher, M. & Juncker, D. Autonomous microfluidic capillaric circuits replicated from 3D-printed molds. *Lab on a Chip* **16**(19), 3804-3814 (2016).

58 Islam, M., Natu, R. & Martinez-Duarte, R. A study on the limits and advantages of using a desktop cutter plotter to fabricate microfluidic networks. *Microfluidics and Nanofluidics* **19**(4), 973-985 (2015).

59 Chandrasekaran, A. *et al.* Thermal scribing to prototype plastic microfluidic devices, applied to study the formation of neutrophil extracellular traps. *Lab on a Chip* **17**(11), 2003-2012 (2017).

60 Guckenberger, D. J., de Groot, T. E., Wan, A. M. D., Beebe, D. J. & Young, E. W. K. Micromilling: a method for ultra-rapid prototyping of plastic microfluidic devices. *Lab on a Chip* **15**(11), 2364-2378 (2015).

61 Ricoult, S. G. *et al.* Nanodot Gradients: Large Dynamic Range Digital Nanodot Gradients of Biomolecules Made by Low-Cost Nanocontact Printing for Cell Haptotaxis (Small 19/2013). *Small* **9**(19), 3186-3186 (2013).

62 Papra, A. *et al.* Microfluidic Networks Made of Poly(dimethylsiloxane), Si, and Au Coated with Polyethylene Glycol for Patterning Proteins onto Surfaces. *Langmuir* **17**(13), 4090-4095 (2001).

63 Delamarche, E., Bernard, A., Schmid, H., Michel, B. & Biebuyck, H. Patterned Delivery of Immunoglobulins to Surfaces Using Microfluidic Networks. *Science* **276**(5313), 779-781 (1997).

64 Mrksich, M. & Whitesides, G. M. Patterning self-assembled monolayers using microcontact printing: A new technology for biosensors? *Trends in Biotechnology* **13**(6), 228-235 (1995).

65 Bernard, A. *et al.* Printing Patterns of Proteins. *Langmuir* **14**(9), 2225-2229 (1998).

66 Coyer, S. R., García, A. J. & Delamarche, E. Facile Preparation of Complex Protein Architectures with Sub-100-nm Resolution on Surfaces. *Angewandte Chemie International Edition* **46**(36), 6837-6840 (2007).

67 Bernard, A., Renault, J. P., Michel, B., Bosshard, H. R. & Delamarche, E. Microcontact Printing of Proteins. *Advanced Materials* **12**(14), 1067-1070 (2000).

68 von Philipsborn, A. C. *et al.* Growth cone navigation in substrate-bound ephrin gradients. *Development* **133**(13), 2487-2495 (2006).

69 Ricoult, S. G., Sanati Nezhad, A., Knapp-Mohammady, M., Kennedy, T. E. & Juncker, D. Humidified Microcontact Printing of Proteins: Universal Patterning of Proteins on Both Low and High Energy Surfaces. *Langmuir* **30**(40), 12002-12010 (2014).

70 Walter, J., Kern-Veits, B., Huf, J., Stolze, B. & Bonhoeffer, F. Recognition of position-specific properties of tectal cell membranes by retinal axons in vitro. *Development* **101**(4), 685-696 (1987).

71 Vielmetter, J., Stolze, B., Bonhoeffer, F. & Stuermer, C. A. O. In vitro assay to test differential substrate affinities of growing axons and migratory cells. *Experimental Brain Research* **81**(2), 283-287 (1990).

72 Weschenfelder, M., Weth, F., Knöll, B. & Bastmeyer, M. in *Neural Development: Methods and Protocols* Vol. 1018 (eds Renping Zhou & Lin Mei) 229-246 (Humana Press, 2013).

73 Yamagishi, S., Kesavamoorthy, G., Bastmeyer, M. & Sato, K. Stripe Assay to Study the Attractive or Repulsive Activity of a Protein Substrate Using Dissociated Hippocampal Neurons. *Journal of Visualized Experiments : JoVE*(112), 54096 (2016).

74 Mai, J., Fok, L., Gao, H., Zhang, X. & Poo, M.-m. Axon Initiation and Growth Cone Turning on Bound Protein Gradients. *The Journal of Neuroscience* **29**(23), 7450-7458 (2009).

75 Ricoult, S. *Axonal Migration and Turning Investigated through Surface-bound Digital Nanodot Gradients.* Doctoral degree thesis, McGill University, (2014).

76 Keenan, T. M. & Folch, A. Biomolecular gradients in cell culture systems. *Lab on a Chip* **8**(1), 34-57 (2008).

77 Chatterjee, K., Young, M. F. & Simon, C. G. Fabricating Gradient Hydrogel Scaffolds for 3D Cell Culture. *Combinatorial chemistry & high throughput screening* **14**(4), 227-236 (2011).

78 Jeon, N. L. *et al.* Generation of Solution and Surface Gradients Using Microfluidic Systems. *Langmuir* **16**(22), 8311-8316 (2000).

79 Włodarczyk-Biegun, M. K. & del Campo, A. 3D bioprinting of structural proteins. *Biomaterials* **134**, 180-201 (2017).

80 Qasaimeh, M. A., Ricoult, S. G. & Juncker, D. Microfluidic probes for use in life sciences and medicine. *Lab on a Chip* **13**(1), 40-50 (2013).

81 Juncker, D., Schmid, H. & Delamarche, E. Multipurpose microfluidic probe. *Nat Mater* **4**(8), 622-628 (2005).

82 Safavieh, M., Qasaimeh, M. A., Vakil, A., Juncker, D. & Gervais, T. Two-Aperture Microfluidic Probes as Flow Dipoles: Theory and Applications. *Scientific Reports* **5**, 11943 (2015).

83 Ricoult, S. G., Kennedy, T. E. & Juncker, D. Substrate-Bound Protein Gradients to Study Haptotaxis. *Frontiers in Bioengineering and Biotechnology* **3**(40), 1-12 (2015).

84 Bélisle, J. M., Mazzaferri, J. & Costantino, S. in *Methods in Cell Biology* Vol. 119 (eds Matthieu Piel & Manuel Théry) Ch. 7, 125-140 (Academic Press, 2014).

85 Costantino, S. in *Immunocytochemistry and Related Techniques* Vol. 101 (eds Adalberto Merighi & Laura Lossi) 423-435 (Springer New York, 2015).

86 Belisle, J. M., Correia, J. P., Wiseman, P. W., Kennedy, T. E. & Costantino, S. Patterning protein concentration using laser-assisted adsorption by photobleaching, LAPAP. *Lab on a Chip* **8**(12), 2164-2167 (2008).

87 Salaita, K., Wang, Y. & Mirkin, C. A. Applications of dip-pen nanolithography. *Nature Nanotechnology* **2**, 145 (2007).

88 Perl, A., Reinhoudt, D. N. & Huskens, J. Microcontact Printing: Limitations and Achievements. *Advanced Materials* **21**(22), 2257-2268 (2009).

89 Geissler, M. *et al.* Microcontact-Printing Chemical Patterns with Flat Stamps. *Journal of the American Chemical Society* **122**(26), 6303-6304 (2000).

90 Dertinger, S. K. W., Jiang, X., Li, Z., Murthy, V. N. & Whitesides, G. M. Gradients of substrate-bound laminin orient axonal specification of neurons. *Proceedings of the National Academy of Sciences* **99**(20), 12542-12547 (2002).

91 Gunawan, R. C., Silvestre, J., Gaskins, H. R., Kenis, P. J. A. & Leckband, D. E. Cell Migration and Polarity on Microfabricated Gradients of Extracellular Matrix Proteins. *Langmuir* **22**(9), 4250-4258 (2006).

92 Lang, S., von Philipsborn, A. C., Bernard, A., Bonhoeffer, F. & Bastmeyer, M. Growth cone response to ephrin gradients produced by microfluidic networks. *Analytical and Bioanalytical Chemistry* **390**(3), 809-816 (2008).

93 Tseng, P., Kunze, A., Kittur, H. & Di Carlo, D. Research highlights: microtechnologies for engineering the cellular environment. *Lab on a Chip* **14**(7), 1226-1229 (2014).

94 MacNearney, D., Mak, B., Ongo, G., Kennedy, T. E. & Juncker, D. Nanocontact Printing of Proteins on Physiologically Soft Substrates to Study Cell Haptotaxis. *Langmuir* **32**(50), 13525-13533 (2016).

95 Donald MacNearney, T. K., David Juncker. *Nanocontact printing on soft substrates: haptotaxis on netrin-1 digital nanodot gradients.* Masters Degree thesis, McGill University, (2016).

96 Sathish, S., Ricoult, S. G., Toda-Peters, K. & Shen, A. Q. Microcontact printing with aminosilanes: creating biomolecule micro- and nanoarrays for multiplexed microfluidic bioassays. *Analyst* **142**(10), 1772-1781 (2017).

97 Hu, S., Chen, T.-H., Zhao, Y., Wang, Z. & Lam, R. H. W. Protein–Substrate Adhesion in Microcontact Printing Regulates Cell Behavior. *Langmuir* **34**(4), 1750-1759 (2018).

98 Gopal, A. A. *et al.* Spatially Selective Dissection of Signal Transduction in Neurons Grown on Netrin-1 Printed Nanoarrays via Segmented Fluorescence Fluctuation Analysis. *ACS Nano* **11**(8), 8131–8143 (2017).

99 Calof, A. L. & Lander, A. D. Relationship between neuronal migration and cell-substratum adhesion: laminin and merosin promote olfactory neuronal migration but are anti-adhesive. *The Journal of Cell Biology* **115**(3), 779-794 (1991).

100 Aebersold, M. J. *et al.* Simple and Inexpensive Paper-Based Astrocyte Co-culture to Improve Survival of Low-Density Neuronal Networks. *Frontiers in Neuroscience* **12**(94), 1-14 (2018).

101 Hamon, C. *et al.* Tunable Nanoparticle and Cell Assembly Using Combined Self-Powered Microfluidics and Microcontact Printing. *Advanced Functional Materials* **26**(44), 8053-8061 (2016).

102 Lautscham, Lena A. *et al.* Migration in Confined 3D Environments Is Determined by a Combination of Adhesiveness, Nuclear Volume, Contractility, and Cell Stiffness. *Biophysical Journal* **109**(5), 900-913 (2015).

103 Ravasio, A. *et al.* Regulation of epithelial cell organization by tuning cell–substrate adhesion. *Integrative Biology* **7**(10), 1228-1241 (2015).

104 Joo, S. *et al.* Effects of ECM protein micropatterns on the migration and differentiation of adult neural stem cells. *Scientific Reports* **5**, 13043-13055 (2015).

105 Randlett, O., Poggi, L., Zolessi, Flavio R. & Harris, William A. The Oriented Emergence of Axons from Retinal Ganglion Cells Is Directed by Laminin Contact In Vivo. *Neuron* **70**(2), 266-280 (2011).

106 Fricke, R. *et al.* Axon guidance of rat cortical neurons by microcontact printed gradients. *Biomaterials* **32**(8), 2070-2076 (2011).

107 Mazia, D., Schatten, G. & Sale, W. Adhesion of cells to surfaces coated with polylysine. Applications to electron microscopy. *The Journal of Cell Biology* **66**(1), 198 (1975).

108 Sitterley, G. in *Attachment and Matrix Factors* Vol. 3 12 (BioFiles, Sigma Life Science, 2008).

109 Hauff, K. *et al.* Matrix-Immobilized BMP-2 on Microcontact Printed Fibronectin as an in vitro Tool to Study BMP-Mediated Signaling and Cell Migration. *Frontiers in Bioengineering and Biotechnology* **3**, 62 (2015).

110 Pesen, D., Heinz, W. F., Werbin, J. L., Hoh, J. H. & Haviland, D. B. Electron beam patterning of fibronectin nanodots that support focal adhesion formation. *Soft Matter* **3**(10), 1280-1284 (2007).

111 Goodhill, G. J. Mathematical guidance for axons. *Trends in Neurosciences* **21**(6), 226-231 (1998).

112 Nguyen, H., Dayan, P., Pujic, Z., Cooper-White, J. & Goodhill, G. J. A mathematical model explains saturating axon guidance responses to molecular gradients. *eLife* **5**, e12248 (2016).

113 Dickson, B. J. Molecular Mechanisms of Axon Guidance. *Science* **298**(5600), 1959-1964 (2002).

114 Boyer, N. P. & Gupton, S. L. Revisiting Netrin-1: One Who Guides (Axons). *Frontiers in Cellular Neuroscience* **12**(221), 1-18 (2018).

115 Missirlis, D. *et al.* Substrate engagement of integrins α5β1 and αvβ3 is necessary, but not sufficient, for high directional persistence in migration on fibronectin. *Scientific Reports* **6**, 23258 (2016).

116 Harms, B. D., Bassi, G. M., Horwitz, A. R. & Lauffenburger, D. A. Directional Persistence of EGF-Induced Cell Migration Is Associated with Stabilization of Lamellipodial Protrusions. *Biophysical Journal* **88**(2), 1479-1488 (2005).

117 Shekarabi, M. & Kennedy, T. E. The Netrin-1 Receptor DCC Promotes Filopodia Formation and Cell Spreading by Activating Cdc42 and Rac1. *Molecular and Cellular Neuroscience* **19**(1), 1-17 (2002).

118 Hoang, A. N. *et al.* Measuring neutrophil speed and directionality during chemotaxis, directly from a droplet of whole blood. *Technology* **1**(1), 49 (2013).

119 Schvartzman, M. *et al.* Nanolithographic Control of the Spatial Organization of Cellular Adhesion Receptors at the Single-Molecule Level. *Nano Letters* **11**(3), 1306-1312 (2011).

120 Cavalcanti-Adam, E. A. *et al.* Cell Spreading and Focal Adhesion Dynamics Are Regulated by Spacing of Integrin Ligands. *Biophysical Journal* **92**(8), 2964-2974 (2007).

121 Kennedy, T. E., Serafini, T., de la Torre, J. & Tessier-Lavigne, M. Netrins are diffusible chemotropic factors for commissural axons in the embryonic spinal cord. *Cell* **78**(3), 425-435 (1994).

122 Brown, L. D., Cai, T. T. & DasGupta, A. Interval Estimation for a Binomial Proportion. *Statistical Science* **16**(2), 101-117 (2001).

123 Moore, S. W., Zhang, X., Lynch, C. D. & Sheetz, M. P. Netrin-1 Attracts Axons through FAK-Dependent Mechanotransduction. *The Journal of Neuroscience* **32**(34), 11574-11585 (2012).

124 Wang, X. *et al.* Effect of RGD nanospacing on differentiation of stem cells. *Biomaterials* **34**(12), 2865-2874 (2013).

125 Rappaz, B., Lai Wing Sun, K., Correia, J. P., Wiseman, P. W. & Kennedy, T. E. FLIM FRET Visualization of Cdc42 Activation by Netrin-1 in Embryonic Spinal Commissural Neuron Growth Cones. *PLOS ONE* **11**(8), e0159405 (2016).

126 Razafiarison, T. *et al.* Biomaterial surface energy-driven ligand assembly strongly regulates stem cell mechanosensitivity and fate on very soft substrates. *Proceedings of the National Academy of Sciences* **115**(18), 4631-4636 (2018).

127 Yu, T. T. & Shoichet, M. S. Guided cell adhesion and outgrowth in peptide-modified channels for neural tissue engineering. *Biomaterials* **26**(13), 1507-1514 (2005).

128 Kim, D.-H. & Wirtz, D. Focal adhesion size uniquely predicts cell migration. *The FASEB Journal* **27**(4), 1351-1361 (2013).

129 Lamalice, L., Le Boeuf, F. & Huot, J. Endothelial Cell Migration During Angiogenesis. *Circulation Research* **100**(6), 782-794 (2007).

130 van Nieuw Amerongen, G. P., Koolwijk, P., Versteilen, A. & van Hinsbergh, V. W. M. Involvement of RhoA/Rho Kinase Signaling in VEGF-Induced Endothelial Cell Migration and Angiogenesis In Vitro. *Arteriosclerosis, Thrombosis, and Vascular Biology* **23**(2), 211-217 (2003).

131 Clark, R. A. F., An, J.-Q., Greiling, D., Khan, A. & Schwarzbauer, J. E. Fibroblast Migration on Fibronectin Requires Three Distinct Functional Domains. *Journal of Investigative Dermatology* **121**(4), 695-705 (2003).

132 Briggs, S. L. The role of fibronectin in fibroblast migration during tissue repair. *Journal of Wound Care* **14**(6), 284-287 (2005).

133 Discher, D. E., Janmey, P. & Wang, Y.-l. Tissue Cells Feel and Respond to the Stiffness of Their Substrate. *Science* **310**(5751), 1139-1143 (2005).

134 Lantoine, J. *et al.* Matrix stiffness modulates formation and activity of neuronal networks of controlled architectures. *Biomaterials* **89**, 14-24 (2016).

135 Flanagan, L. A., Ju, Y.-E., Marg, B., Osterfield, M. & Janmey, P. A. Neurite branching on deformable substrates. *Neuroreport* **13**(18), 2411-2415 (2002).

136 Koeberle Paulo, D. & Bähr, M. Growth and guidance cues for regenerating axons: Where have they gone? *Journal of Neurobiology* **59**(1), 162-180 (2004).

137 Webber, A. & Raz, Y. Axon guidance cues in auditory development. *The Anatomical Record Part A: Discoveries in Molecular, Cellular, and Evolutionary Biology* **288A**(4), 390-396 (2006).